(12)

FG.

AFOSR Scientific Report

Volume I

THE DEVELOPMENT OF A COMPUTER AIDED AIRFOIL DESIGN PROCEDURE INCLUDING PRELIMINARY WIND TUNNEL EXPERIMENTS ON A LOW REYNOLDS NUMBER HIGH LIFT SECTION

Jimmy Charles Narramore

Ralph Dean Olander

and

Ronald Oran Stearman

AFOSR Scientific Report

This research was sponsored by the

AIR FORCE OFFICE OF SCIENTIFIC RESEARCH

~~Office of Aerospace Research~~

through Grant AF-AFOSR 71-1998

January 1976

UNCLASSIFIED
SECURITY CLASSIFICATION OF THIS PAGE (When Data Entered)

REPORT DOCUMENTATION PAGE		READ INSTRUCTIONS BEFORE COMPLETING FORM
1. REPORT NUMBER AFOSR - TR - 76 - 0536	2. GOVT ACCESSION NO.	3. RECIPIENT'S CATALOG NUMBER
4. TITLE (and Subtitle) Volume I THE DEVELOPMENT OF A COMPUTER AIDED AIRFOIL DESIGN PROCEDURE INCLUDING PRELIMINARY WIND TUNNEL EXPERIMENTS ON A LOW REYNOLDS NUMBER HIGH LIFT SECTION		5. TYPE OF REPORT & PERIOD COVERED FINAL 1 Dec 70-30 Nov 75 6. PERFORMING ORG. REPORT NUMBER
7. AUTHOR(s) JIMMY C NARRAMORE RALPH D OLANDER RONALD O STEARMAN		8. CONTRACT OR GRANT NUMBER(s) AFOSR 71-1998
9. PERFORMING ORGANIZATION NAME AND ADDRESS UNIVERSITY OF TEXAS AT AUSTIN DEPT OF AEROSPACE ENGR & ENGR MECHANICS AUSTIN, TEXAS 78712		10. PROGRAM ELEMENT, PROJECT, TASK AREA & WORK UNIT NUMBERS 681307 9782-04 61102F
11. CONTROLLING OFFICE NAME AND ADDRESS AIR FORCE OFFICE OF SCIENTIFIC RESEARCH/NA BUILDING 410 BOLLING AIR FORCE BASE, D C 20332		12. REPORT DATE Jan 76 13. NUMBER OF PAGES 150
14. MONITORING AGENCY NAME & ADDRESS(if different from Controlling Office)		15. SECURITY CLASS. (of this report) UNCLASSIFIED 15a. DECLASSIFICATION/DOWNGRADING SCHEDULE
16. DISTRIBUTION STATEMENT (of this Report) Approved for public release; distribution unlimited.		
17. DISTRIBUTION STATEMENT (of the abstract entered in Block 20, if different from Report)		
18. SUPPLEMENTARY NOTES		
19. KEY WORDS (Continue on reverse side if necessary and identify by block number) AIRFOIL OPTIMIZATION HIGH LIFT COMPUTER AIDED DESIGN		

20. ABSTRACT (Continue on reverse side if necessary and identify by block number)

An investigation on the state of the art of subsonic airfoil section design, including a review of the historical development of airfoil design methodology, was carried out. A computer aided airfoil design procedure employing current technology was developed and utilized to design a low-Reynolds number, high-lift airfoil section. Preliminary wind tunnel studies were carried out on this high-lift section and the influence of flow disturbances on its performances evaluated. This study represents the first phase in determining how changes in airfoil design parameters influence the dynamical properties of the airfoil.

DD FORM 1473 EDITION OF 1 NOV 65 IS OBSOLETE UNCLASSIFIED

(18) AFOSR (19) TR-76-Ø536

AFOSR Scientific Report

(16) AF-9782

Air Force Office of Scientific Research (17) 9782Ø4

(15) ~~Grant~~ AF-AFOSR [redacted]-1998-71

(6) THE DEVELOPMENT OF A COMPUTER AIDED AIRFOIL DESIGN PROCEDURE INCLUDING PRELIMINARY WIND TUNNEL EXPERIMENTS ON A LOW REYNOLDS NUMBER HIGH LIFT SECTION. Volume I.

(9) Final rept. 1 Dec 7Ø-3Ø Nov 75,

by

(10) Jimmy Charles Narramore

Ralph Dean Olander

[redacted]

Ronald Oran Stearman

(12) 151p.

Department of Aerospace Engineering and Engineering Mechanics

The University of Texas at Austin

Austin, Texas 78712

(11) Jan~~uary 19~~76

Approved for public release;

Distribution of this document is unlimited.

ACKNOWLEDGMENTS

The authors wish to acknowledge the support and assistance of the staff of the Aerospace Structural Dynamics and Aeroelasticity Laboratory of The University of Texas during the development of this research program. They also express their appreciation to the Computation Center of The University of Texas for the extended use of their facilities.

Finally, the authors wish to extend their thanks to William Walker, Aeromechanics Division, Air Force Office of Scientific Research, Office of Aerospace Research, for his continued financial support of this program.

Austin, Texas
January 1976

ABSTRACT

An investigation on the state of the art of subsonic airfoil section design was carried out. This included a review of the historical development of airfoil design methodology. A computer aided airfoil design procedure employing current technology was developed and was utilized to design a low-Reynolds-number high-lift airfoil section. Preliminary wind tunnel studies were carried out on this high-lift section and the influence of flow disturbances on its performances evaluated. The present study represents the first phase of an investigation to determine how changes in airfoil design parameters influence the dynamical properties of the airfoil. Such considerations are important in stall flutter prevention, a problem encountered in rotor-craft and turbine engine design.

TABLE OF CONTENTS

Table of Contents (continued)

LIST OF SYMBOLS

a,b	integration constants in Stratford's equations
c	airfoil chord
C_D	airfoil section drag coefficient
C_L	airfoil section lift coefficient
C_{L_u}	upper surface lift coefficient with lower surface held at stagnation
C_p	pressure coefficient
$\bar{C}_p$	Stratford's modified pressure coefficient
H	boundary layer shape factor, $\frac{\delta^*}{\theta}$
M	Mach number
q	dynamic pressure
R	gas constant
Re	Reynolds number based on chord length
Re_{δ^*}	Reynolds number based on displacement thickness
Re_{θ_i}	Reynolds number based on momentum thickness evaluated at the instability point
Re_{θ_t}	Reynolds number based on momentum thickness evaluated at the transition completion point
S	airfoil surface length
S_P	stagnation point location
S_T	total surface parameter length
T	static temperature
V	velocity along airfoil surface
V_o	maximum velocity
V_∞	freestream velocity

X	chord position
α	airfoil angle of attack (measured from zero lift line)
β	slack variable
δ	boundary layer displacement thickness
Γ	circulation about the airfoil
γ	ratio of specific heats $\frac{C_P}{C_V}$
ν	kinematic viscosity
ρ	fluid density
θ	boundary layer momentum thickness
σ	surface coordinate originating at the effective origin of the flat rooftop boundary layer
σ_o	effective flat rooftop length

Subscripts

o	refers to conditions at velocity peak on airfoil surface
T	refers to conditions at the trailing edge
P	refers to conditions at the stagnation point
l	refers to local conditions
∞	refers to freestream conditions
c	corrected
u	uncorrected

Abbreviations

db	decibels
SPL	sound power level

LIST OF TABLES

LIST OF FIGURES

LIST OF FIGURES (continued)

List of Figures (continued)

List of Figures (continued)

PART I

DEVELOPMENT OF A COMPUTER AIDED

AIRFOIL DESIGN PROCEDURE

INTRODUCTION

The problem of selecting optimum shapes to satisfy a given operational requirement has been a basic problem since the beginning of aerodynamic applications. An illustration is the requirement of producing a given airfoil design more resistant to stall flutter. This leads to an optimization problem to minimize the undesirable hysteresis found in the airfoil's force and moment versus angle of attack curves. Unfortunately, hardly any information is available within the literature illustrating how an airfoil's shape influences its dynamical force characteristics.[63] In this present study, airfoil design for stall flutter suppression is investigated by first focusing on the high lift airfoil designs employing a Stratford type pressure region. It has been suggested that an airfoil designed to a Stratford type of pressure recovery should have little hysteresis in the static lift versus angle of attack curves. Further investigation of this observation is needed.

The purpose of this part of the present study is to develop a practical computer aided high lift airfoil design procedure based upon the current state of the art found within the literature. Initially the calculus of variations is employed to determine the form of an optimum velocity distribution; next a computer program is used to determine the numerical values of the optimal velocity distribution as a function of the Reynolds number and trailing edge pressure (it should be noted that other airfoil optimization problems could be attacked with this computer program if the calculus of variations problem corresponding to these problems could be solved.); and finally the Eppler inverse computer program is used to determine what practical two dimensional airfoil shape will produce a near optimum velocity distribution. This airfoil will then be called an optimal airfoil for the requirements stipulated.

This part of the report will be divided into four sections. First the historical development of the airfoil design will be discussed. This will include a philosophy of airfoil design and a discussion of the problems encountered. Comparisons of newer airfoil sections will be made to the well known NACA airfoils and the reasons for improved performance for specific missions will be mentioned.

Next the foundations for the analytical investigation will be developed through the concept of component velocity distributions (i.e., by considering different regions on the airfoil) and their application to the general velocity distribution on the airfoil surface.

A limited case optimization will then be presented in which only the acceleration region and the pressure recovery region are incorporated. The lift coefficient will be maximized using standard calculus of variations methods.

Finally an example of the methodology used in the practical design of an airfoil section from a specified velocity distribution will then be given and the theoretical performance of an optimal airfoil presented.

HISTORICAL DEVELOPMENT

There is not much doubt that early attempts at flight were inspired by the birds. The first airfoils, as one would expect, were copies of Nature's shapes. The invention of the airfoil is usually credited to Horatio F. Phillips who patented an airfoil shape in 1884 closely resembling the highly cambered wing of a gull.[1] This pattern of using thin, highly cambered airfoils was followed for the first two decades of aviation. Later, with the advent of monoplanes, thicker airfoils were needed and at this time man started a long and rarely interrupted quest for better airfoils for a wide variety of missions.

In 1915 NACA was established, and with it came a large and expensive experimental research program. Families of wing sections were developed by a systematic experimental approach.[2] The general method used included: selecting a thickness distribution (usually empirical based on previous experience); selecting a camber line shape; then changing the maximum camber, the maximum camber position and the maximum thickness; and sometimes varying the maximum thickness position and the leading edge radius. All this led to an immense amount of data, but only a gradual improvement in performance which came through experience.

The tests had indicated that a laminar boundary layer could be maintained even at comparatevely large Reynolds numbers if the wing surface was sufficiently smooth and a slightly favorable pressure gradient was imposed. This led to the development of the 6-series or laminar airfoils. In design of these airfoils, new methods of deriving the airfoil shape were used. The criterion used for design was to maintain laminar flow back to a certain aft position at a certain angle of attack. Beyond this point the pressure increased linearly back to its trailing edge value. Improvements in drag reduction were noticeable. These laminar airfoils attained 30 to 50% smaller minimum profile drag than older airfoils having the same thickness.

Figure 1 shows the velocity distribution of three symmetrical NACA airfoils which possess a maximum thickness ratio of 12%. The 0012 is of the older type and the other two represent the laminar airfoils. The laminar flow airfoils produce much less drag than the 0012 at the design angle of attack due to the fact that the favorable pressure gradient maintains laminar flow producing the least frictional drag to the position of peak suction. This indicates that the drag might be reduced by moving the peak suction further and further back, but this is not the case. Moving the peak suction aft increases the unfavorable pressure gradient required which can cause separation near the trailing edge, and eventually the pressure drag, due to the growing turbulent boundary layer thickness, increases faster than the frictional drag decreases. Therefore, for a given thickness and Reynolds number there exists, with respect to drag, an optimum aft limit of chordwise position of peak suction.

When the airfoils in Figure 1 are placed at an angle of attack of 1.3°, the characteristics of the laminar airfoils change. The position of peak suction moves suddenly to near the leading edge, and the adverse gradient causes the laminar flow to become unstable, transition to turbulence near the nose, and greatly increase the frictional drag. This sudden increase in the drag causes the well known "bucket" in the polar of

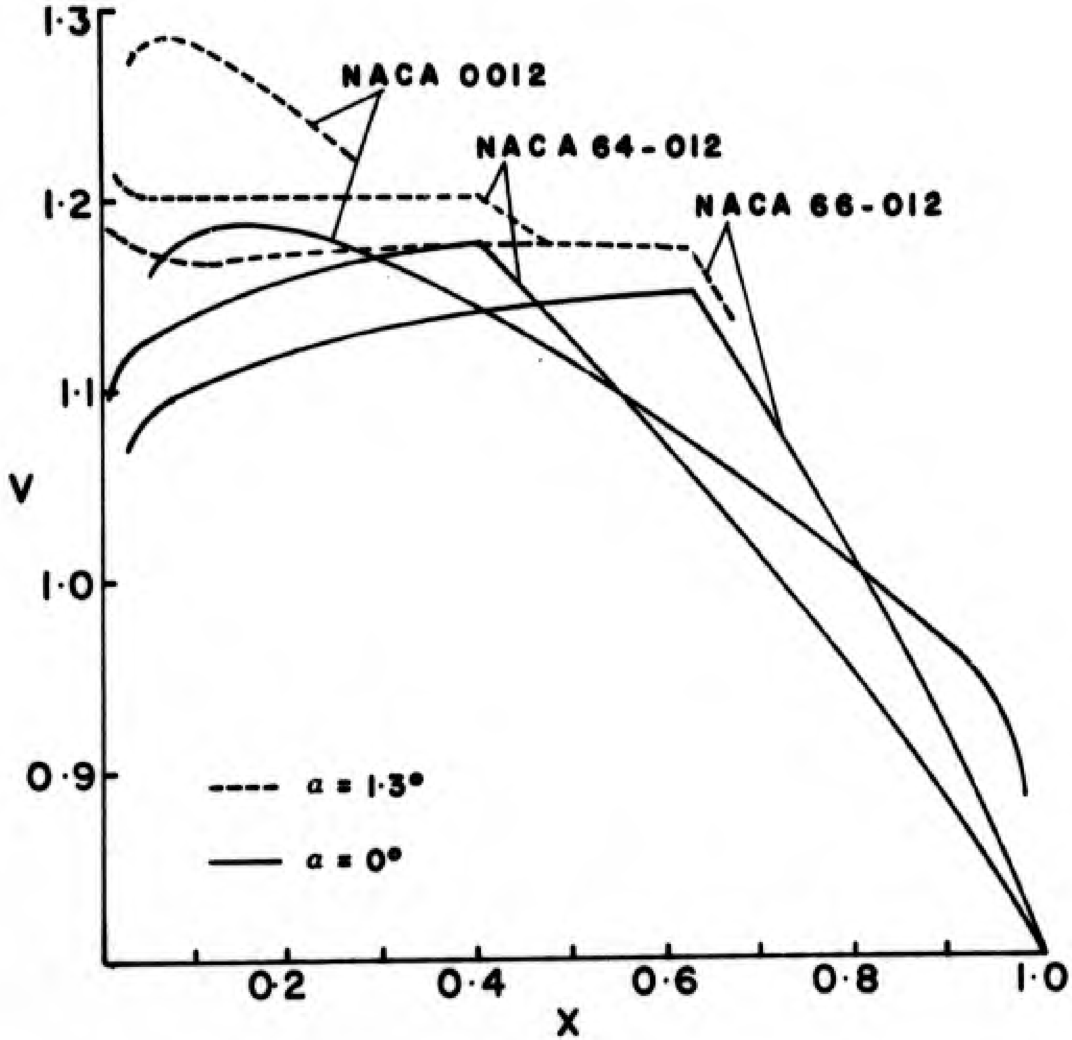

Figure 1. Velocity distributions of three 12 per cent thick NACA airfoils at two angles of attack

laminar airfoils. Older airfoils do not exhibit this bucket since the transition position changes only gradually throughout the angle of attack range. For maximum efficiency the drag of the airfoil should be as low as possible, but it is also desirable to have a range of angles of attack to operate within. The low drag bucket, therefore, should have a low minimum drag and a large lift coefficient range. The width of the low drag bucket is closely connected with the minimum drag and thickness of the section in NACA laminar airfoils. It is shown in Figure 2 that the thicker the section the wider the bucket and the wider the bucket the larger the drag. This can also be observed by scanning the low drag airfoils in Abbot and von Doenhoff and noting that a width of the drag bucket (subscript) is always associated with a certain thickness (last two numbers) e.g., 65_2 - 415, 65_2 - 015, 66_2 - 215, 63_2 - 615, etc., and that minimum drag increases with thickness. Until this interdependence is altered (until a smaller drag has been obtained with the same operating C_L range or a wider low drag range has been achieved with the same drag) no improvement can be claimed.[3] Now methods to improve airfoil design by boundary layer control will be discussed.

Soon after the development of laminar airfoils the push for faster and faster planes put subsonic airfoil research in the closet in the United States. The research completed had done very much for the aircraft designer. It had produced a catalogue from which the best airfoil available for the required mission could be chosen; but, also, it had given a hint to future developments in airfoil design.

The hint stems from the fact that the low drag airfoils were designed from a specified velocity distribution used to control the boundary

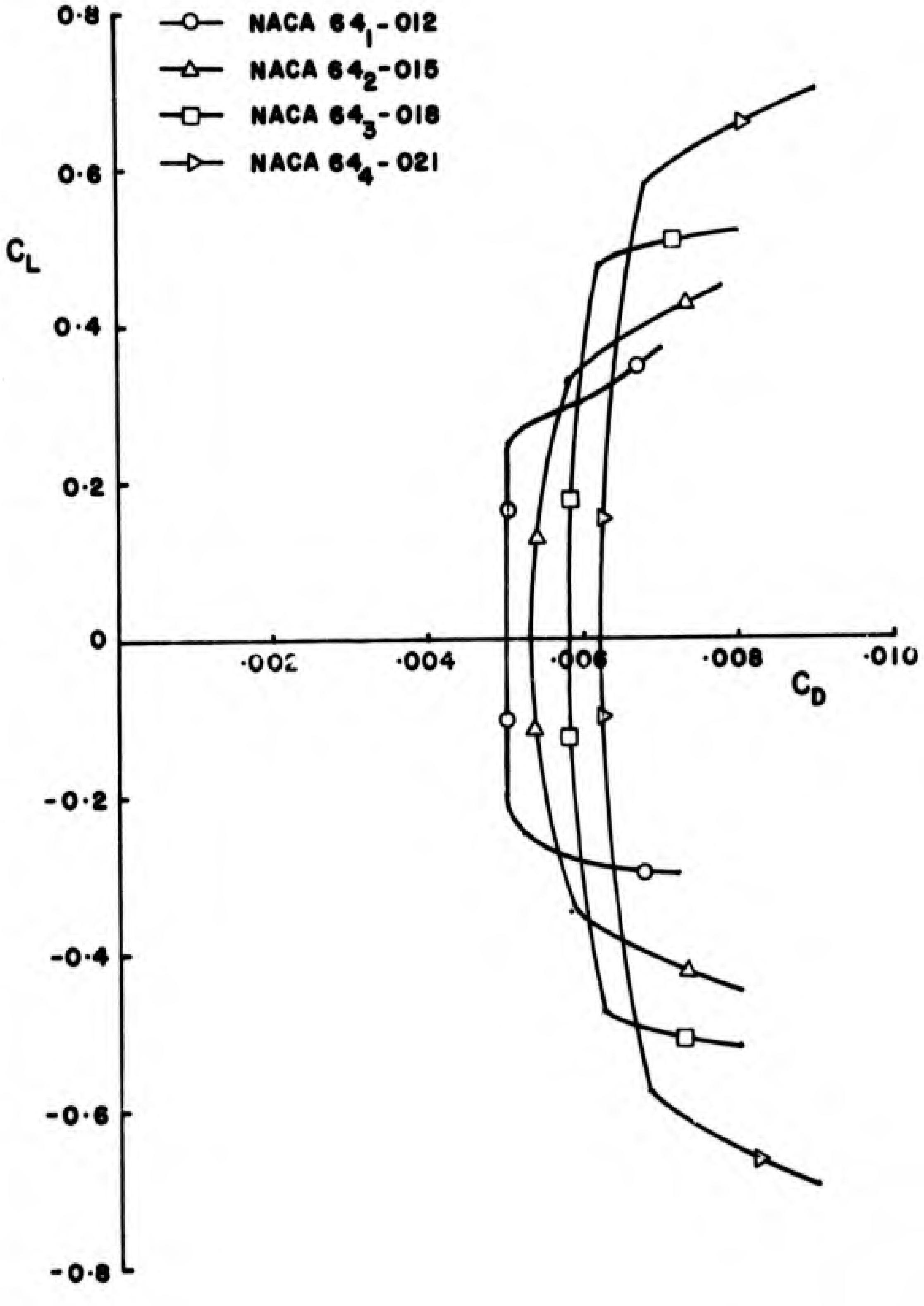

Figure 2. Drag polars of four NACA laminar airfoils

layer.[4] The properties of an airfoil can best be described by its velocity distribution. The lift, moment, and the theoretical development of the boundary layer (drag) are direct results of the velocity distribution, and from these the polar of the airfoil can be defined. The shape of the airfoil is of secondary concern!

The NACA laminar airfoils were designed to maintain laminar flow to a certain aft position. Thwaites[5] and Lighthill[6] have shown that if magnitude and position of peak suction are the design parameters the velocity distribution upstream of the peak should be chosen so that it is constant at some angle of attack α . The pressure gradient is favorable for all angles of attack less than α, maintaining laminar flow. Therefore, the width of the low drag bucket is a maximum for the two design parameters.

Control of the Turbulent Boundary Layer

Since there is always an adverse pressure on the aft part of airfoils and since this gradient usually results in transition to turbulence, turbulent boundary layers exist on the aft end of airfoils.[7] Therefore, careful control of the turbulent boundary layer to insure that no separation takes place by a suitable velocity distribution can bring further improvements. In order to shape the pressure recovery region it is necessary to have a method for testing for boundary layer separation. B.S. Stratford devised a method to do this and to provide a velocity distribution which recovers a given pressure difference in the shortest possible distance while just avoiding separation along its entire length.[8] Matsumiya and Uchida also produced similar results.[9] The resulting concave distribution is shown in Figure 3 and compared to the recovery region

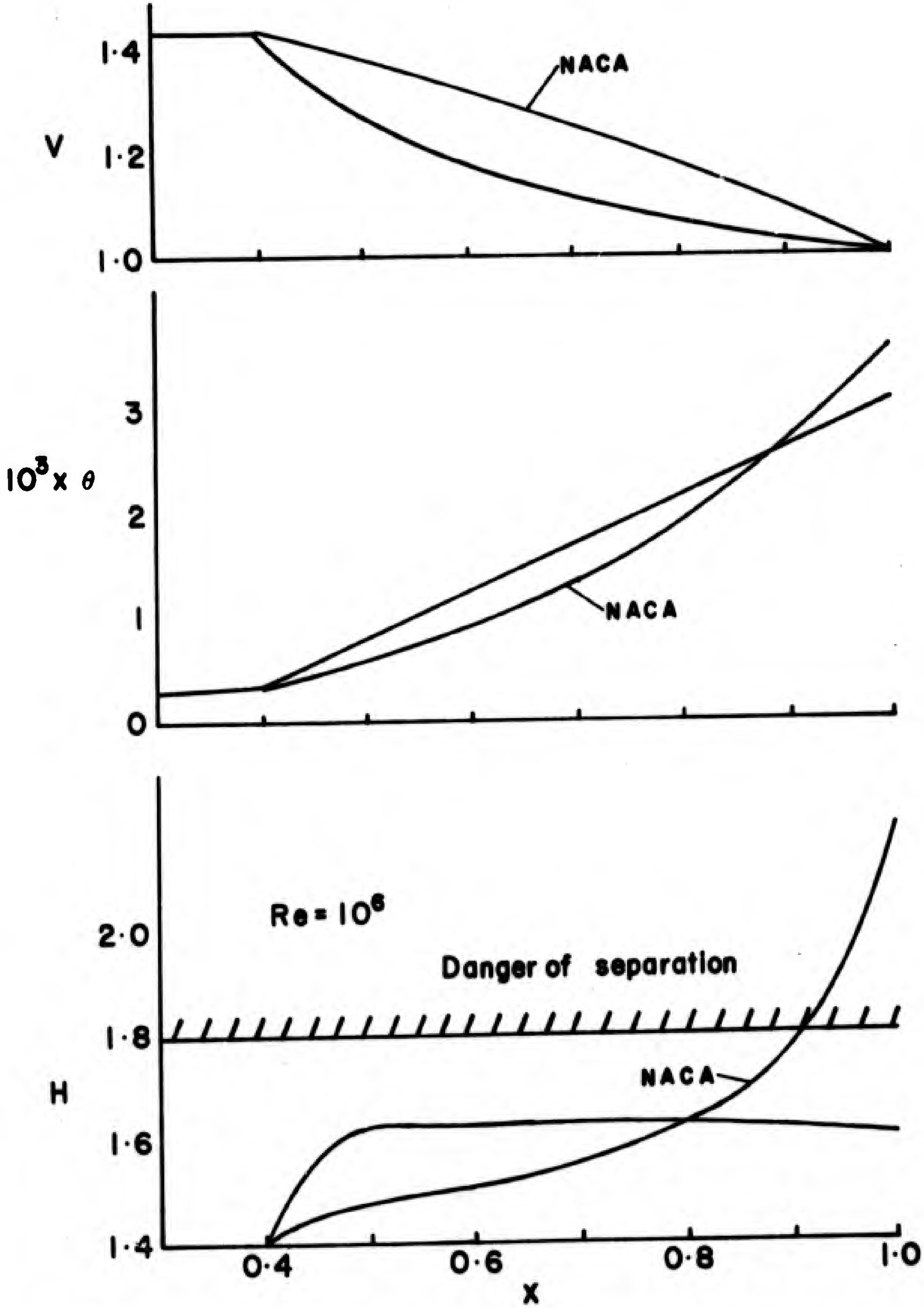

Figure 3. Development of the turbulent boundary layer for two different velocity distributions

of NACA laminar airfoils. The paper mentioned above shows that the most favorable development occurs when the shape parameter ($H = \frac{\text{displacement thickness}}{\text{momentum thickenes}}$) remains constant at a value of about 1.8 in the turbulent boundary layer. Also, Squire and Young have shown that the drag of an airfoil is proportional to the momentum thickness and the velocity at the trailing edge.[10] So the favorable development of the turbulent boundary layer is very important.

Control of Transition

On NACA laminar airfoils or airfoils with a concave pressure recovery the favorable pressure gradient changes more or less abruptly into a steep negative velocity gradient. At this point with a Reynolds number as high as 10^7 a laminar separation bubble occurs and the flow reattaches after it transitions to turbulence.[11] The separation bubble causes an unnecessary thickening of the initial turbulent boundary layer. Figure 4 shows the unpleasant effect of a separation bubble that extends into a region of steep adverse pressure gradient. At $Re = 1.5\times10^6$ the separation bubble is removed by trip wires and the lift-drag curve shows normal character. At $Re = 1.0\times10^6$ the trip wires are smaller than the critical roughness height and a separation bubble is formed which although of small size, causes a very large increase in drag. It must be noted that the turbulent boundary layer aft of the bubble remained completely attached to the trailing edge. Since boundary layer tripping is somewhat of an art and since there is added drag due to the tripping device, this does not seem to be the best method to control transition.

F.X. Wortmann has found that it is possible to control transition by not connecting the positive and negative gradients directly but by

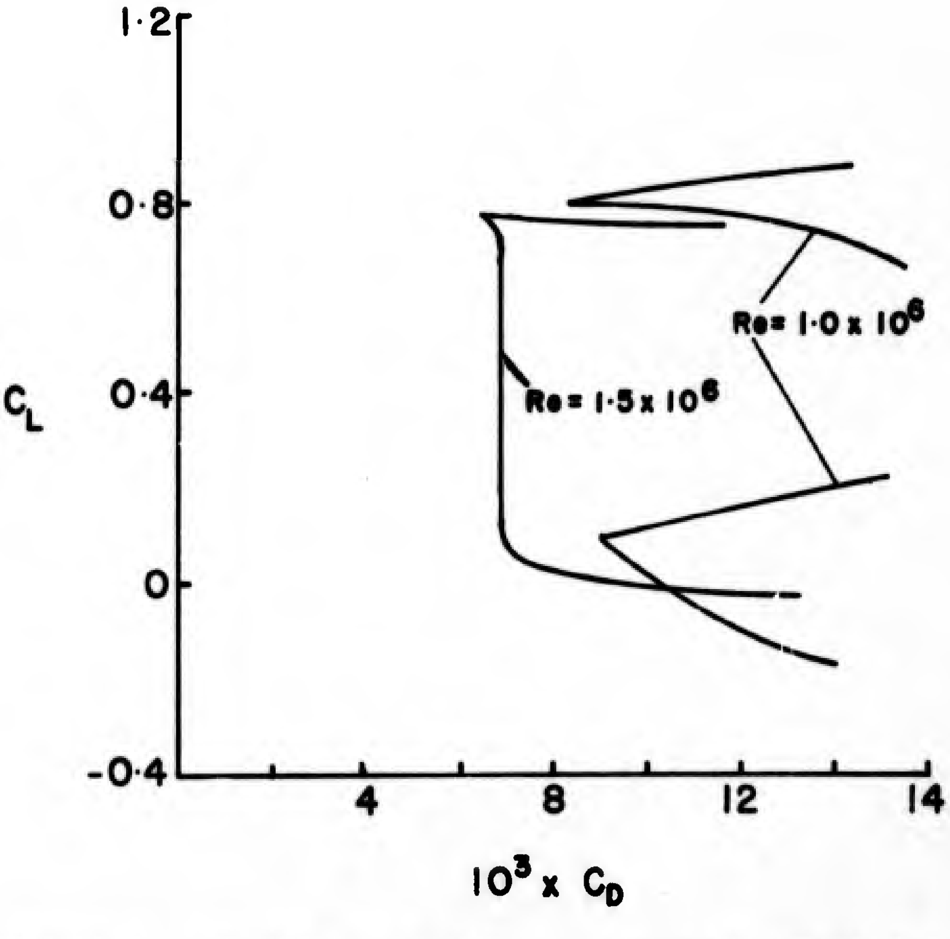

Figure 4. Lift-drag curve of 20 per cent thick airfoil for two Reynolds numbers illustrating effect of laminar separation bubble in pressure recovery region

inserting between them a transition region called the "instability range" where a slight negative gradient occurs.[12] By this means separation of the laminar boundary layer is avoided, but at the same time a high degree of instability of the laminar boundary layer is obtained. Wortmann chose a velocity distribution similar to the Falkner-Skan solutions which allowed no separation within the region.[13] Work done by Granville produced a procedure for calculating the length of the instability range required for transition.[14]

Wortmann has shown how the instability range and concave turbulent pressure recovery region enhance the performance of airfoils.[15] A Wortmann airfoil and a NACA laminar airfoil with the same width drag bucket are compared in Figures 5, 6, and 7. The figures illustrate that the 19.1% thick FX airfoil has approximately 18% less drag than the 18% thick NACA airfoil and the maximum lift is somewhat higher. This is noted to be an improvement since the thicker section with the wider bucket has the lower minimum profile drag.

For very low Reynolds numbers (below 0.7×10^6) S.J. Miley advocates placing a turbulent development region after the instability region which allows the new turbulent boundary to fully develop before encountering the steep adverse pressure gradient of the concave pressure recovery region.[16] Figure 8 illustrates the resulting velocity distribution (on the upper surface only).

Stall

Very often it is not the maximum lift which is of primary interest but the behavior of the airfoil at and beyond the maximum lift. A properly

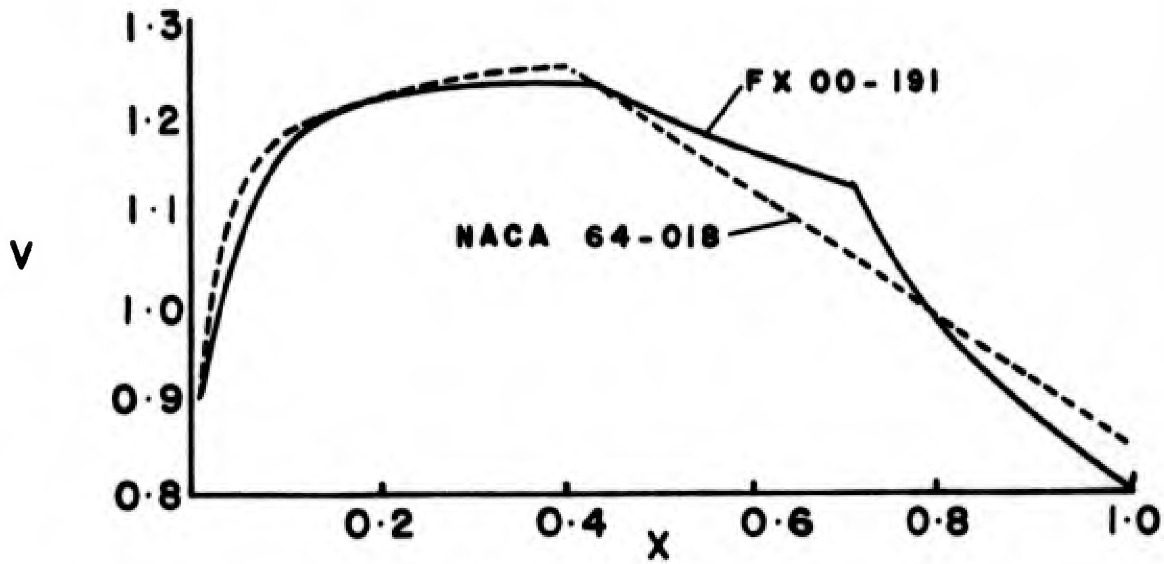

Figure 5. Comparison of the lift-drag curves of the NACA 64-018 airfoil section with a 19.1 per cent thick FX airfoil section

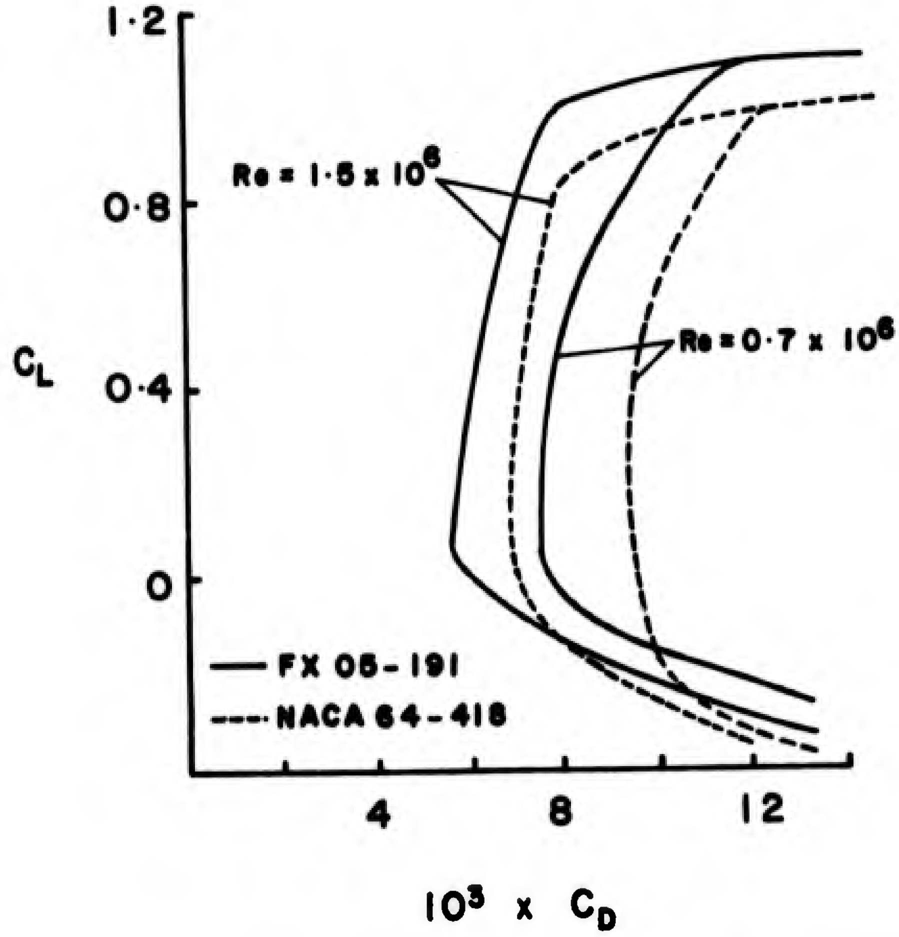

Figure 6. Comparison of the lift-drag curves of the NACA 64-418 and the FX05-191 airfoil sections at two Reynolds numbers

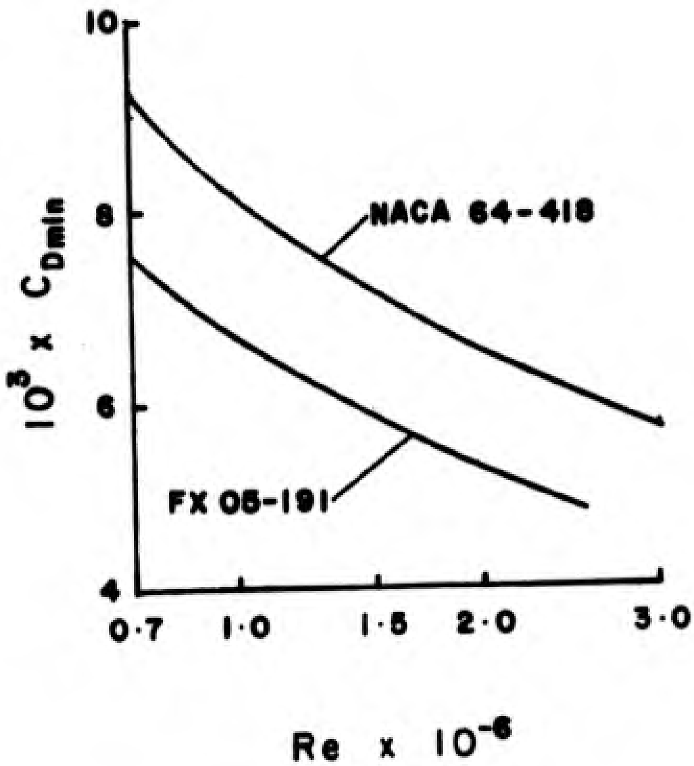

Figure 7. Summary of the minimum profile drag coefficients of sections NACA 64-418 and FX05-191 in relation to Reynolds number

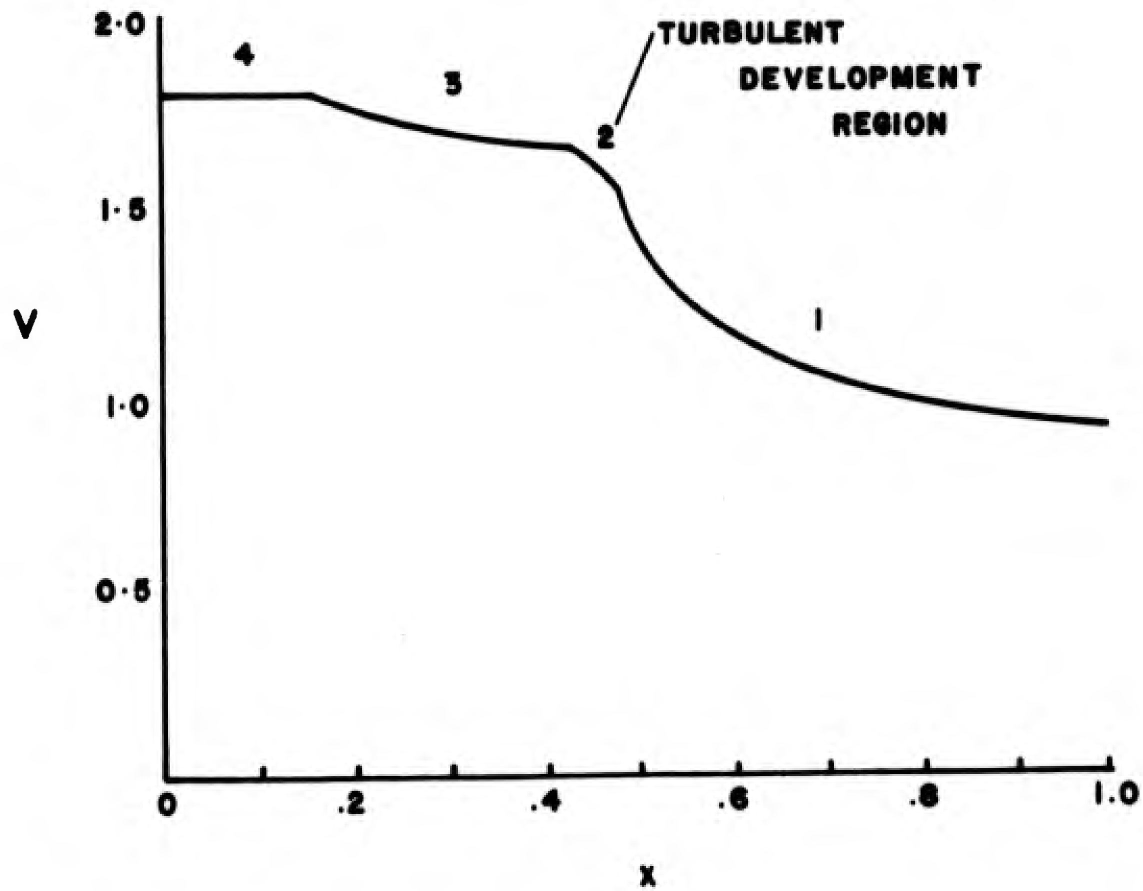

Figure 8. Upper surface velocity distribution showing Miley's turbulent development region

designed airfoil should at least avoid the dangerous leading edge stall. Leading edge stall is encountered when the short laminar separation bubble at the leading edge at some critical angle of attack suddenly transforms into a long bubble extending over the whole upper surface. The sudden change causes a complete collapse of lift or catastrophic stall. Owen and Klanfer have shown that the laminar separation bubble remains short without sudden extension if the Reynolds number based on the displacement thickness at the separation point remains greater than some value.[17] It has already been shown that a laminar separation bubble extending into an adverse pressure gradient can severely effect performance. Figure 9 shows that decreasing the peak velocity at high angles of attack can limit the length of the separation bubble and Figure 10 shows the corresponding lift-drag curve. Wortmann has shown that a minor change in the nose of NACA laminar airfoils can increase the maximum lift coefficient by 8%.[18]

Calculation Methods

A prerequisite for the analyses given above is a method of calculating the airfoil shape from the desired velocity distribution. There are many such methods, but the author was familar with only one which is exact and is available. This method was developed by R. Eppler and has been incorporated into a FØRTRAN program.[19] Another method which has only recently been developed at McDonnell Douglas is the James Method.[20] The new method has caused some excitement since the airfoil shape automatically closes. The output will produce the nearest velocity distribution to the one specified that will give a closed airfoil.[21]

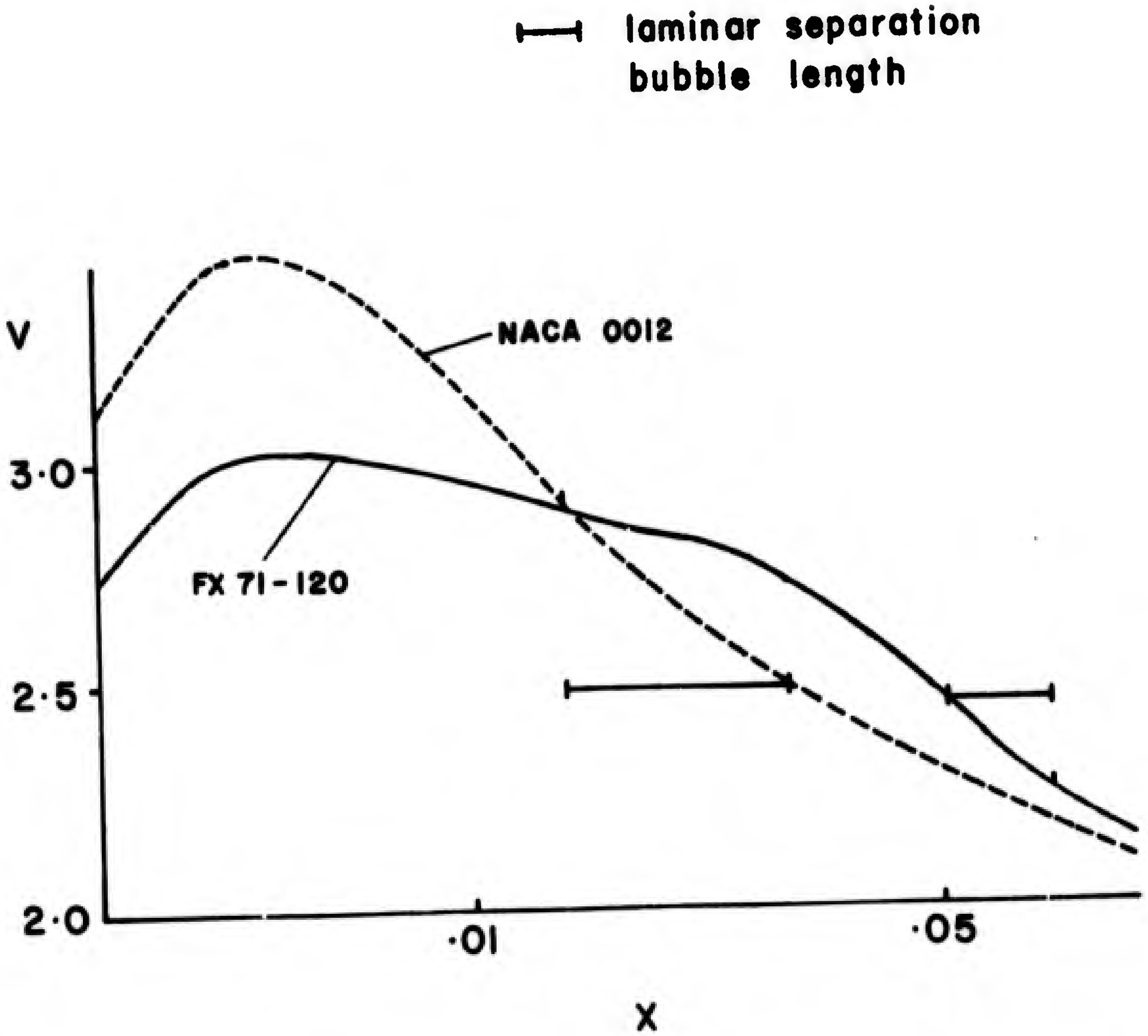

Figure 9. Illustration of the effect of the velocity distribution in the first few per cent chord on the laminar separation bubble length

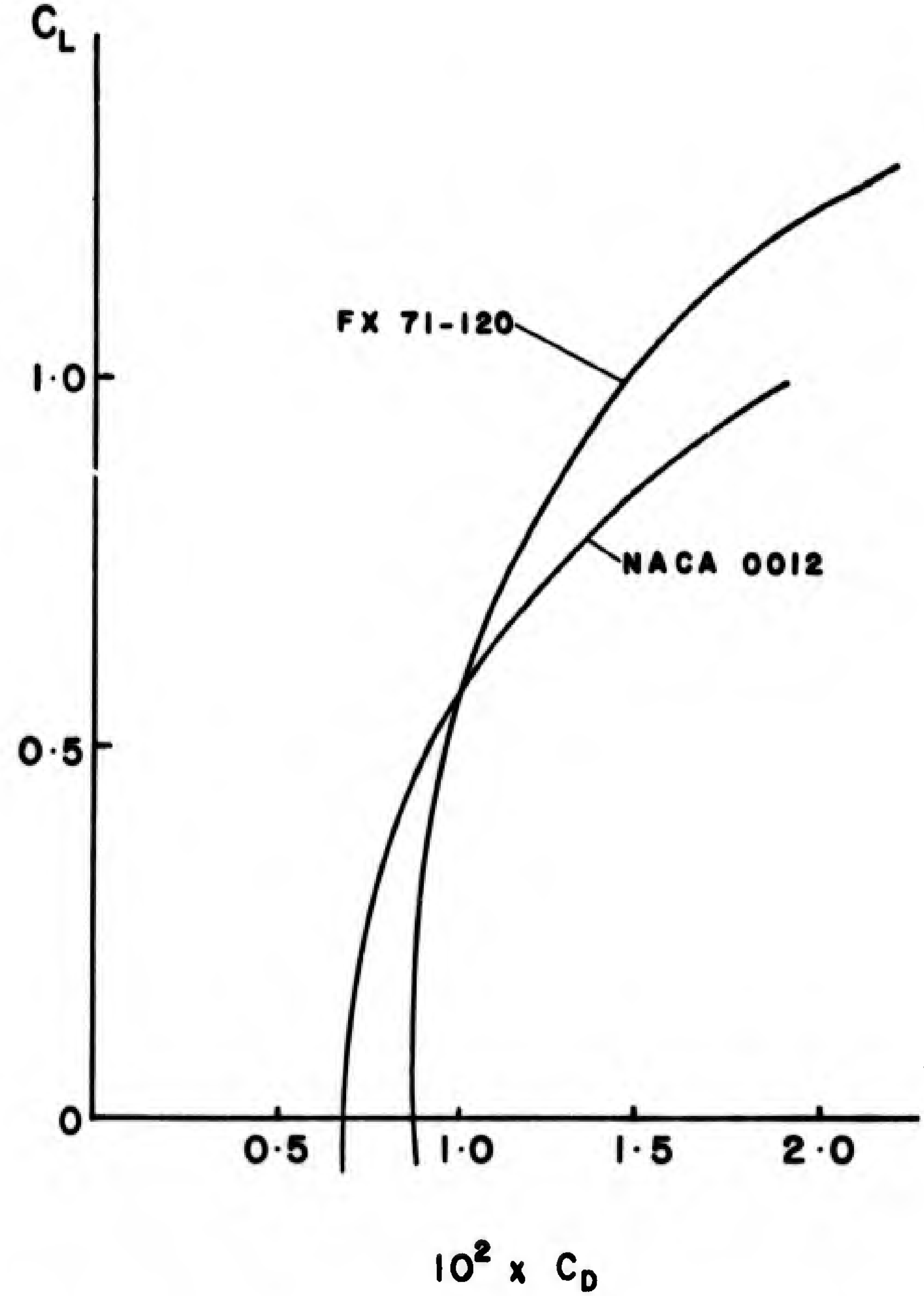

Figure 10. Comparison of lift-drag curves of FX airfoil with modified nose velocity distribution and NACA airfoil without modification

Another problem which is probably the most important, is the boundary layer model. The model for laminar flow is fairly accurate, but transition and turbulent models still leave something to be desired.[22] Stevens, Goradra and Braden have developed a program using fairly recent boundary layer theory which gives reasonable results.[23]

NASA Emphasis on Airfoil Design

The renewed interests of the NASA in general aviation problems in recent years has revived their in house research and external support of low speed aerodynamics and subsonic airfoil design. An excellent survey of their work in this area has been presented in a recent survey article by Pierpont.[63] The reader is referred to this reference for further details on this new NASA program. It is sufficient here to add that currently new mission oriented familes of airfoils are under investigation by the NASA.

Summary

With the change in the approach to airfoil design which has occurred in the last fifteen years, from manipulations of profile geometry to manipulations of the airfoil boundary layer, the volumes of low Reynolds number section data have become essentially obsolete. This is due to the fact that an individual airfoil section's performance is directly controlled by its boundary layer and not specifically by its geometric shape. The geometry, of course, creates the boundary layer through the associated pressure distribution; however, the origin of an airfoil design today is a prescribed boundary layer which dictates the pressure distribution which in turn dictates the geometric shape.

FOUNDATIONS FOR THE ANALYTICAL INVESTIGATION

As was indicated in the last section of this paper, the design of an airfoil consists of the determination of a geometric shape which will meet the specified mission requirements and most favorably effect the boundary layer along its surface. With the use of state of the art techniques, this problem was attacked by dividing the airfoil perimeter into a series of regions as illustrated in Figure 11, and an independent analysis of each region carried out. In this section the separate surface components are discussed beginning with the upper surface which is defined as the region between the leading edge stagnation point and the trailing edge. This upper surface is divided into four regions: the nose region, the acceleration region, the instability range, and the pressure recovery region. A similar division can be carried out on the lower surface.

Nose Region

For airfoils at high angles of attack, the nose shape plays an important role in the development of the boundary layer. Usually at high angles of attack large velocity peaks occur in the first few percent of chord followed by a large adverse slope in the velocity distribution curve which separates the laminar flow and spoils the initial conditions of the turbulent boundary layer.[24] The peak causes a local separation bubble to form and the turbulent boundary layer may separate near the trailing edge forming an extensive wake. With further increase in angle of attack different phenomena may occur in these two separate regions.[25] For very thin airfoils (less than 10% thickness) the bubble bursts very early but then

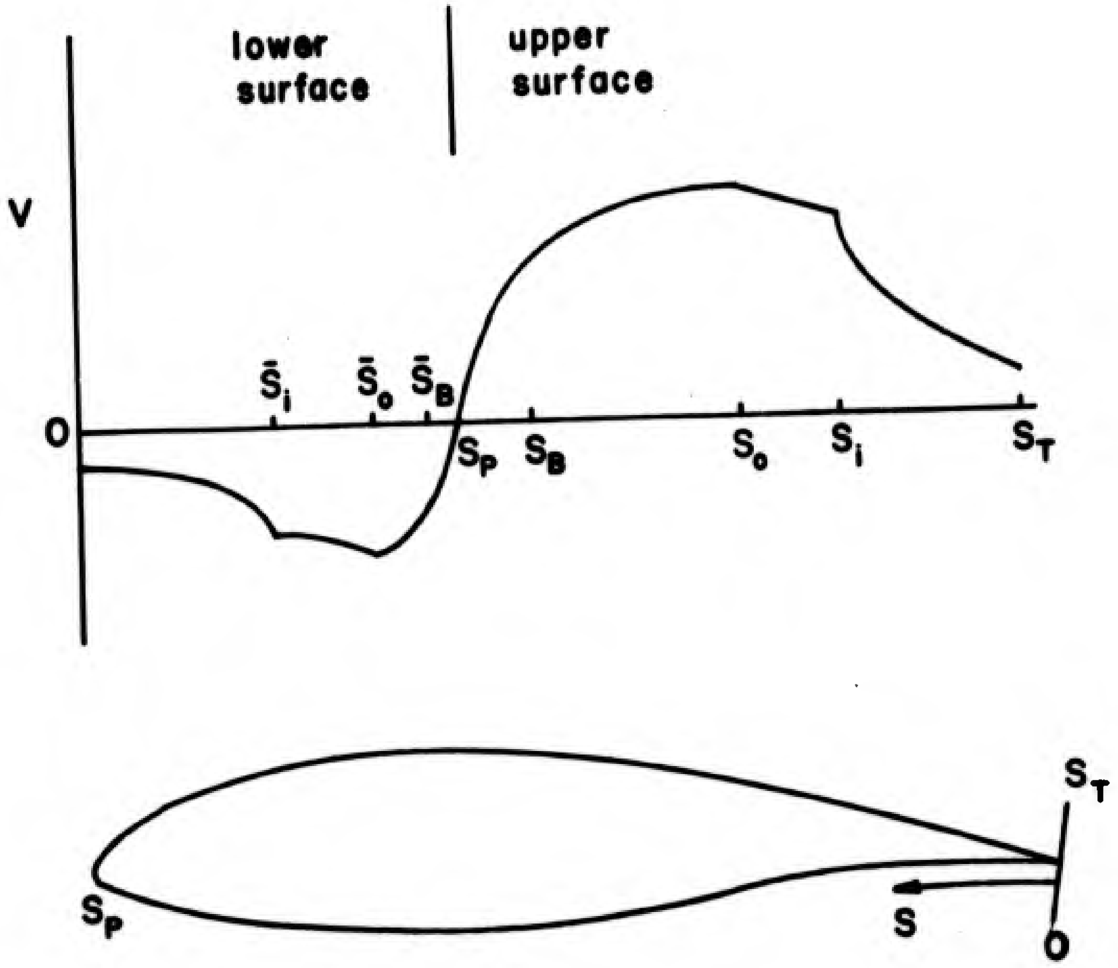

Figure 11. General form of the airfoil velocity distribution

transitions to turbulence and reattaches. Increasing the angle of attack makes the bubble grow until the reattachment line reaches the trailing edge. The maximum lift is moderate and the stall is steady. With airfoils of medium thickness the length of the laminar separation bubble decreases with increasing angle of attack and reaches an unstable break up condition at a high critical angle of attack. The bursting of the bubble causes the flow to completely separate from the upper surface. The resulting sudden and significant loss of lift is called leading edge stall. On thicker airfoils the separation of the turbulent boundary layer moves forward from the trailing edge with increasing angle of attack. The stalled condition is reached before the laminar separation bubble at the nose becomes unstable. This trailing edge stall may be more or less steady depending upon how fast the separation point of the turbulent boundary layer moves forward.[26] A properly designed airfoil should avoid the leading edge stall at high angles of attack. It has been shown[27] that the laminar separation bubble will not burst as long as the Reynolds number based on displacement thickness at the separation point remains greater than about 450. Since each bubble which occurs within a steep negative velocity gradient exerts an extremely unfavorable influence on the development of the turbulent boundary layer, care should be taken to avoid the laminar separation at the nose if possible. In other words, the velocity distribution over the upper surface of the airfoil should be such that at high angles of attack an instability range is formed (boundary layer transition is initiated and the laminar separation bubble avoided) near the leading edge.[28] Modifying the nose in the first five to ten percent of chord length is sufficient to provide a gain in the maximum lift of 15% to 20% and an increase in the associated stall angle of attack of 2 or 3 degrees.[29]

Acceleration Region

The acceleration region consists of the airfoil surface from the nose region to the start of the boundary layer instability range. Since the skin friction coefficient for a laminar boundary layer is less than that for a turbulent boundary layer, the acceleration region should be designed so that a stable laminar boundary layer will exist there if possible. (Of course, perturbations such as surface waviness and roughness, skin steps, access openings, leakage, insects, erosion, and turbulence of the free stream can decrease the stability margin of a laminar boundary layer and cause premature transition.) At very high Reynolds numbers the stability of the laminar boundary layer seems to fade out so that the maintenance of laminar flow may be impossible, whereas, at low Reynolds numbers the stability of the laminar boundary layer increases so that transition to turbulence is difficult. Increasing the length of the acceleration region (laminar flow) decreases the skin friction drag for the airfoil but increases the adverse gradient required downstream. This adverse gradient soon causes the pressure drag due to separation to grow faster than the skin friction drag is decreasing. Therefore, there exists for a certain Reynolds number an optimum length for the acceleration region.

Instability Range

The instability range was first devised in 1957 by F.X. Wortmann.[30] It came about as a result of some of his experiments while trying to improve the low drag performance of NACA laminar flow airfoils. The flow over aerodynamically smooth airfoils at low and moderate Reynolds numbers is characterized by laminar flow from the leading edge back to approximately the location of the first minimum pressure point on both the upper and lower surfaces. For NACA laminar flow airfoils, laminar separation occurs immediately downstream from the location of minimum pressure and the flow returns to the surface almost immediately as a turbulent boundary layer.[31] It has been shown (Figure 4) that this short bubble may adversely effect the initial development of the turbulent boundary layer. The momentum thickness at the trailing edge is, then, increased; and the Squire-Young drag law shows that the skin friction drag is increased.[32] Wortmann solved the laminar separation bubble problem by introducing an "instability gradient" upstream of the pressure rise to control transition. The instability range consists of a slight negative velocity gradient in which separation of the laminar boundary layer is avoided but a high degree of instability of the laminar boundary layer is achieved and transition initiated.

For the instability range, velocity distributions at some angle of attack are chosen by Wortmann of the type

$$\frac{V}{V_\infty} = k(x - x_1)^m \tag{1}$$

which is a Falkner-Skan similar solution for laminar boundary layers. For $m > -0.091$ no separation of the laminar layer occurs and hence no bubble can form. The constants k and x_1 are determined so that the velocity and the momentum thickness are continuous at the beginning of the instability range.

The all important position of the completion of transition in the instability range is governed by two factors: the degree of instability of the laminar boundary layer and the perturbations introduced into the laminar boundary layer. The degree of instability in turn depends on one hand on the Reynolds number and on the other hand on the pressure gradient in the flow direction.

The length of the instability range is determined by the degree of turbulence in the freestream and the rate at which perturbations are amplified downstream of the instability point. Granville[33] evaluated measurements in a flow of very low turbulence and found that in a positive pressure gradient $Re_{\theta t} - Re_{\theta i} \geq 400$.

Ideally, the instability range causes the flow to transition to a fully developed turbulent form before encountering the pressure recovery region. This not only eliminates the laminar separation bubble but also relieves the adverse effects on the turbulent boundary layer. Wortmann has shown the instability region is maintained over a whole range of Reynolds numbers and even over a large range of angles of attack.[34]

Pressure Recovery Region

There is always an adverse velocity gradient on the aft part of airfoils, and in order to have sufficient energy to remain attached this region must necessarily have turbulent flow. Much work has been done to determine the form of the velocity distribution in this region which will produce the most favorable effect upon the turbulent boundary layer.

In 1955 Wortmann[35] investigated the problem of choosing a pressure distribution which makes the turbulent boundary layer remain attached but recovers a maximum amount of pressure in a minimum distance. Using integral methods based on work done by Truckenbrodt[36], he developed an equation defining a velocity distribution for the pressure recovery region which would not separate and was of the form

$$\frac{V}{V_\infty} = \frac{V_o}{V_\infty}\left[1 + \left(\frac{\beta_\omega}{\theta_o}\right)(X - X_o)\right]^{-M_\omega} \tag{2}$$

where the subscript o denotes the start of the pressure recovery region, and θ_o is the momentum thickness at point o. β_ω and M_ω are functions computed in Truckenbrodt's procedure.

A more general form of this equation was employed by Eppler. It is given by

$$V = V_o[1 + K' (X - X_o)]^{-\mu'} \tag{3}$$

where the quantities K' and μ' may be related to the required turbulent boundary layer characteristics or to the degree of desired pressure recovery and the initial velocity distribution slope at point o.

More recently B.S. Stratford[37], using newer techniques to model the turbulent boundary layer, devised a method to check for separation and extended his work to derive the velocity distribution which just maintains zero skin friction throughout the region of pressure recovery. His method is convenient to use, and he has provided results so that it may be applied to airfoil sections. The general result of Stratford's investigation is

$$\bar{C}_p = 0.49\{Re_{\sigma_o}{}^{1/5}[(\frac{\sigma}{\sigma_o})^{1/5} - 1]\}^{1/3} \quad \text{for } \bar{C}_p \le \frac{4}{7} \tag{4}$$

and

$$\bar{C}_p = 1 - \frac{a}{[\frac{\sigma}{\sigma_0} + b]^{1/2}} \quad \text{for } \bar{C}_p \ge \frac{4}{7} \tag{5}$$

where

$$\bar{C}_p = \frac{p - p_o}{\frac{1}{2}\rho V_o^2} \tag{6}$$

This analysis and its application to airfoil design will be discussed in more detail in a later section.

Summary

In the preceding section the idea of component design distributions which may be integrated into a single airfoil was introduced. It should be noted that all of the regions discussed in this section may be employed on the lower surface.

The general form of the velocity distribution is represented in Figure 11. The design of an airfoil section may be interpreted as the determination of the location and size of a number of regions around the surface of the profile. Obviously, this amounts to a varational problem for the required velocity distribution to minimize or maximize some performance parameter.

SUBSONIC AIRFOIL OPTIMIZATION

Only quite recently has the application of variational techniques to applied aerodynamics through the study of the optimum shapes for vehicles been brought into the spotlight.[38] The idea of building a vehicle which is the best for its mission is very appealing. In this section a calculus of variations problem will be developed in the very new area of subsonic aerodynamic optimization.

An Optimal Velocity Distribution

As an example of how optimal processes may be applied to the design of subsonic airfoil sections a restricted case will be analyzed in detail. In this analysis the lift on a monoelement airfoil will be maximized by determining an optimal velocity distribution which does not allow separation of the boundary layer. It must be noted that the term optimal distribution is justified only as far as the model used for boundary layer development can be justified. The problem to be analyzed may be interpreted as a form of variational problem where an extremum of the lift coefficient is sought.

The lift coefficient may be expressed in terms of the circulation about the airfoil, and the optimization problem becomes that of finding the velocity distribution V(s) which maximizes

$$C_L = \frac{L}{\frac{1}{2}\rho V_\infty^2 C} = \frac{2\Gamma}{V_\infty C} = 2 \oint \frac{V(s)}{V_\infty} \frac{ds}{C} \tag{7}$$

where V(s) is the velocity tangential to the airfoil surface.

Figure 11 shows the general form of the velocity distribution and the notation used in this analysis. The velocity distribution is a function of the surface distance; and since the flow direction on the lower surface is in the opposite direction of increasing S, it is always negative there. This is consistent with the definition of the lift coefficient given in Equation 7.

The expression for the lift coefficient may be expanded to separate the upper and lower surface flows giving

$$C_L = \frac{2}{C} \int_0^{S_P} \frac{V}{V_\infty} ds + \frac{2}{C} \int_{S_P}^{S_T} \frac{V}{V_\infty} ds \quad . \tag{8}$$

Contributions from the lower surface are always less than zero so that the lower surface integral's maximum value is zero. As a result, it appears that the optimum velocity distribution on the lower surface is a constant equal to zero.

This leaves, to be optimized, the upper surface velocity distribution

$$C_{L_u} = \frac{2}{C} \int_{S_P}^{S_T} \frac{V}{V_\infty} ds \tag{9}$$

The chord length may be approximated by $S_T - S_P$ so that the upper surface lift coefficient may be written as

$$C_{L_u} = \frac{2}{S_T - S_P} \int_{S_P}^{S_T} \frac{V}{V_\infty} ds \tag{10}$$

According to Figure 11, Equation 10 may be expanded to the form

$$C_{L_u} = \frac{2}{S_T - S_P}\left\{\int_{S_P}^{S_B} \frac{V}{V_\infty}\,ds + \int_{S_B}^{S_o} \frac{V}{V_\infty}\,ds + \int_{S_o}^{S_i} \frac{V}{V_\infty}\,ds + \int_{S_i}^{S_T} \frac{V}{V_\infty}\,ds\right\} \qquad (11)$$

Certain constraints must be imposed upon the problem to make it realistic. The nose region between S_P and S_B should be constrained by the fact that $Re_{\delta^*} \geq 450$ should be maintained to avoid a leading edge stall. In the accelerating region from S_B to S_o the velocity is constrained by the local Mach number ($M_1 \leq 0.4$) so that compressibility effects are not encountered in the subsonic airfoil design. In the instability range from S_o to S_i the velocity is restricted to the form $\frac{V}{V_\infty} = K(X - X_1)^m$ which avoids laminar separation bubbles and initiates boundary layer transition. Within the pressure recovery region the velocity distribution is given by the Stratford zero skin friction equations (Equations 4 and 5) which allow maximum pressure recovery in a minimum distance.

Obviously, this general problem could be solved and a maximum of the lift coefficient found. Since the different regions on the airfoil and the parameters in the constraint equations bring the boundary layer characteristics into the problem, the solution would require that some model of the boundary layer be used so that the displacement thickness and momentum thickness be explicit functions of the velocity distribution or that these be implicitly matched at the joints of the regions.

In the example problem, to be worked here, the velocity distribution will be made less general and only two regions distinguished on the airfoil upper surface, the acceleration region and the pressure recovery region. This simplification makes the variational problem more manageable and allows the direct use of Stratford's results.

The general form of the velocity distribution used in the variational analysis is shown in Figure 12. The upper surface lift coefficient equation given above is now reduced to

$$C_{L_u} = \frac{2}{S_T - S_P}\left\{\int_{S_P}^{S_o} \frac{V}{V_\infty}\, ds + \int_{S_o}^{S_T} \frac{V}{V_\infty}\, ds\right\}. \tag{12}$$

<u>Stratford Zero Skin Friction Distribution</u>

Stratford's result provides a pressure distribution which recovers a given pressure difference in the shortest possible distance while just avoiding separation along its entire length. The basic result was derived for a pressure distribution of the form shown in Figure 13 where the boundary layer is taken to be turbulent over the entire region. A pressure coefficient and Reynolds number may be defined as

$$\bar{C}_P = \frac{P - P_o}{\frac{1}{2}\rho V_o^{\,2}} \tag{13}$$

and

$$Re_{\sigma_o} = \frac{V_o \sigma_o}{\upsilon} \tag{14}$$

The resulting pressure distribution for zero shear stress with a shape parameter $(H = \frac{\delta^*}{\theta})$ of two is

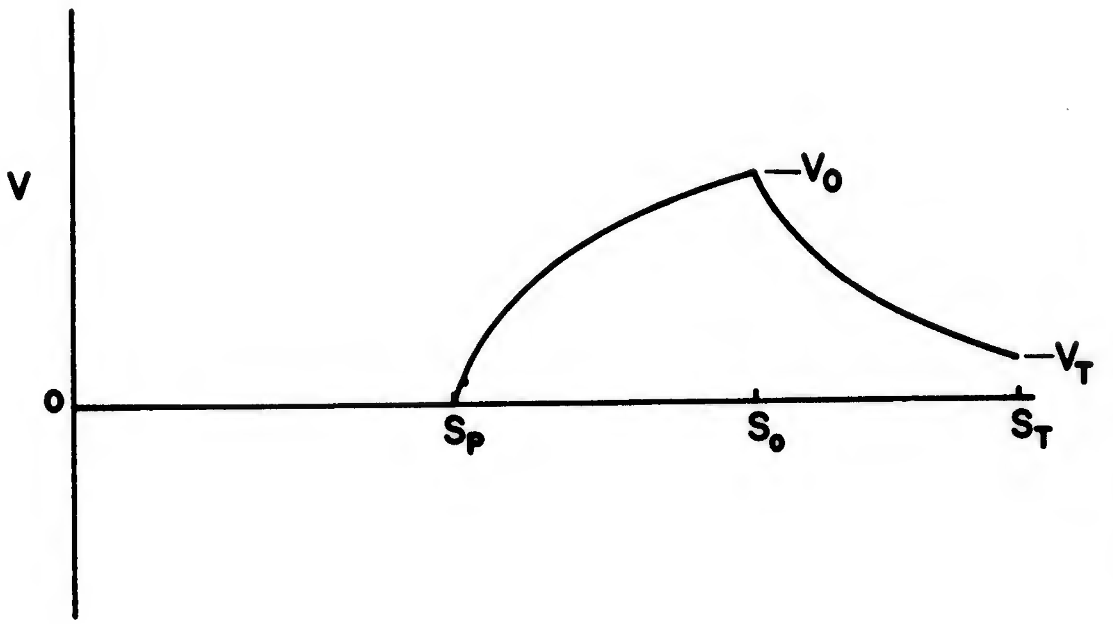

Figure 12. General form of the upper surface velocity distribution to be analyzed in the variational problem

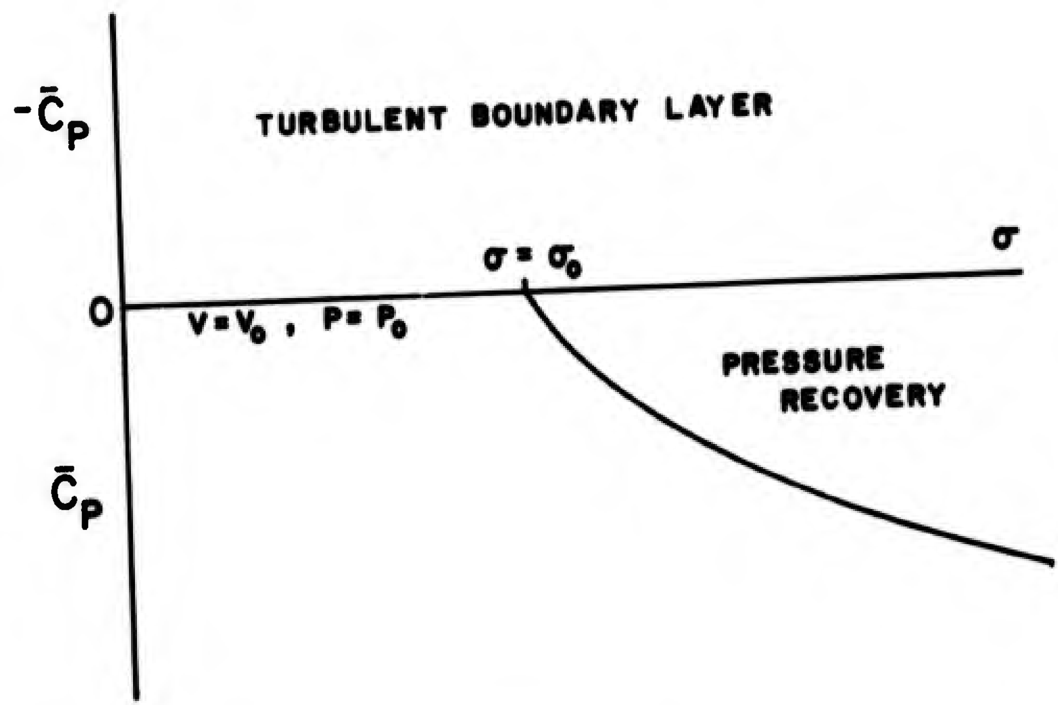

Figure 13. Pressure distribution used by Stratford

$$\bar{C}_P\left(\frac{\sigma}{\sigma_o}\right) = 0.49\left\{Re_{\sigma_o}^{1/5}\left[\left(\frac{\sigma}{\sigma_o}\right)^{1/5} - 1\right]\right\}^{1/3} \quad \text{for } \bar{C}_P \le \frac{4}{7} \tag{15}$$

$$\bar{C}_P\left(\frac{\sigma}{\sigma_o}\right) = 1 - \frac{a}{\left[\frac{\sigma}{\sigma_o} + b\right]^{1/2}} \quad \text{for } \bar{C}_P \ge \frac{4}{7} \tag{16}$$

The constants a and b are chosen to match $\bar{C}_P$ and $\frac{d\bar{C}_P}{d\left(\frac{\sigma}{\sigma_o}\right)}$ at $\bar{C}_P = \frac{4}{7}$. The resulting values are

$$b = \left\{\frac{15\left(1 - \frac{4}{7}\right)\left[\left(\frac{\sigma}{\sigma_o}\right)^{1/5}_{\bar{C}_P=\frac{4}{7}} - 1\right]^{2/3}\left(\frac{\sigma}{\sigma_o}\right)^{4/5}_{\bar{C}_P=\frac{4}{7}}}{2(0.49)\, Re_{\sigma_o}^{1/15}} - \left(\frac{\sigma}{\sigma_o}\right)_{\bar{C}_P=\frac{4}{7}}\right\} \tag{17}$$

$$a = \left(1 - \frac{4}{7}\right)\left[\left(\frac{\sigma}{\sigma_o}\right)_{\bar{C}_P=\frac{4}{7}} + b\right]^{1/2} \tag{18}$$

$$\left(\frac{\sigma}{\sigma_o}\right)_{\bar{C}_P=\frac{4}{7}} = \left\{\left[\frac{4}{(0.49)7}\right]^3 Re_{\sigma_o}^{-1/5} + 1\right\}^5 \tag{19}$$

The airfoil problem requires a stagnation point at $S = S_P$ with the velocity monotonically increasing to V_o at $S = S_o$. Stratford has provided two straightforward relations which modify the previous result to account for an initial region of favorable pressure gradient where the boundary layer may be laminar or turbulent by using an effective virtual origin σ_o. For a turbulent acceleration region

$$\sigma_o = \left(\frac{V_o}{V_\infty}\right)^{-3} \int_{S_P}^{S_o} \left(\frac{V}{V_\infty}\right)^3 ds \tag{20}$$

while for laminar acceleration region

$$\sigma_o = 38.2\ Re_{\sigma_o}^{-3/8} \left(\frac{V_o}{V_\infty}\right)^{-1} \left[\int_{\frac{S_T}{S_o-S_P}}^{\frac{S_o}{S_o-S_P}} \left(\frac{V}{V_\infty}\right) d\left(\frac{S}{S_o-S_P}\right)\right]^{5/8} (S_o-S_P) \tag{21}$$

The relations are derived from the requirement that the boundary layer momentum thickness match at the beginning of the pressure rise for laminar, turbulent, and flat rooftop flow.

From the definition of $\overline{C}_P$ in Equation 13, it may be shown that

$$C_P = \left(\frac{V_o}{V_\infty}\right)^2 (\overline{C}_P - 1) + 1 \tag{22}$$

with the use of Bernouilli's equation. Evaluating this equation at the trailing edge gives

$$C_{P_T} = \left(\frac{V_o}{V_\infty}\right)^2 (\overline{C}_{P_T} - 1) + 1 \quad . \tag{23}$$

Now the length required for the recovery region may be calculated. If $\overline{C}_{P_T} \leq \frac{4}{7}$, it is given by

$$\left(\frac{\sigma}{\sigma_o}\right)_T = \left[1 + Re_{\sigma_o}^{-1/5} \left(\frac{\overline{C}_{P_T}}{0.49}\right)^3\right]^5 \quad . \tag{24}$$

If $\bar{C}_{P_T} \geq \frac{4}{7}$, it is given by

$$\left(\frac{\sigma}{\sigma_o}\right)_T = \left[\frac{a}{1 - \bar{C}_{P_T}}\right]^2 - b \tag{25}$$

with a and b determined from the Equations 17 and 18.

Calculus of Variations Problem

These results may now be applied to the variational problem of maximizing the lift coefficient of a two dimensional, subsonic airfoil section. Figure 14 shows the general form of the upper surface velocity distribution with the Stratford pressure recovery region.

The variational problem may be expressed as

Maximize

$$C_{L_u} = \frac{2}{S_T - S_P}\left\{\int_{S_P}^{S_o} \frac{V}{V_\infty}\, ds + \int_{S_o}^{S_T} \frac{V}{V_\infty}\, ds\right\} \tag{26}$$

Subject to the Constraints

for $S \leq S_o$

$$\frac{V_o}{V_\infty} \leq \left(\frac{V}{V_\infty}\right)_{max} \tag{27}$$

turbulent acceleration region

$$\sigma_o = \left(\frac{V_o}{V_\infty}\right)^{-3} \int_{S_P}^{S_o} \left(\frac{V}{V_\infty}\right)^3 ds \tag{28}$$

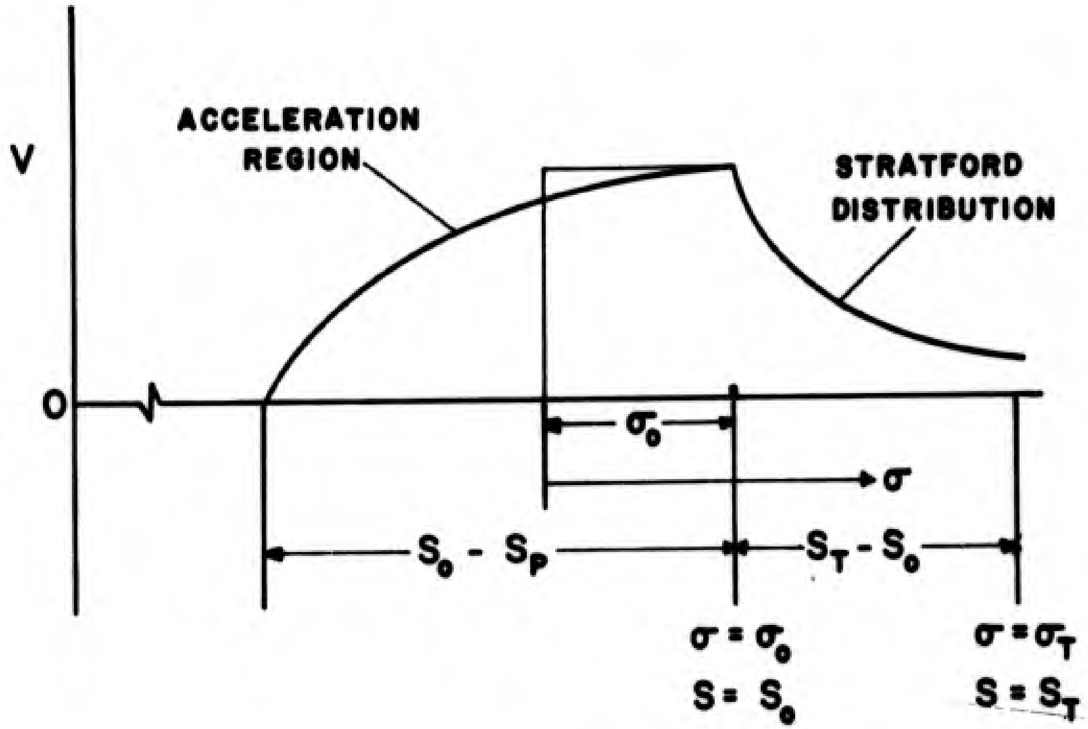

Figure 14. Upper surface velocity distribution with a Stratford recovery region

laminar acceleration region

$$\sigma_o = 38.2\, Re_{\sigma_o}^{-3/8} \left(\frac{V_o}{V_\infty}\right)^{-1} \left[\int_{\frac{S_P}{S_o - S_P}}^{\frac{S_o}{S_o - S_P}} \left(\frac{V}{V_\infty}\right) d\left(\frac{S}{S_o - S_P}\right)\right]^{5/8} (S_o - S_P) \tag{29}$$

for $S \geq S_o$

$$\frac{V}{V_\infty} = \frac{V_o}{V_\infty}\left[1 - 0.49\left\{Re_{\sigma_o}^{1/5}\left[\left(\frac{\sigma}{\sigma_o}\right)^{1/5} - 1\right]\right\}^{1/3}\right]^{1/2} \tag{30}$$

$$\text{if } \frac{V}{V_\infty} \geq \frac{V_o}{V_\infty}\sqrt{1 - 4/7}$$

$$\frac{V}{V_\infty} = \frac{V_o}{V_\infty}\left[\frac{a}{\left[\frac{\sigma}{\sigma_o} + b\right]^{1/2}}\right]^{1/2} \quad \text{if } \frac{V}{V_\infty} \leq \frac{V_o}{V_\infty}\sqrt{1 - 4/7} \tag{31}$$

For convenience in this example I will assume turbulent flow over all the surface so the equations will be shorter.

The inequality constraint listed above may be limited by the local Mach number. For this example the limit will be set such that $M_{max} \leq 0.4$ so that

$$\frac{V_o}{V_\infty} \leq \frac{0.4\sqrt{\gamma RT}\,(S_T - S_P)}{Re_C\,\nu} \tag{32}$$

Converting this by a slack variable to an equality constraint gives

$$\frac{V_o}{V_\infty} = \frac{0.4\sqrt{\gamma RT}\,(S_T - S_P)}{Re_C\,\nu} - \beta^2 \tag{33}$$

or

$$\frac{V_o}{V_\infty} = \alpha(S_T - S_P) - \beta^2 \tag{34}$$

where $\alpha = \dfrac{0.4\sqrt{\gamma RT}}{Re_C \nu}$

In order to simplify the problem, this expression may be substituted into the other constraints so that the problem becomes

Maximize

$$C_{L_u} = \frac{2}{S_T - S_P}\int_{S_P}^{S_o} \frac{V}{V_\infty}\, ds + \frac{2}{S_T - S_P}\int_{S_o}^{S_T} \frac{V}{V_\infty}\, ds \tag{35}$$

Subject to the Constraints

for $S \le S_o$

$$\sigma_o = [\alpha(S_T - S_P) - \beta^2]^{-3} \int_{S_P}^{S_T} \left(\frac{V}{V_\infty}\right)^3 ds \tag{36}$$

for $S \ge S_o$

$$\frac{V}{V_\infty} = [\alpha(S_T - S_P) - \beta^2]\left[1 - 0.49\left\{Re_{\sigma_o}^{1/5}\left[\left(\frac{\sigma}{\sigma_o}\right)^{1/5} - 1\right]\right\}^{1/3}\right]^{1/2}$$

$$\text{if } \frac{V}{V_\infty} \ge [\alpha(S_T - S_P) - \beta^2]\sqrt{1 - 4/7} \tag{37}$$

$$\frac{V}{V_\infty} = [\alpha(S_T - S_P) - \beta^2]\left[\frac{a}{\left[\frac{\sigma}{\sigma_o} + b\right]^{1/2}}\right]^{1/2}$$

$$\text{if } \frac{V}{V_\infty} \le [\alpha(S_T - S_P) - \beta^2]\sqrt{1 - 4/7} \tag{38}$$

If the last two constraints are placed in the performance index, the last integral in this equation may be expressed as:

$$\int_{S_o}^{S_T} \frac{V}{V_\infty}\, ds = G\left[\left(\frac{\sigma}{\sigma_o}\right)_T, C_{P_T}, Re_{\sigma_o}\right] \tag{39}$$

Setting up an analogous calculus of variations notation for this problem yields

Maximize

$$I = \int_{X_o}^{X_C} f(x,y)dx + I_S \tag{40}$$

Subject to

$$C = \int_{X_o}^{X_C} g(x,y)dx. \tag{41}$$

Also, the corner condition $f(x,y)\big|_{x_C^-} = f(x,y)\big|_{x_C^+}$ must be satisfied, which yields continuity in velocity between the acceleration and pressure recovery region.

So that this problem may be solved, the Lagrange multiplier approach is used. The augmented performance index is

$$I = \int_{X_o}^{X_C} (f + \lambda g)dx - \lambda C \tag{42}$$

or

$$I = \int_{X_o}^{X_C} F(x,y)dx - \lambda C \tag{43}$$

where

$$F = \frac{2\frac{V}{V_\infty}}{S_T - S_P} + \lambda \frac{\left(\frac{V}{V_\infty}\right)^3}{[\alpha(S_T - S_P) - \beta^2]^3} \tag{44}$$

and

$$y = \frac{V}{V_\infty} \tag{45}$$

In order to find a curve making the functional in Equation 43 an extremum, Euler's equation must be solved. Euler's equation may be written

$$\frac{\partial F}{\partial y} - \frac{d}{dx}\frac{\partial F}{\partial y'} = 0. \tag{46}$$

Since no derivatives of the velocity distribution appear in the equation to be solved this reduces to

$$\frac{\partial F}{\partial y} = 0 \tag{47}$$

The partial derivative of the function is

$$\frac{\partial F}{\partial y} = \frac{2}{S_T - S_P} + 3\lambda \frac{\left(\frac{V}{V_\infty}\right)^2}{[\alpha(S_T - S_P) - \beta^2]^3} = 0 \tag{48}$$

Solving for the velocity distribution yields

$$\frac{V}{V_\infty} = \sqrt{\frac{-2[\alpha(S_T - S_P) - \beta^2]^3}{3\lambda(S_T - S_P)}} \tag{49}$$

This equation implies that the velocity is constant in the acceleration region if the Lagrange multiplier is a constant.

In this case it may easily be shown that the Lagrange multiplier is constant. Equation 48 may be put in the form

$$\lambda = \frac{1}{\left(\frac{V}{V_\infty}\right)^2} \frac{A}{B} \quad . \tag{50}$$

Therefore, the multiplier may vary at most as the inverse of the velocity squared. The derivative of Equation 28 is

$$0 = \left(\frac{V_o}{V_\infty}\right)^{-3} \int_{S_P}^{S_T} \left(\frac{V}{V_\infty}\right)^2 \left[\frac{\partial}{\partial s}\left(\frac{V}{V_\infty}\right)\right] ds \tag{51}$$

Since harmonic functions are excluded from the solution, the value of $\left[\frac{\partial}{\partial s}\left(\frac{V}{V_\infty}\right)\right]$ must be zero. This means that the velocity in the acceleration region and therefore the Lagrange multiplier are constant.

In order to determine the value of the Lagrange multiplier, Equation 49 is substituted into the constraint equation so that

$$\sigma_o = [\alpha(S_T - S_P) - \beta^2]^{-3} \int_{S_P}^{S_o} \sqrt{\frac{-2[\alpha(S_T - S_P) - \beta^2]^3}{3\lambda(S_T - S_P)}}\, ds \tag{52}$$

Integration yields

$$\sigma_o = \frac{\left[\frac{-2[\alpha(S_T - S_P) - \beta^2]^3}{3\lambda(S_T - S_P)}\right]^{3/2}}{[\alpha(S_T - S_P) - \beta^2]^3} \left\{S_o - S_P\right\} \tag{53}$$

Solving this equation for the Lagrange multiplier gives

$$\lambda = \frac{-2[\alpha(S_T - S_P) - \beta^2]}{3(S_T - S_P)} \left[\frac{S_o - S_P}{\sigma_o}\right]^{2/3} \tag{54}$$

Plugging this back into Equation 49 yields

$$\frac{V}{V_\infty} = [\alpha(S_T - S_P) - \beta^2]\left[\frac{\sigma_o}{S_o - S_P}\right]^{1/3} \tag{55}$$

which says that the optimum velocity distribution in the acceleration region is a constant. In order to satisfy the corner condition, the velocity must be continuous at the joint of the acceleration region and the pressure recovery region. Since the velocity in the acceleration region is constant

$$\frac{V(S)}{V_\infty} = \text{constant} = \frac{V_o}{V_\infty} \tag{56}$$

which is the value of the velocity at the start of the pressure recovery region.

The velocity distribution which maximizes lift consists of a constant value in the acceleration region followed by the Stratford distribution in the pressure recovery region. Liebeck and Ormsbee[39] have shown that this is the same result that occurs when the acceleration region is laminar.

The equation for the lift coefficient may now be written as (assuming $\bar{C}_P \geq 4/7$)

$$C_{L_u} = \frac{2}{S_T - S_P} \int_{S_P}^{S_o} [\alpha(S_T - S_P) - \beta^2]\, ds$$

$$+ \frac{2}{S_T - S_P} [\alpha(S_T - S_P) - \beta^2] \int_{S_o}^{S_Z} \left[1. - 0.49\left\{Re_{\sigma_o}^{1/5}\left[\left(\frac{\sigma}{\sigma_o}\right)^{1/5} - 1\right]\right\}^{\frac{1}{3}}\right]^{\frac{1}{2}} ds$$

$$+ \frac{2}{S_T - S_P} [\alpha(S_T - S_P) - \beta^2] \int_{\left(\frac{\sigma}{\sigma_o}\right)_{\bar{C}_P = \frac{4}{7}}}^{\left(\frac{\sigma}{\sigma_o}\right)_T} \left[\frac{a}{\left[\frac{\sigma}{\sigma_o} + b\right]}\right]^{\frac{1}{2}} \sigma_o\, d\left(\frac{\sigma}{\sigma_o}\right) \tag{57}$$

where $S_Z = S\big|_{\bar{C}_P = \frac{4}{7}}$

Upon integration this yields

$$C_{L_u} = \frac{2}{S_T - S_P} [\alpha(S_T - S_P) - \beta^2]\left\{(S_o - S_P) + J + \frac{4}{3} a^{1/2}\left[\left(\frac{\sigma}{\sigma_o}\right)_T + b\right]^{3/4} \sigma_o - \frac{4}{3} a^{1/2}\left[\left(\frac{\sigma}{\sigma_o}\right)_{\bar{C}_P = \frac{4}{7}} + b\right]^{3/4} \sigma_o\right\} \tag{58}$$

where $J = \int_{S_o}^{S_Z} \left[1. - 0.49\left\{Re_{\sigma_o}^{1/5} \left[\left(\frac{\sigma}{\sigma_o}\right)^{1/5} - 1\right]\right\}^{1/3}\right]^{1/2} ds$

Obviously, in order to maximize this function the slack variable must be zero; or interpreted differently, the maximum of the lift occurs on the constraining boundary.

The equation for the lift coefficient can now be expressed as a function of $\left(\frac{\sigma}{\sigma_o}\right)_T$

$$C_{L_u} = \frac{2}{\left[\frac{S_o}{\sigma_o} - 1 + \left(\frac{\sigma}{\sigma_o}\right)_T\right]\sigma_o - S_P} \left\{ \frac{(1 - C_{P_T})^{1/2}\left[\left(\frac{\sigma}{\sigma_o}\right)_T + b\right]^{1/4}}{a^{1/2}} \right\} \left\{ (S_o - S_P) + J + \frac{4}{3}\, a^{1/2}\left[\left(\frac{\sigma}{\sigma_o}\right)_T + b\right]^{3/4} \sigma_o - \frac{4}{3}\, a^{1/2}\left[\left(\frac{\sigma}{\sigma_o}\right)_{\bar{C}_P = \frac{4}{7}} + b\right]^{3/4} \sigma_o \right\} \tag{59}$$

To find the proper value of $\left(\frac{\sigma}{\sigma_o}\right)_T$ solve

$$\frac{\partial C_{L_u}}{\partial\left[\left(\frac{\sigma}{\sigma_o}\right)_T\right]} = 0 \tag{60}$$

A computer program called MAXLFT (see Appendix I) was written to determine the proper solution numerically. Program MAXLFT produces optimum velocity distributions which maximize lift as a function of Reynolds number, trailing edge pressure, and a local Mach number constraint on the maximum velocity. With program MAXLFT an airfoil velocity distribution is defined which has been optimized using a boundary layer theory model and the calculus of variations.

AIRFOIL DESIGN PROCEDURE

With the idealized optimum velocity distributions available as a guide, a practical airfoil design will be carried out in this section. The current state of the art in airfoil design techniques are employed and illustrated here. The actual design under consideration should be suitable for ultralight gliders, axial flow fans and turbines, inboard sections of helicopter blades, high lift flap systems, and very high aspect ratio sailplanes.

Design Mission

In order to design an airfoil section it is necessary to know what performance is desired and in what Reynolds and Mach number regime this performance is needed. Since there seems to be a growing interest in a low speed, inexpensive type of aircraft, the design of an airfoil section suitable for a high performance ultralight glider was chosen as a case study in airfoil design methodology.

To determine the desired Reynolds number regime and lift coefficient range of interest, a survey of existing ultralights was made with one model being picked as an example of a high performance ultralight glider. Volmer Jensen's Swingwing was chosen because of its superior performance. Table 1 gives data as presented in Low and Slow number 17 for Volmer Jensen's estimated performance of the Swingwing.

TABLE 1

SWINGWING DATA

Weight		Wing		Velocity	
Empty	100 lb.	Span	32 ft. 7 in.	Cruise	20 mph
Gross	240 lb.	Area	179 $ft.^2$	Stall	15 mph

In order to determine the Reynolds number and lift coefficient range, the mean chord was determined to be 5.5 ft. from $\bar{c} = \frac{S}{b}$. Using sea level atmospheric conditions the maximum lift coefficient, cruise lift coefficient, minimum Reynolds number, and cruise Reynolds number were determined from Equation 61 and Equation 62.

$$C_L = \frac{2W}{\rho S V^2} \tag{61}$$

$$Re = \frac{V\bar{c}}{\nu} \tag{62}$$

The results are presented in Table 2.

TABLE 2

SWINGWING PERFORMANCE REGIME

	Lift Coefficient	Flight Reynolds Number
Cruise	1.31	1.022×10^6
Stall	2.34	0.767×10^6

As a result of the review of the performance of Volmer Jensen's Swingwing, specific design requirements for an airfoil section which might be applicable to an ultralight glider were chosen. At a Reynolds number of 7×10^5 and at the cruise angle of attack, the following specifications must be met: 1) A low moment coefficient so that a large tail surface will not be required, 2) Little or no tendency for the boundary layer to separate or to form a separation bubble at any point along the surface, 3) Practical thickness so that a structure could be made which would support the loads, 4) Gentle stall characteristics since the airfoil will be operated at high lift values, 5) High lift coefficients so that a low flight velocity is achieved.

Low Moment

In order to insure that a large tail structure is not required, the moment of the airfoil about its quarter chord position should be kept small. The moment coefficient decreases with increasing laminar length (acceleration region) on the lower surface and with decreasing laminar length on the upper surface.[40] Therefore, the type of velocity distribution around the surface of the airfoil is dictated somewhat by the requirement of a small moment coefficient.

Since no high pressures are allowed on the lower surface near the trailing edge (for low moment), large adverse gradients on the lower surface are excluded. This implies that the lower surface should have only laminar (accelerating) flow from the stagnation point to the trailing edge at the design angle of attack. The upper surface must have an adverse pressure gradient with turbulent flow near the trailing edge so that the laminar (accelerating) flow on this surface is not too long.

These requirements, for a low moment coefficient, rule out the possibility of having a high lift airfoil which has no adverse gradient on the upper surface at the design angle of attack (ie., all laminar flow) and a lower surface velocity distribution which has an adverse gradient near the trailing edge. Therefore, the velocity distribution is limited to the type obtained from the MAXLFT program (see previous section and Appendix I).

The optimal maximum lift velocity distributions provided by MAXLFT gives the airfoil designer a goal for which to strive in a practical high lift airfoil design prodecure. So that the variation of the lift coefficient (C_{L_u}) and the flat rooftop length (S_o) with the rooftop velocity ratio (V_o) could be determined the MAXLFT program was run with provisions to calculate a series of maximum lift velocity distributions. Figure 15 shows the results for a Reynolds number of 7×10^5. This indicates that there is a peak in the lift coefficient at a maximum velocity ratio of about 1.9.

<u>No Separation</u>

Table 2 indicates that the Reynolds number range of interest is in the very low flight Reynolds number regime. It is advantageous to investigate the pecularities of this type of flow before proceeding.

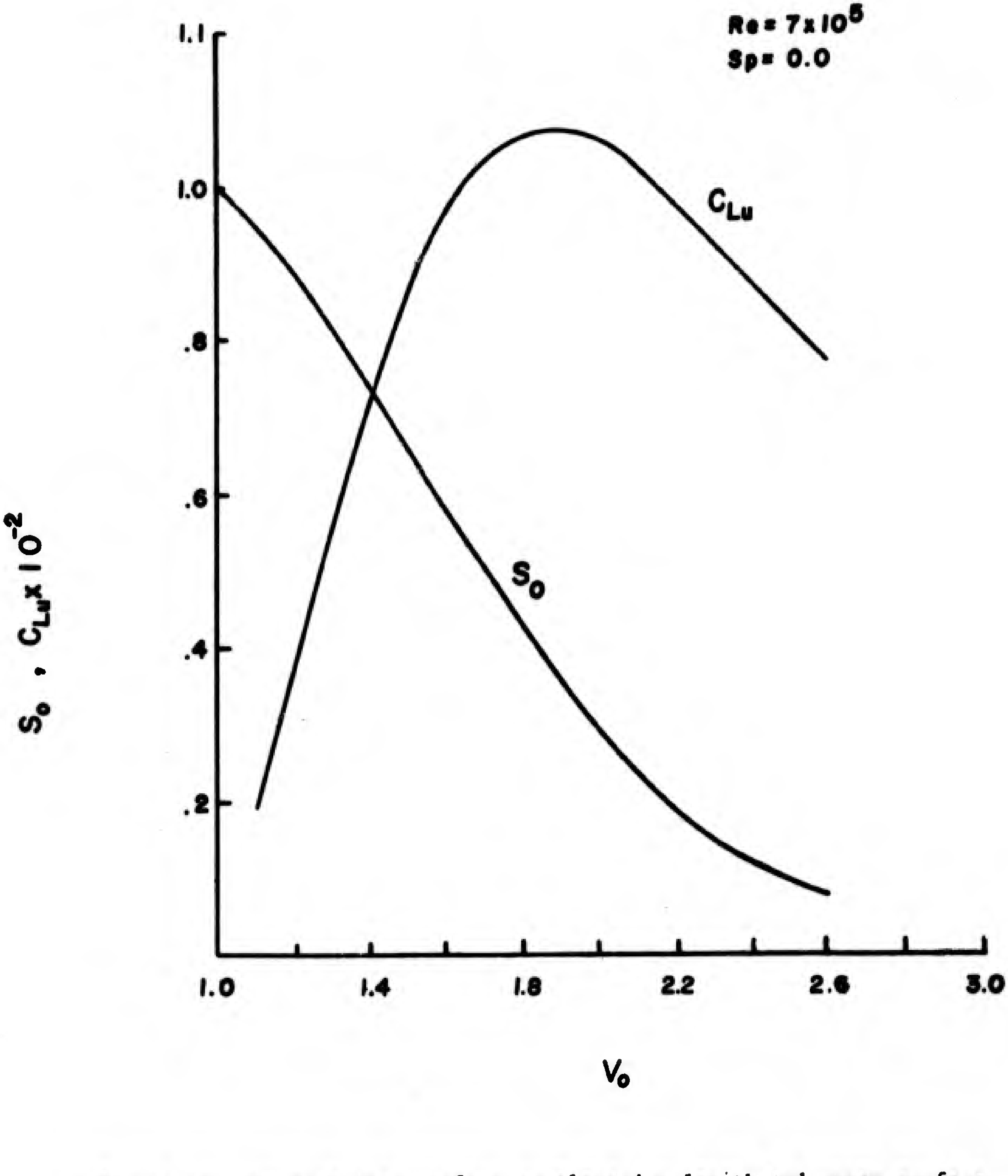

Figure 15. Optimum flat rooftop acceleration length and upper surface lift coefficient as a function of the maximum velocity ratio.

Problem of Low Reynolds Number Airfoils

If the steady state equations of motion of a flow about a body are nondimensionalized properly, the Reynolds number appears. The Reynolds number represents the ratio of inertial forces to viscous forces and is used in the limit to develop boundary layer theory.

When the Reynolds number is large enough, the flow about an airfoil may be divided into two regions: the invisid or potential flow region where the viscosity of the flow may be neglected, and the boundary layer close to the wall where the effect of viscosity, laminar and eddie, is of primary importance.

Generally boundary layers are classified in two types, laminar and turbulent. Laminar boundary layers are characterized by smooth, stratified flows, while the flow in turbulent boundary layers is characterized by the presence of random eddies. The eddies transfer momentum from the outer parts of the boundary layer to portions closer to the surface. This implies that the mean velocity near the surface and therefore the skin friction and energy within the layer is higher for turbulent boundary layers than for laminar boundary layers under similar conditions.

Transition from laminar to turbulent flow is a function of the stability of the laminar boundary layer, and as the Reynolds number is decreased the stability of the laminar flow is increased. Lowering the Reynolds number also reduces the degree of adverse pressure gradient in which the laminar boundary layer will remain attached without separation.

The problem encountered in the design of low Reynolds number airfoils may now be assessed. There is always an adverse pressure gradient on the aft region of airfoils (on the upper, lower, or both surfaces), and for a useful range of lift coefficients this requires the existence of a turbulent boundary layer in this region. Because the laminar boundary layer is more stable at low Reynolds numbers, the promotion and control of transition prior to the steep adverse gradient at the start of the pressure recovery region is a demanding requirement.

Control of Transition

Since the control of transition is so important for maintaining lift and keeping the drag low in the low Reynolds number regime, an instability range must be incorporated into the upper surface velocity distribution before the start of the pressure recovery region. This is to insure a fully developed turbulent boundary layer profile at the start of the pressure recovery region. As the Reynolds number is lowered, the length of the instability range required to insure transition to fully developed turbulence becomes greater since the laminar boundary layer becomes more stable. This implies that the surface length from the stagnation point to the start of the pressure recovery region must be sufficient to insure transition at the design Reynolds number and angle of attack.

Stan Miley[41] has provided, in his dissertation, charts which give the minimum length required for transition in a pressure distribution which incorporates constant velocity region followed by an instability range and verified his results experimentally with measurements on a sailplane. The transition length (S_{TR}) at a Reynolds number of 7×10^5

from Miley's charts can be seen in Figure 16. At a surface length value of about 0.35 the transition length curve crosses the rooftop length curve indicating , that at a value of V_o higher than about 2.1 there is no chance for transition before the start of the pressure recovery region. Therefore there is a transition length constraint upon the value of S_o since it must be greater than or equal to S_{TR}.

In order to be conservative, a design value V_o of 2.0 was chosen with an S_o of about 0.42. This gives about a 14.3% increase over the minimum transition length (S_{TR}) at this value. Miley's charts indicated that the instability range should have a surface length in excess of 13% chord. Again being conservative, a length of about 16% chord was chosen for the instability range.

The Eppler inverse solution program (see Appendix II) was used to generate the airfoil section profile from the prescribed velocity distribution which satisfies the requirements given thus far. The resulting profile and velocity distribution at the design (cruise) angle of attack are shown in Figure 17 and Figure 18 respectively. The section number designation here is one adopted only for reference and is of no particular coded form. For this airfoil, the calculated lift and drag coefficients at the design point of $\alpha = 17°$ and $Re = 7 \times 10^5$ are $C_L = 2.02$ and $C_D = 0.0138$. The design point is actually a cruise condition, and the maximum sectional lift coefficient will be somewhat higher than this. Some final modifications to this design are now carried out to satisfy the remaining mission design requirements.

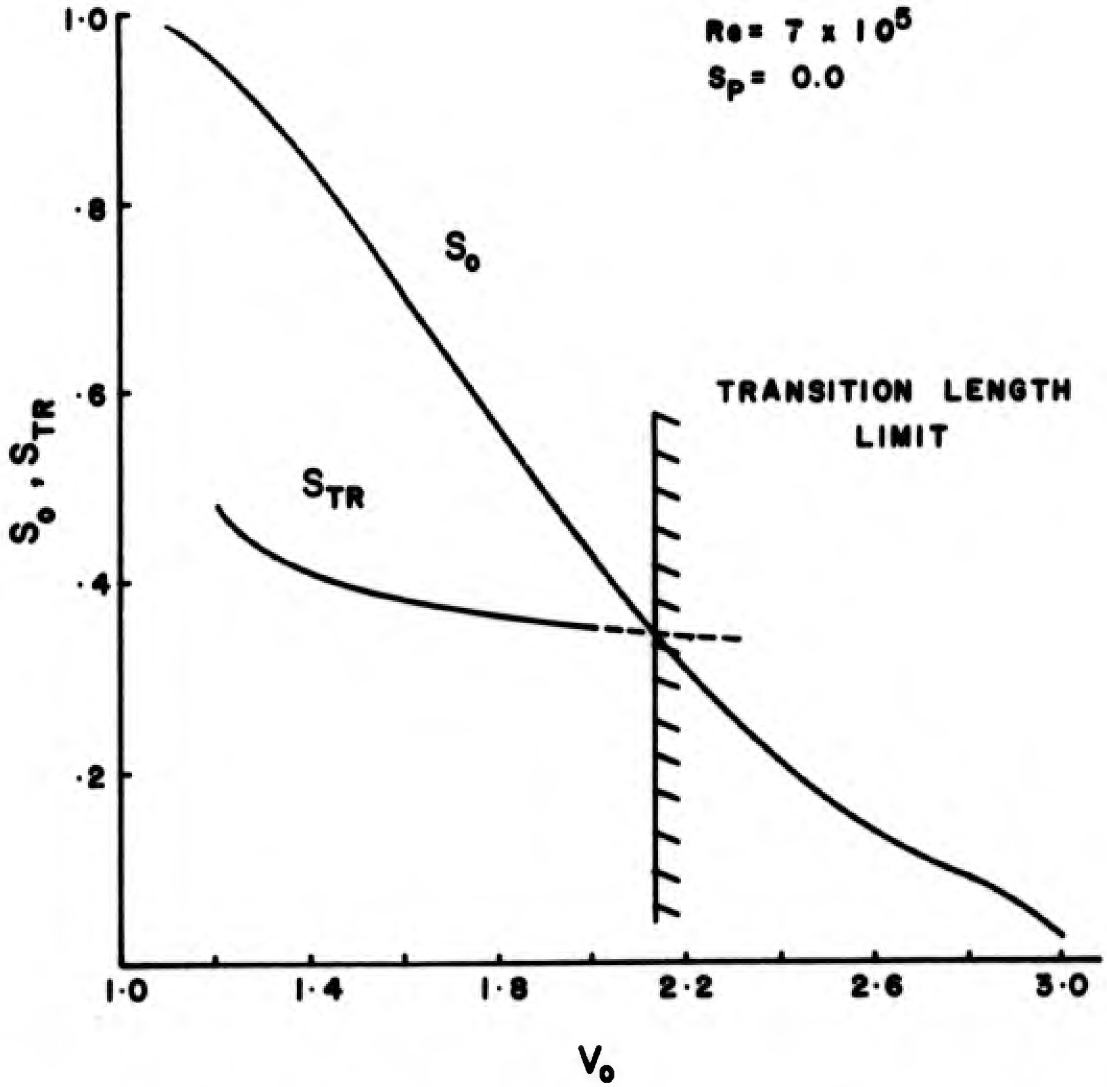

Figure 16. Optimum flat rooftop acceleration length and minimum transition length as a function of the maximum velocity ratio

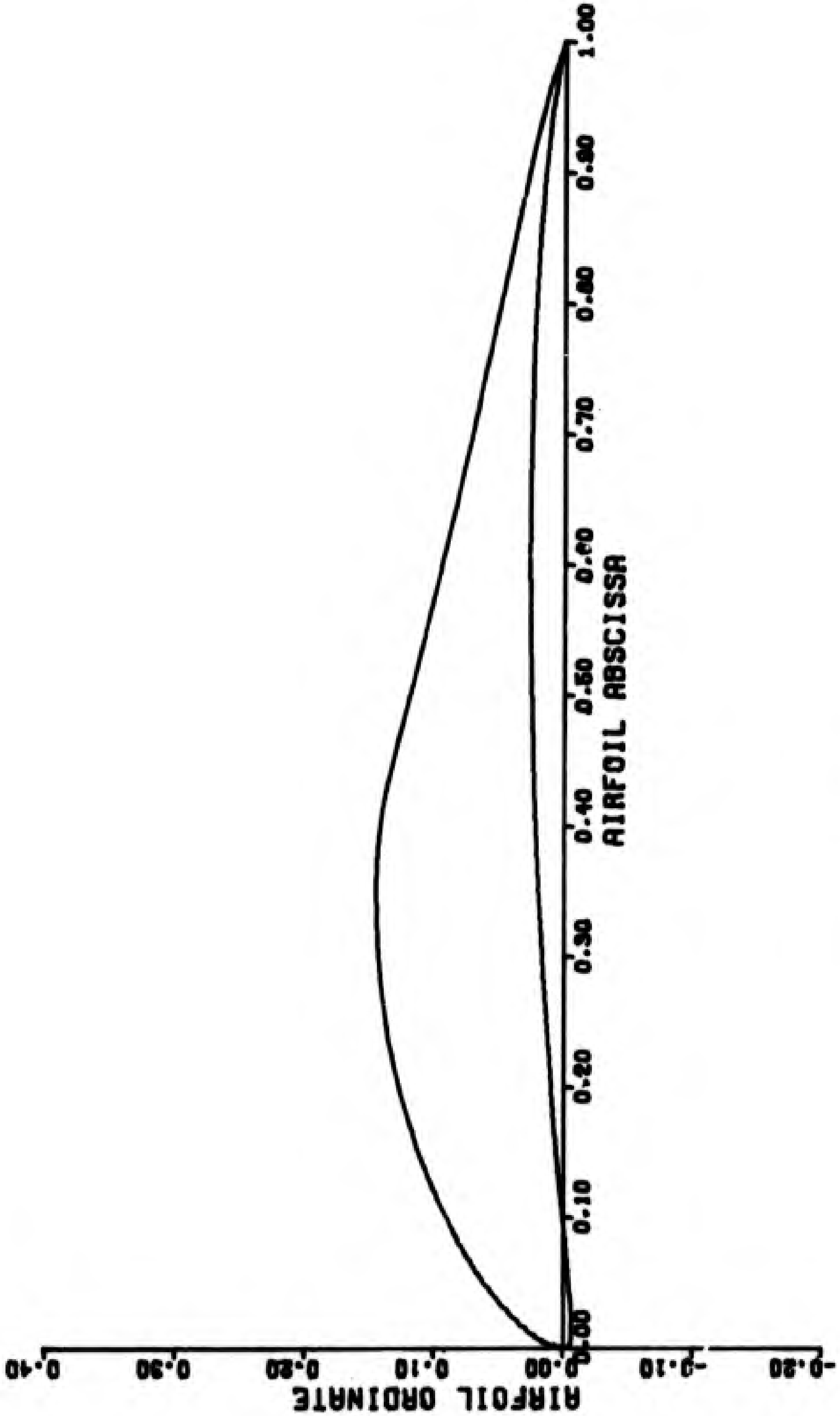

Figure 17. JN-128

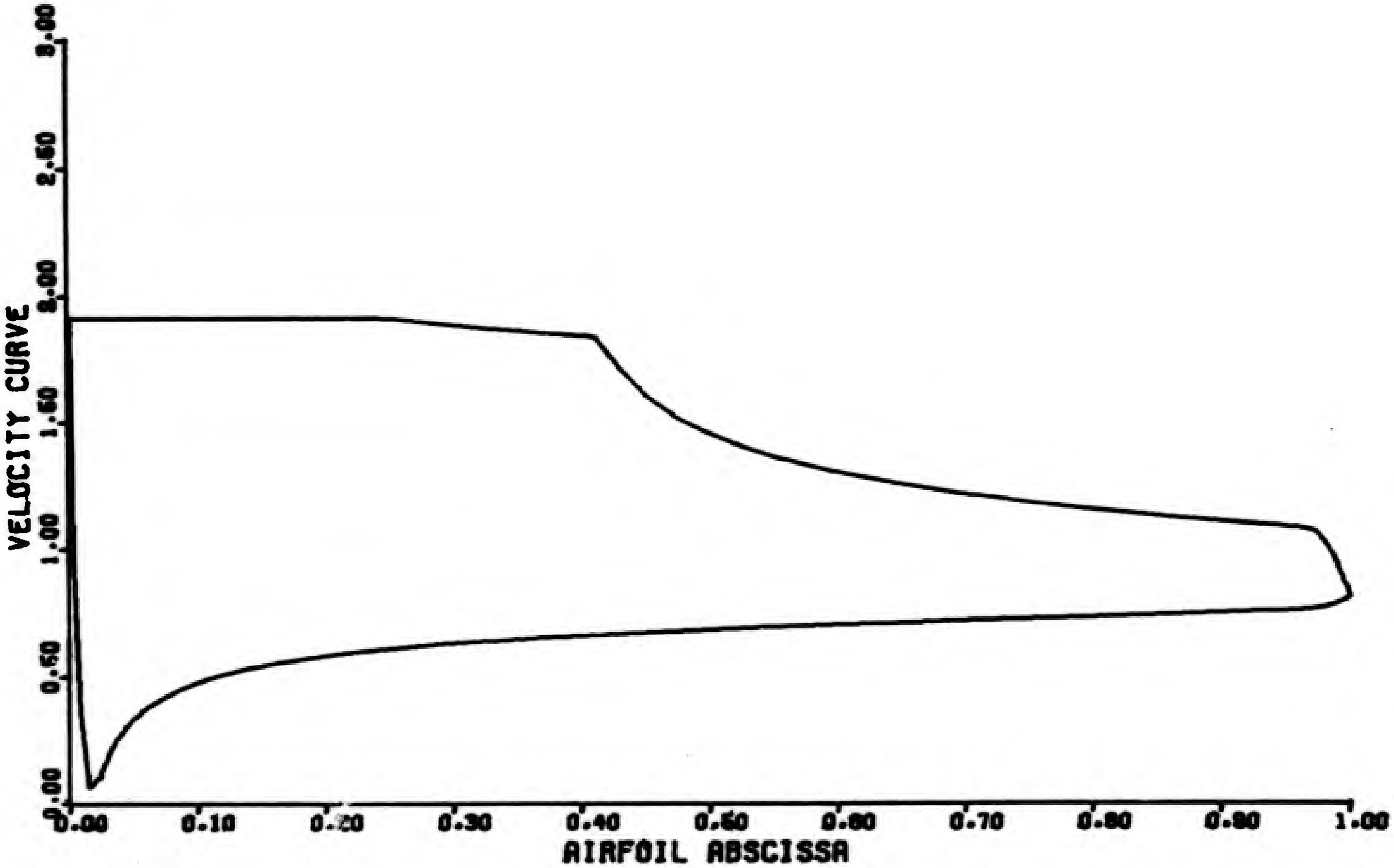

Figure 18. Velocity distribution of JN-128 at an angle of attack of 17°

Practical Thickness

In order to make the airfoil thicker, the input for the lower surface velocity distribution was modified, but still only laminar acceleration gradients were allowed at the design angle of attack. The slight modification resulted in a thicker airfoil and a small increase in the lift coefficient at the design angle of attack of 17° and Reynolds number of 7×10^5. The resulting airfoil is shown in Figure 19 and its velocity distribution at the design angle of attack in Figure 20. For the design condition the lift coefficient and drag coefficient are 2.04 and 0.0142 respectively.

Gentle Stall

Since this airfoil will be flown in the high lift range of angles of attack and since a sudden catastrophic stall is undesirable for low altitude flying, the airfoil section should be designed so that the leading edge laminar separation bubble stall does not occur. In order to insure that the leading edge stall does not occur, the optimum velocity distribution must be further modified on the upper surface near the nose so that velocity peaks do not occur there at angles of attack near the design angle of attack.

This is accomplished by modifying the velocity distribution on the upper surface in the first eight percent chord. The velocity at the design angle of attack was lowered in this region (Figure 22). It can be seen that the airfoil then became thicker near the nose by examining the resulting airfoil shown in Figure 21. The velocity distribution at

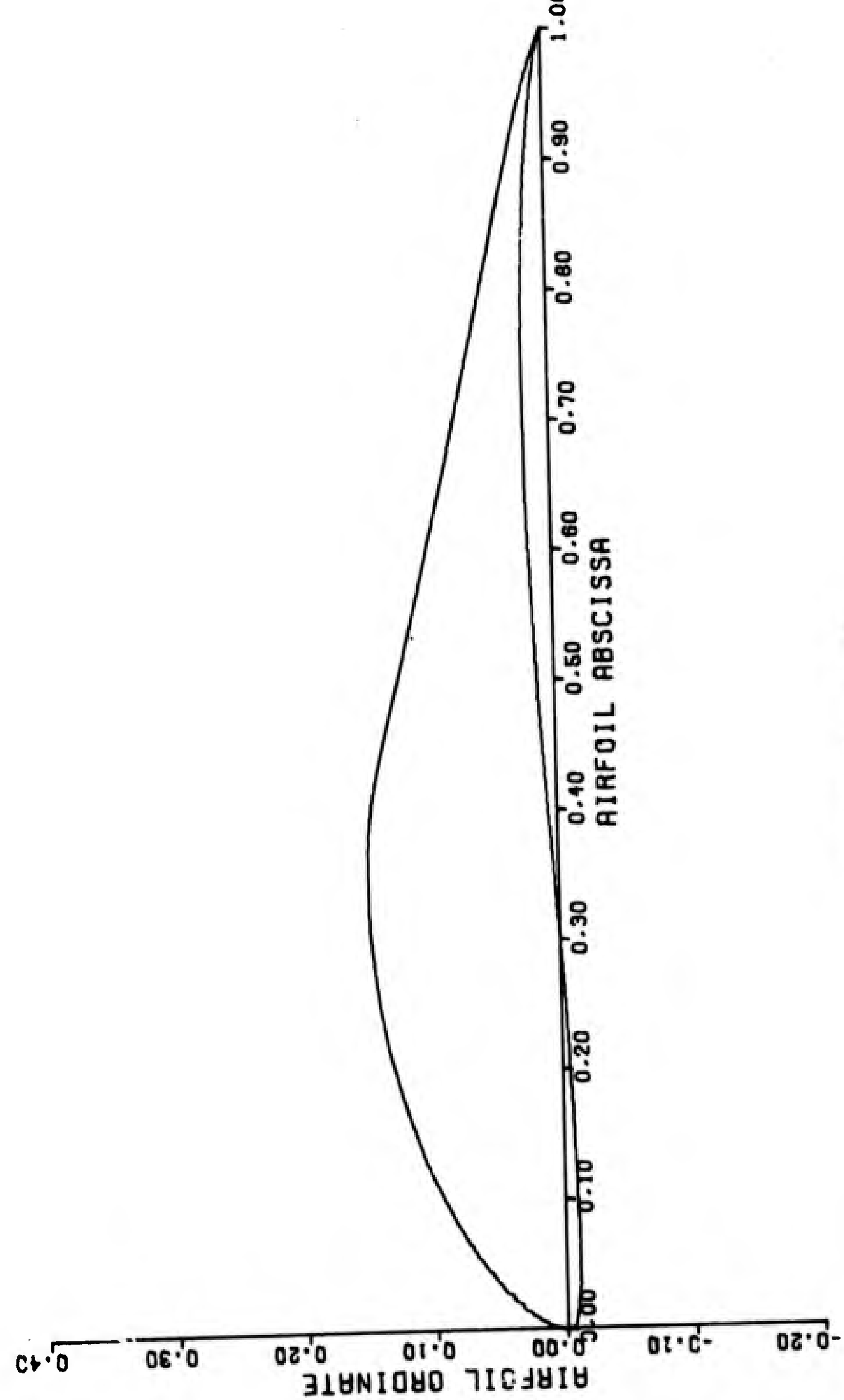

Figure 19. JN-131

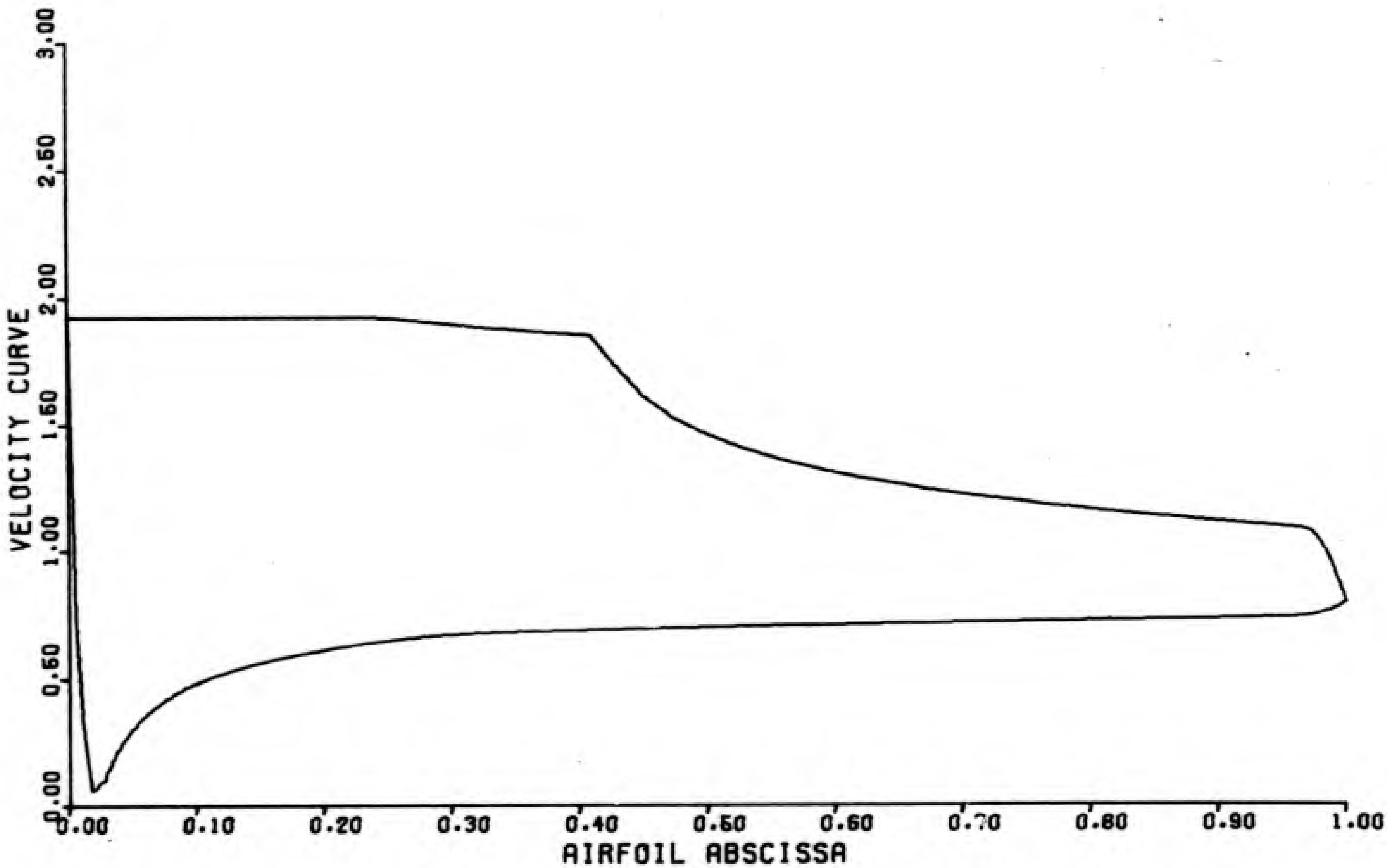

Figure 20. Velocity distribution of JN-131 at an angle of attack of 17°

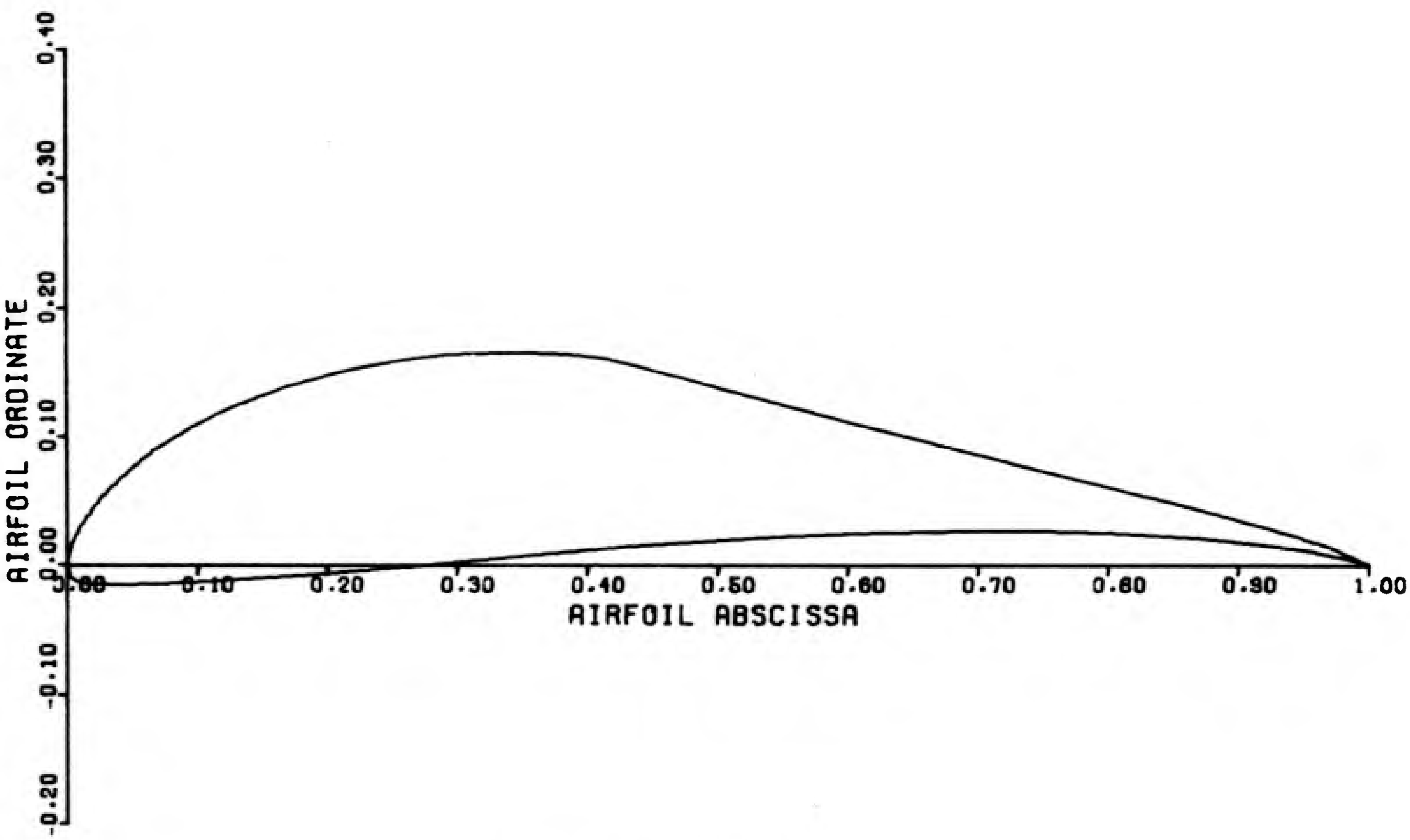

Figure 21. JN-133

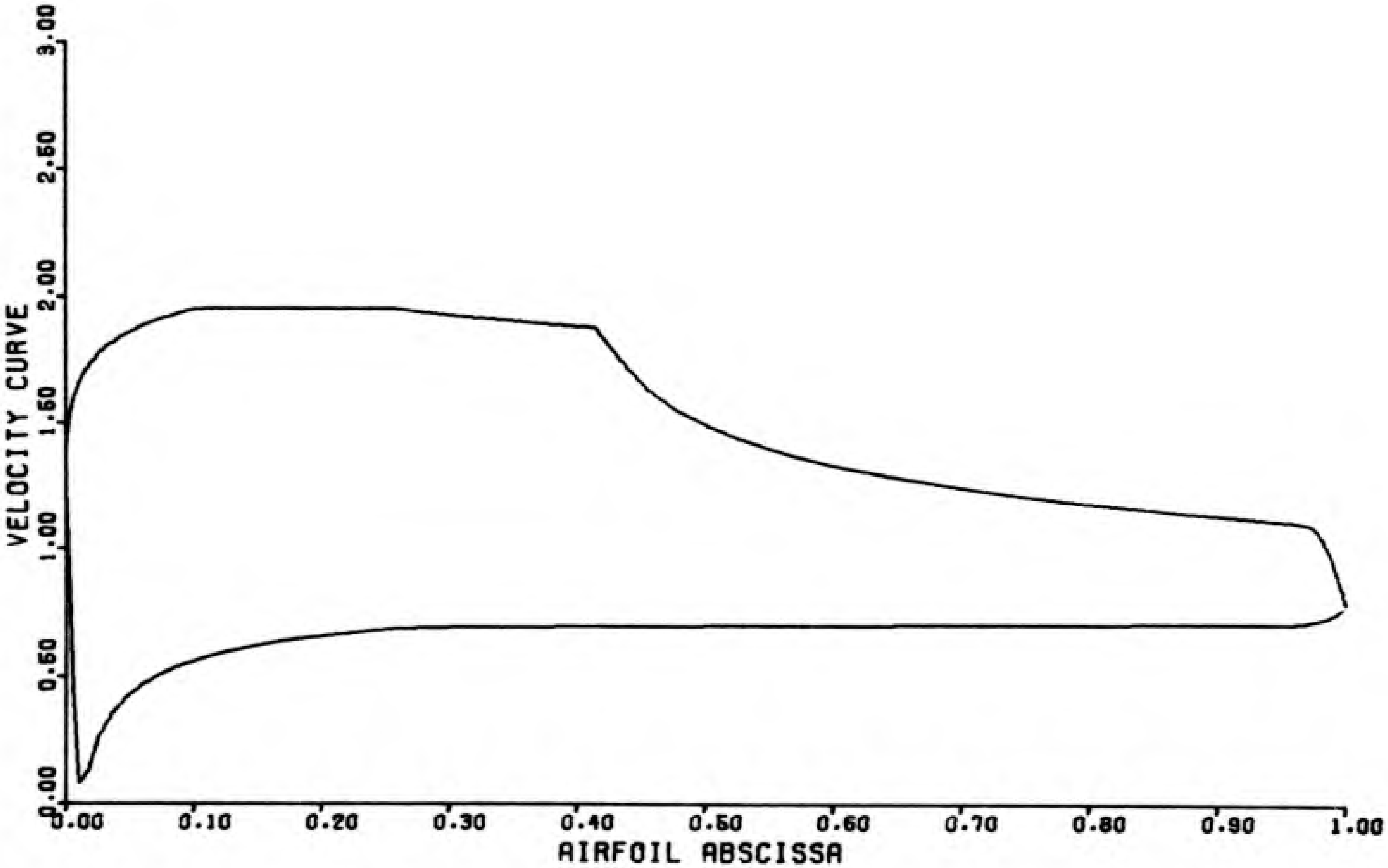

Figure 22. Velocity distribution of JN-133 at an angle of attack of 17°

the design angle of attack of 17° and Reynolds number of 7×10^5 is shown in Figure 22, and the lift coefficient is 2.08 while the drag coefficient is 0.0137.

High Lift

So that the shape of the trailing edge could be improved and transition to fully developed turbulent flow in the instability range could be insured, one final modification (1.-ω in Fig. 37) was made to produce an optimal airfoil which satisfied all of the design mission requirements. The resulting profile and velocity distribution at the design angle of attack of 17° are shown in Figure 23 and Figure 24 respectively, while the computed profile coordinates are presented in Table 3. For this airfoil, the calculated lift and drag coefficients at the design point of $\alpha = 17°$ and $Re = 7 \times 10^5$ are $C_L = 2.09$ and $C_D = 0.0149$.

Summary

The object of this section was to develop an airfoil employing as a guide the optimal velocity distributions produced by MAXLFT. Since the design Reynolds number was small, the optimum velocity distribution had to be modified to insure transition before the start of the pressure recovery region at the design angle of attack. The JN-153 airfoil was designed to produce high lift at a low Reynolds number and represents what is thought to be a near optimal airfoil. Of course the results can only be as good as the model used for the boundary layer.

Figure 28 shows the location of transition and separation on the upper and lower surfaces as a function of angle of attack at a Reynolds

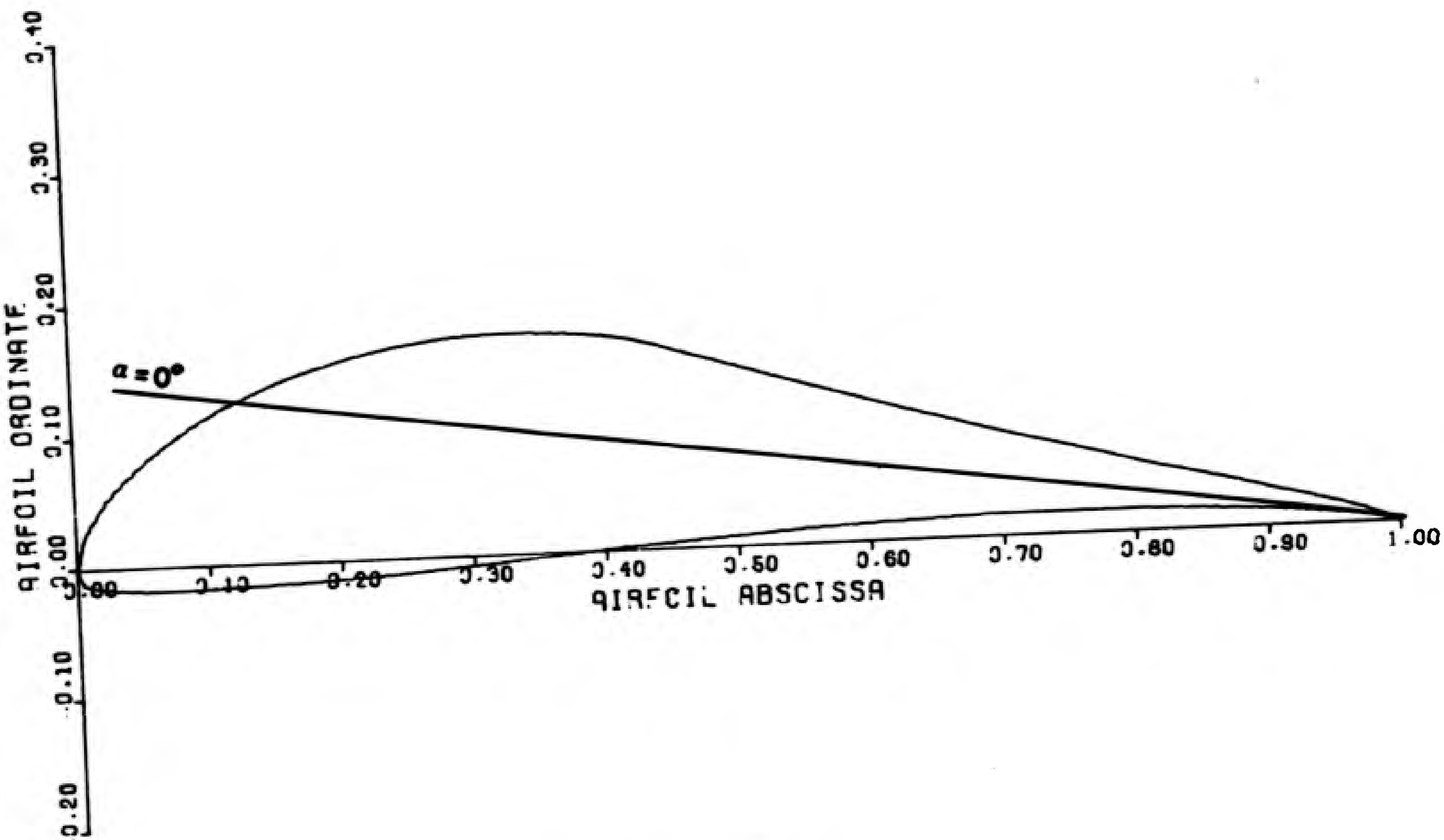

Figure 23. JN-153

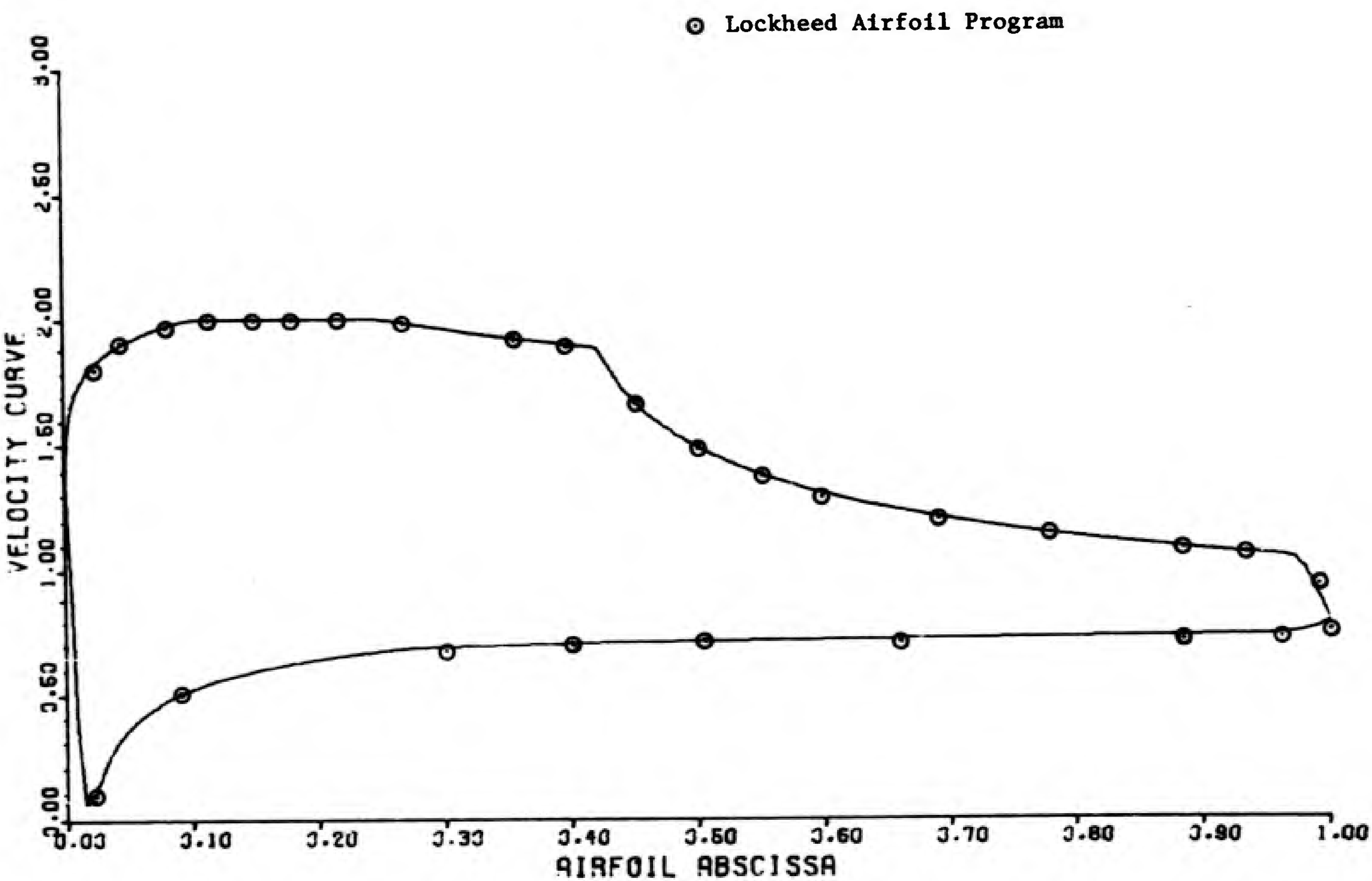

Figure 24. Velocity distribution of JN-153 at an angle of attack of 17°

TABLE 3

COMPUTED COORDINATES OF THE JN-153

X	Y	X	Y	X	Y
100.000	0.000	28.213	16.701	13.792	-1.695
99.910	.029	26.333	16.487	15.819	-1.607
99.650	.123	24.497	16.208	17.951	-1.504
99.241	.284	22.700	15.864	20.181	-1.386
98.702	.503	20.946	15.464	22.501	-1.252
98.043	.762	19.238	15.011	24.903	-1.103
97.265	1.042	17.582	14.511	27.379	-.932
96.354	1.332	15.982	13.968	29.929	-.732
95.301	1.637	14.442	13.385	32.561	-.512
94.107	1.963	12.968	12.764	35.268	-.282
92.776	2.313	11.563	12.111	38.039	-.049
91.314	2.687	10.233	11.426	40.866	.181
89.724	3.088	8.980	10.709	43.736	.405
88.014	3.514	7.803	9.962	46.641	.620
86.188	3.968	6.701	9.192	49.569	.822
84.254	4.449	5.676	8.404	52.509	1.008
82.218	4.957	4.731	7.604	55.451	1.178
80.090	5.493	3.867	6.796	58.384	1.328
77.878	6.056	3.087	5.988	61.296	1.457
75.589	6.645	2.392	5.182	64.176	1.565
73.235	7.260	1.783	4.386	67.014	1.650
70.825	7.900	1.262	3.604	69.800	1.711
68.371	8.563	.830	2.843	72.521	1.749
65.881	9.247	.488	2.109	75.169	1.762
63.370	9.949	.235	1.410	77.731	1.753
60.848	10.668	.074	.753	80.200	1.720
58.330	11.398	.003	.149	82.563	1.666
55.827	12.136	.025	-.391	84.813	1.590
53.355	12.877	.141	-.848	86.940	1.495
50.928	13.611	.371	-1.175	88.934	1.383
48.564	14.331	.778	-1.389	90.788	1.255
46.218	15.020	1.388	-1.551	92.493	1.114
44.103	15.663	2.172	-1.674	94.041	.962
42.055	16.194	3.119	-1.765	95.426	.804
40.064	16.543	4.223	-1.825	96.639	.641
38.057	16.765	5.477	-1.858	97.672	.477
36.052	16.899	6.876	-1.867	98.515	.324
34.057	16.953	8.412	-1.853	99.168	.192
32.081	16.935	10.082	-1.819	99.632	.089
30.131	16.850	11.877	-1.766	99.908	.023
				100.000	-.000

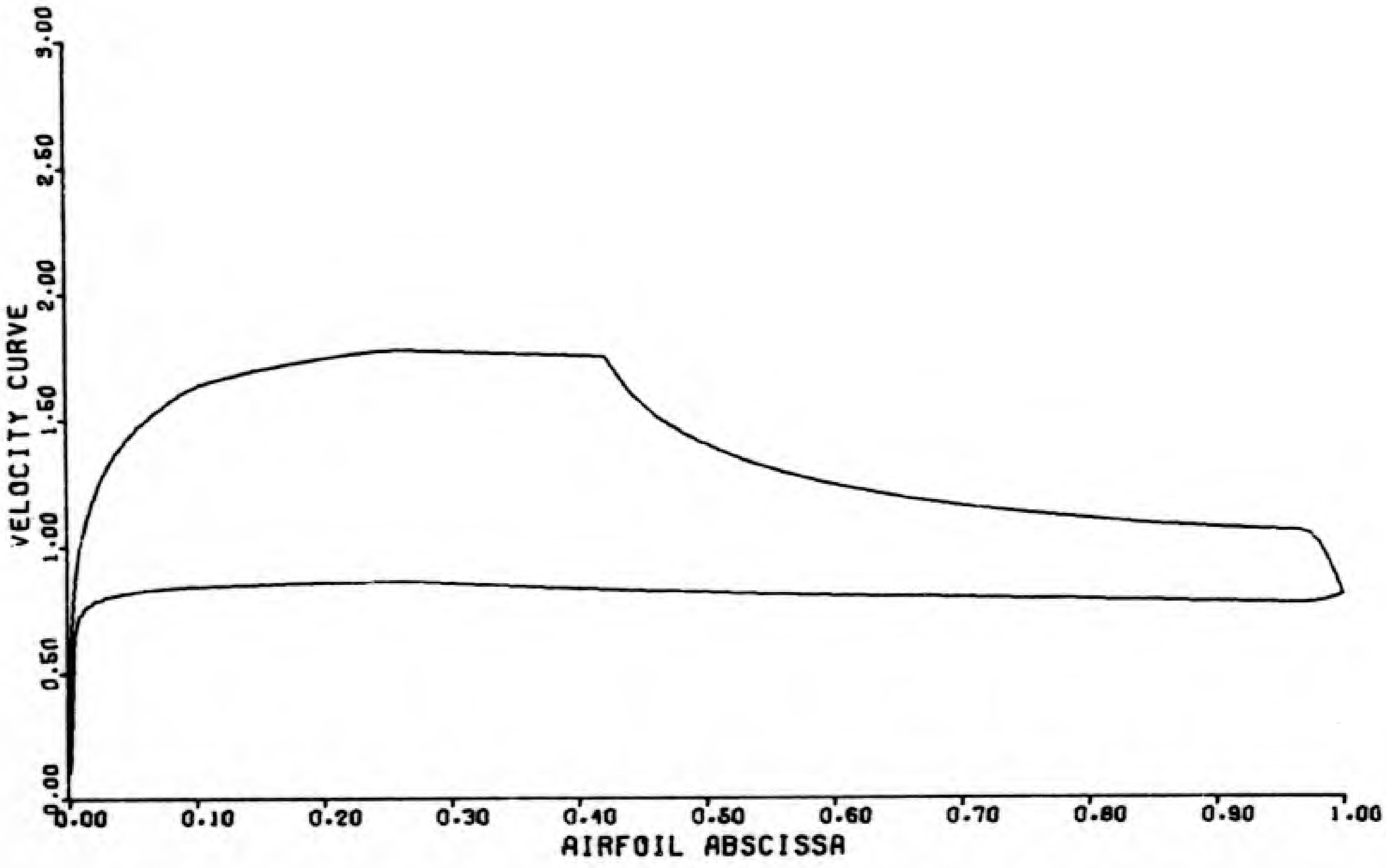

Figure 25. Velocity distribution of JN-153 at an angle of attack of 11°

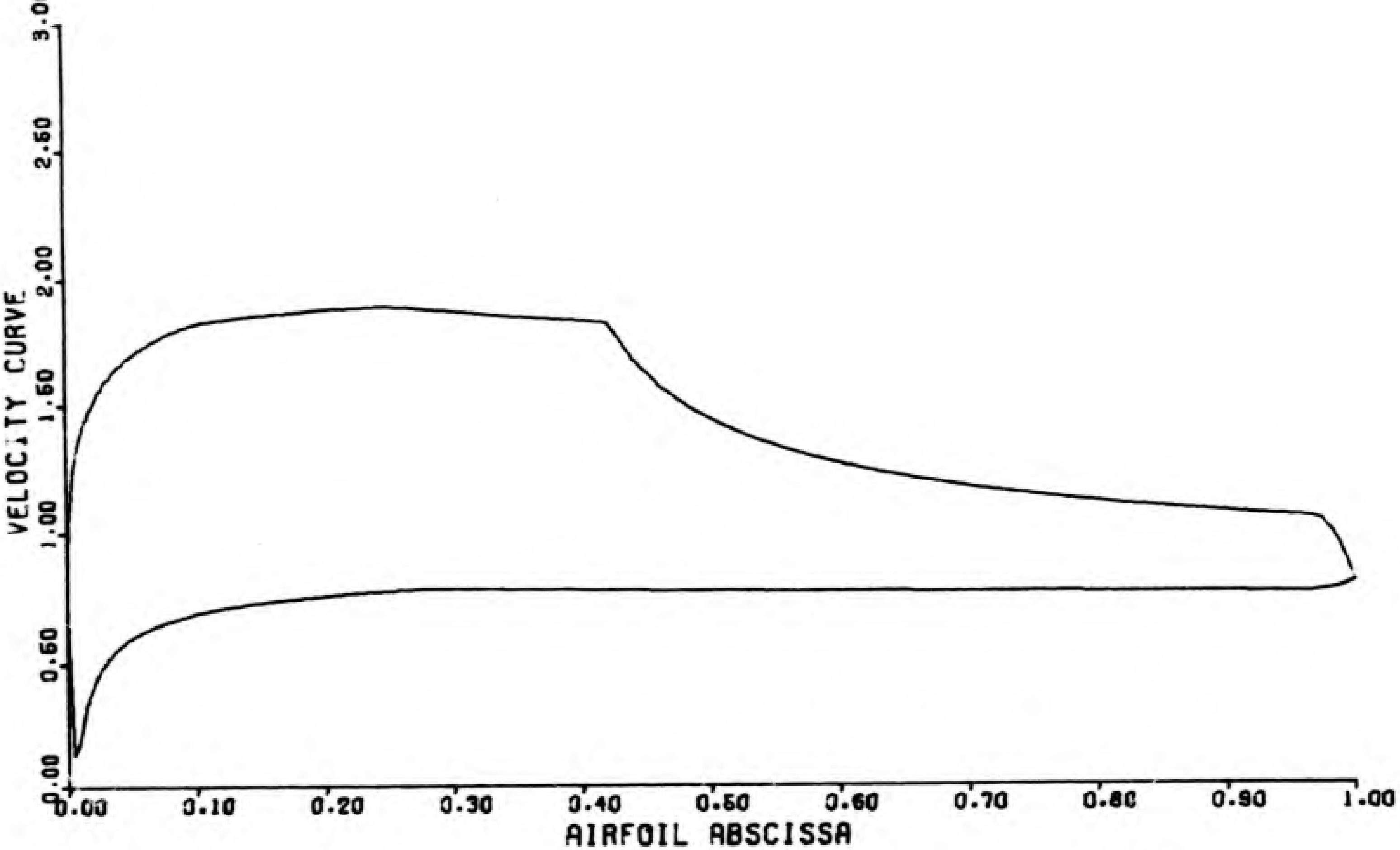

Figure 26. Velocity distribution of JN-153 at an angle of attack of 14°

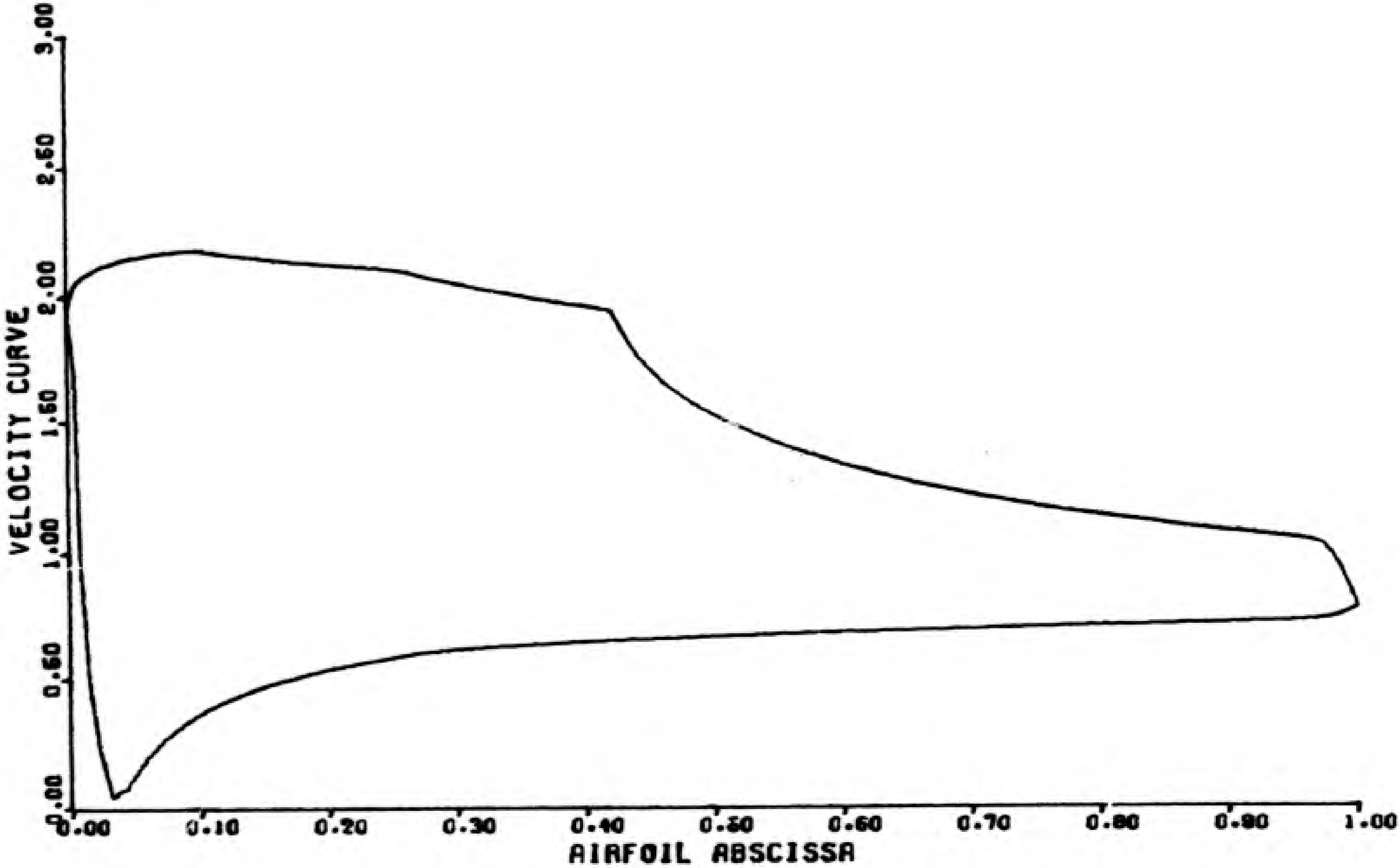

Figure 27. Velocity distribution of JN-153 at an angle of attack of 20°

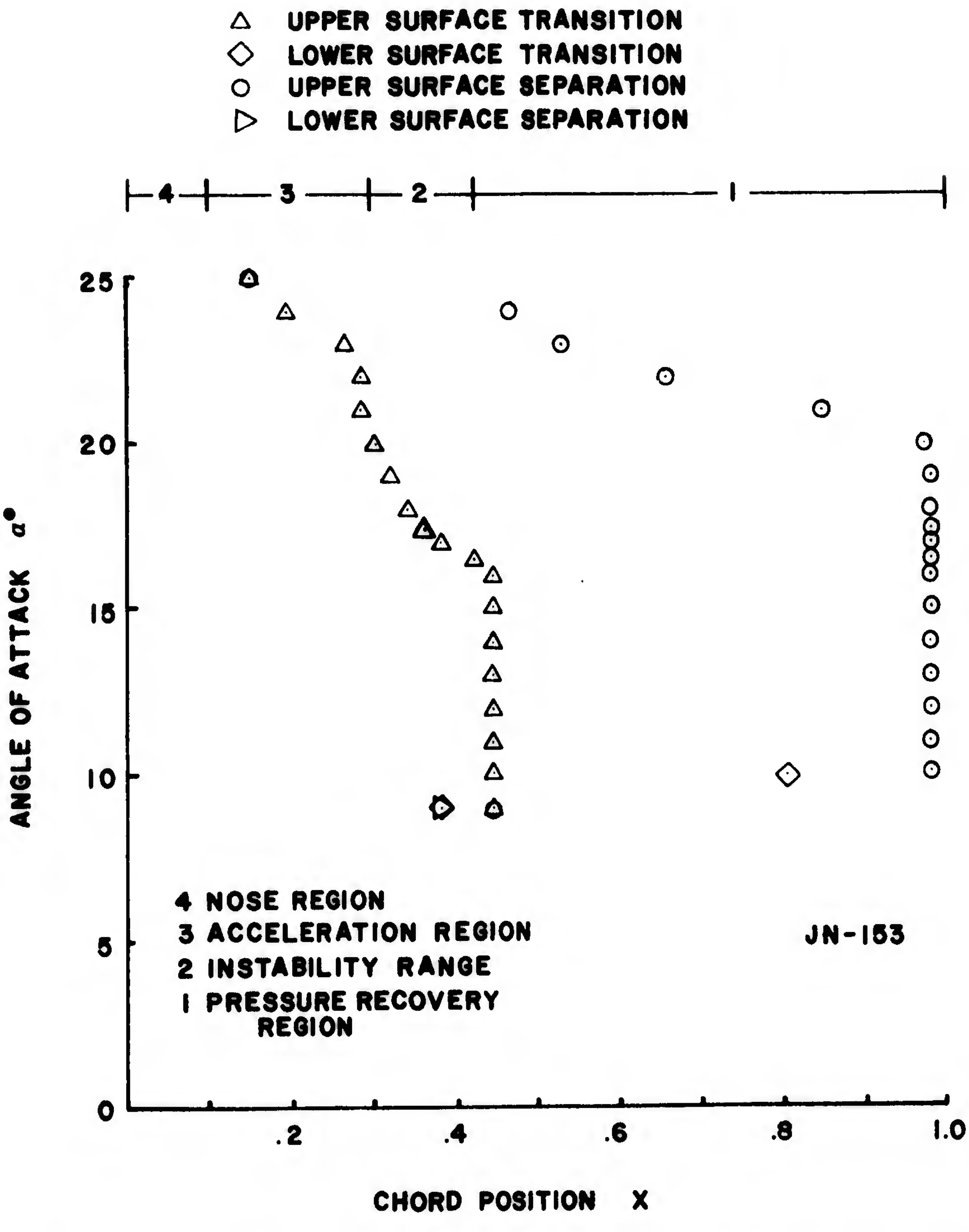

Figure 28. Transition and separation position on the upper and lower surface as a function of angle of attack at a Reynolds number of 7×10^5 for the JN-153

number of 7×10^5. It can be seen that transition takes place in the instability range at angles of attack between 17° and 23°. At angles of attack lower than 17° transition takes place in the pressure recovery region indicating the possibility of a laminar separation bubble (Note that if an ultralight glider was designed around this airfoil a Reynolds number of 7×10^5 would occur at $\alpha = 17°$ and at lower angles of attack the Reynolds number would be higher since the velocity would be higher, and the transition point would move forward into the instability range.) and below 10° laminar separation occurs on both the upper and lower surfaces. At angles of attack above 24° the airfoil is probably stalled since the separation on the upper surface covers over 50% of the chord length. Figure 28 shows that the stall is not a leading edge stall since the separation point moves forward from the trailing edge as the angle of attack increases.

Figures 29, 30, 31, and 32 show the estimated theoretical aerodynamic characteristics of the JN-153. As an indication of the performance capability of the JN-153, the sink speed parameter (to be maximized for minimum sink speed) of several current high lift airfoils is shown in Figure 33. The preliminary wind tunnel studies outlined in the next section indicate that the JN-153 estimated performance is somewhat optimistic. The actual characteristics will most likely fall somewhat below the experimentally established performance of the FX72-MS-150A. At its design Reynolds number of 7×10^5 the JN-153 should be competitive, however, with the FX63-137 which was designed for a manpowered aircraft.

With the use of lifting line theory, the two-dimensional section

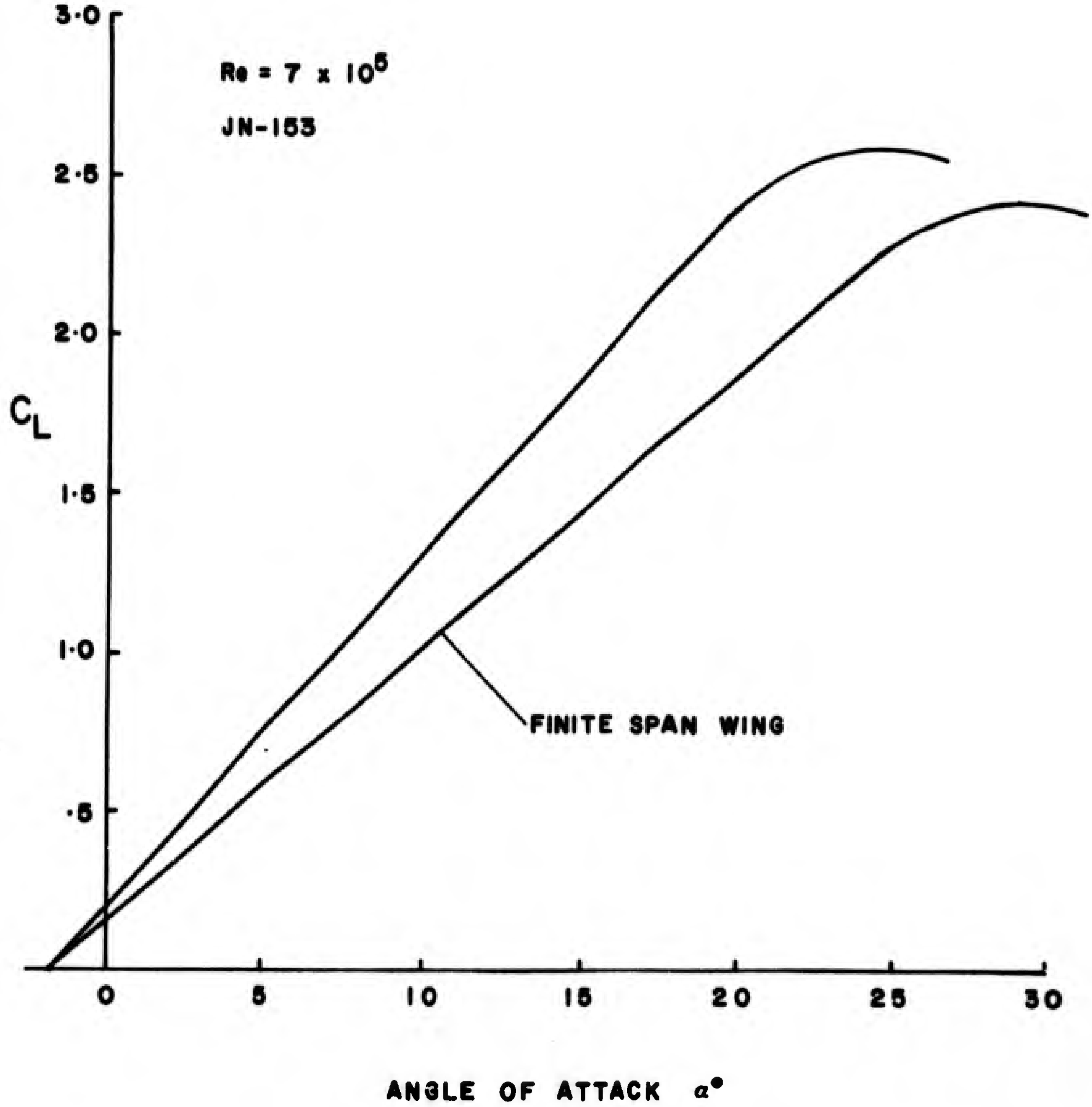

Figure 29. Theoretical lift coefficient as a function of angle of attack for the JN-153 at a Reynolds number of 7×10^5 (estimated stall region)

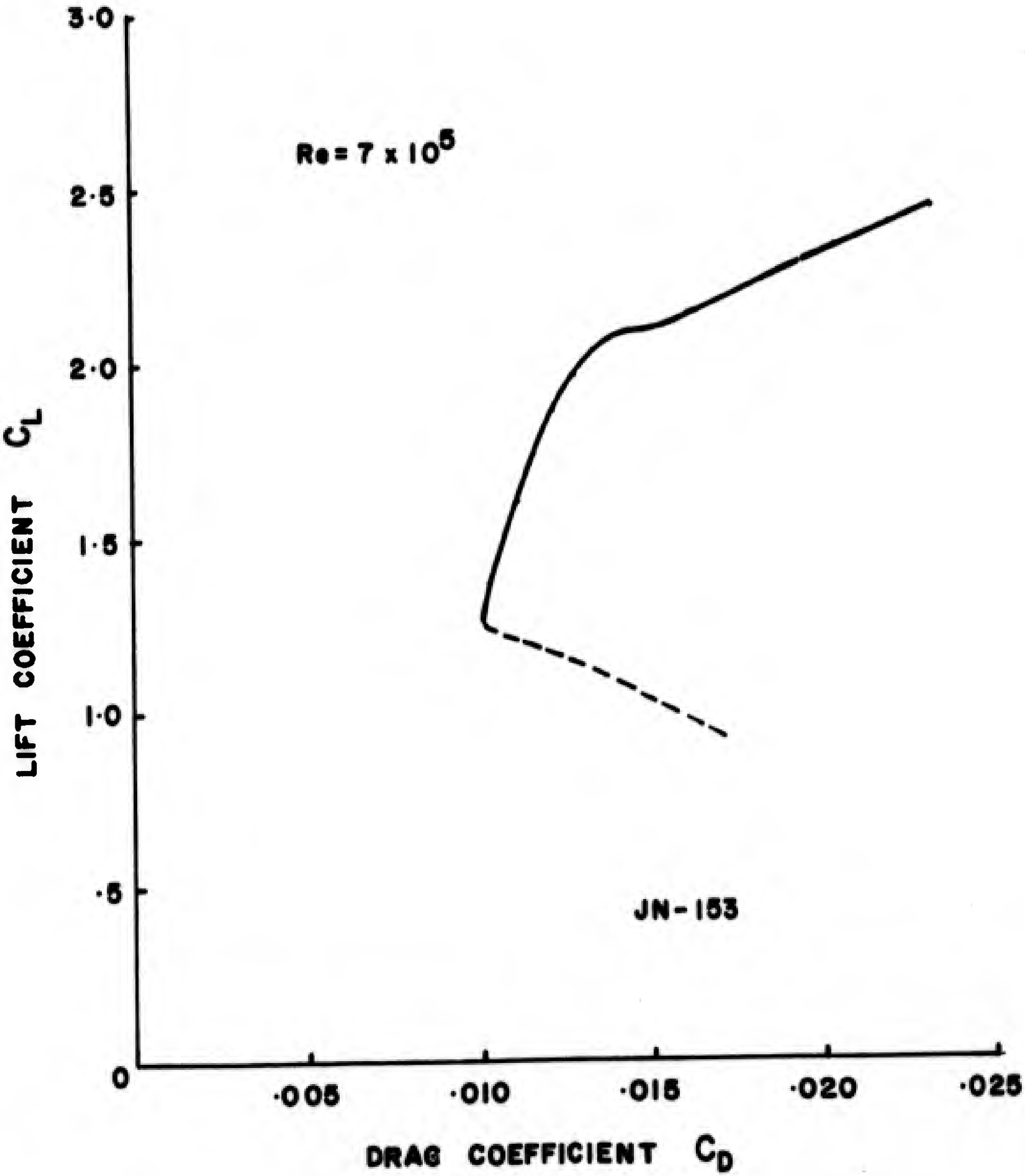

Figure 30. Theoretical lift-drag curve for the JN-153 at a Reynolds number of 7×10^5

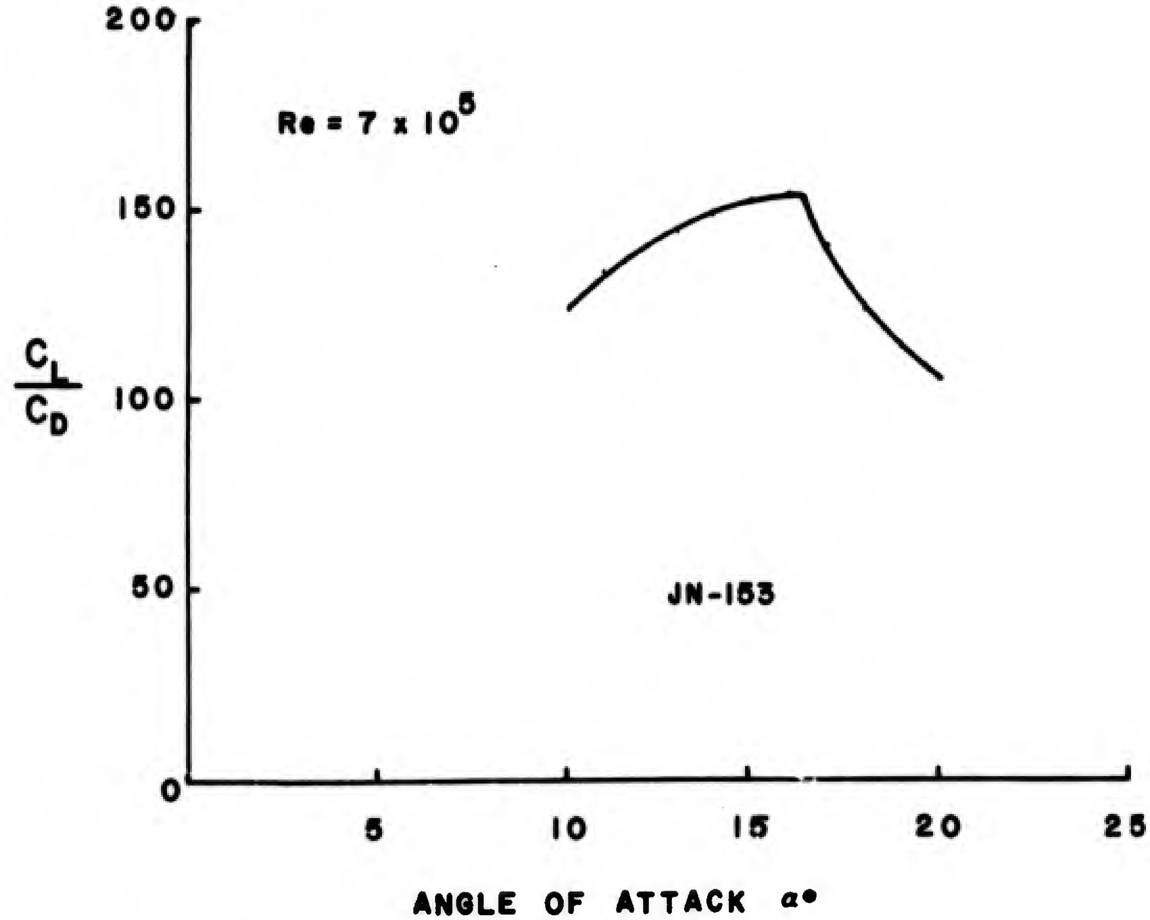

Figure 31. Theoretical lift-drag ratio as a function of angle of attack for the JN-153 at a Reynolds number of 7×10^5

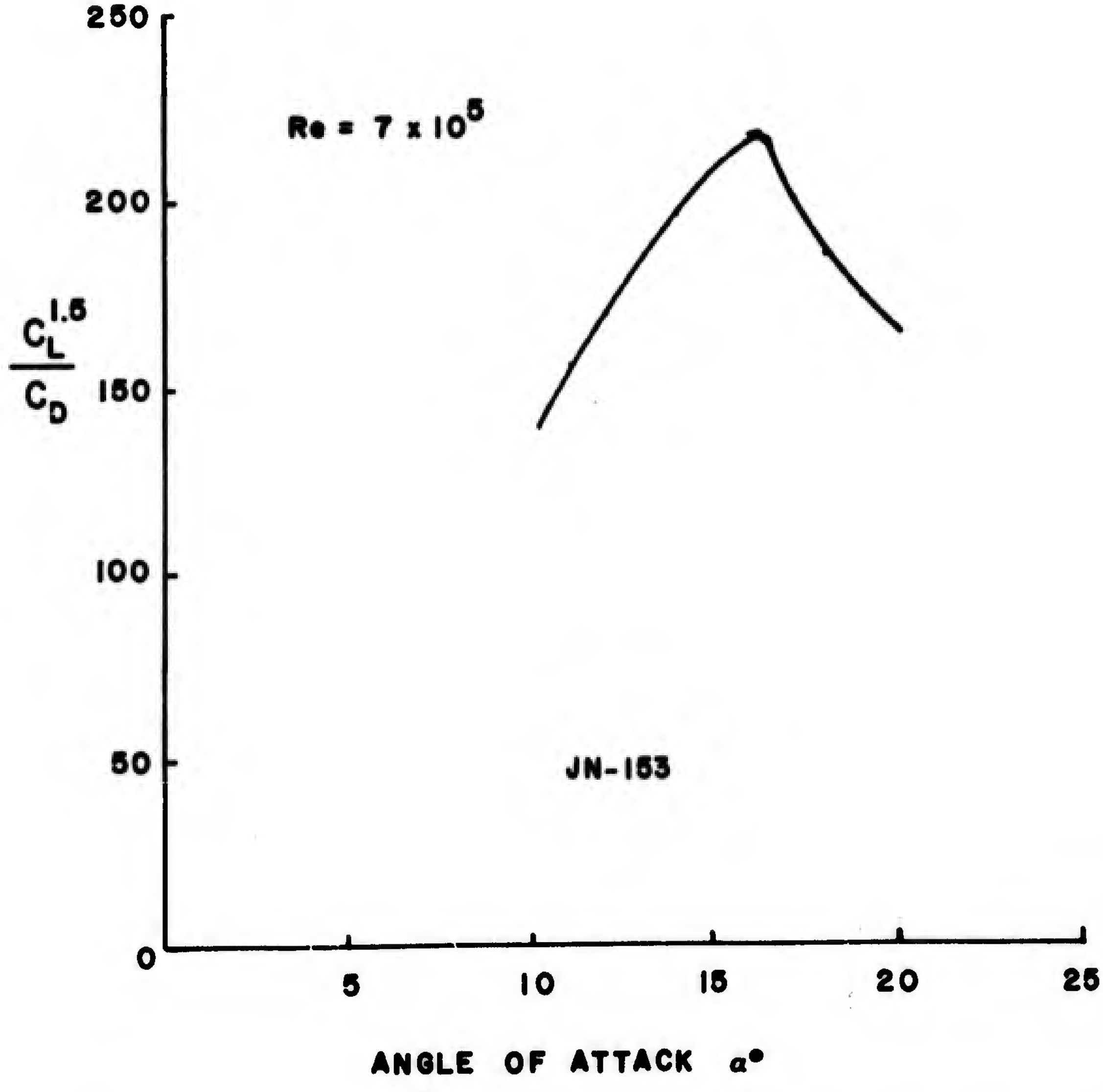

Figure 32. Theoretical sink speed parameter of the JN-153 as a function of angle of attack at a Reynolds number of 7×10^5

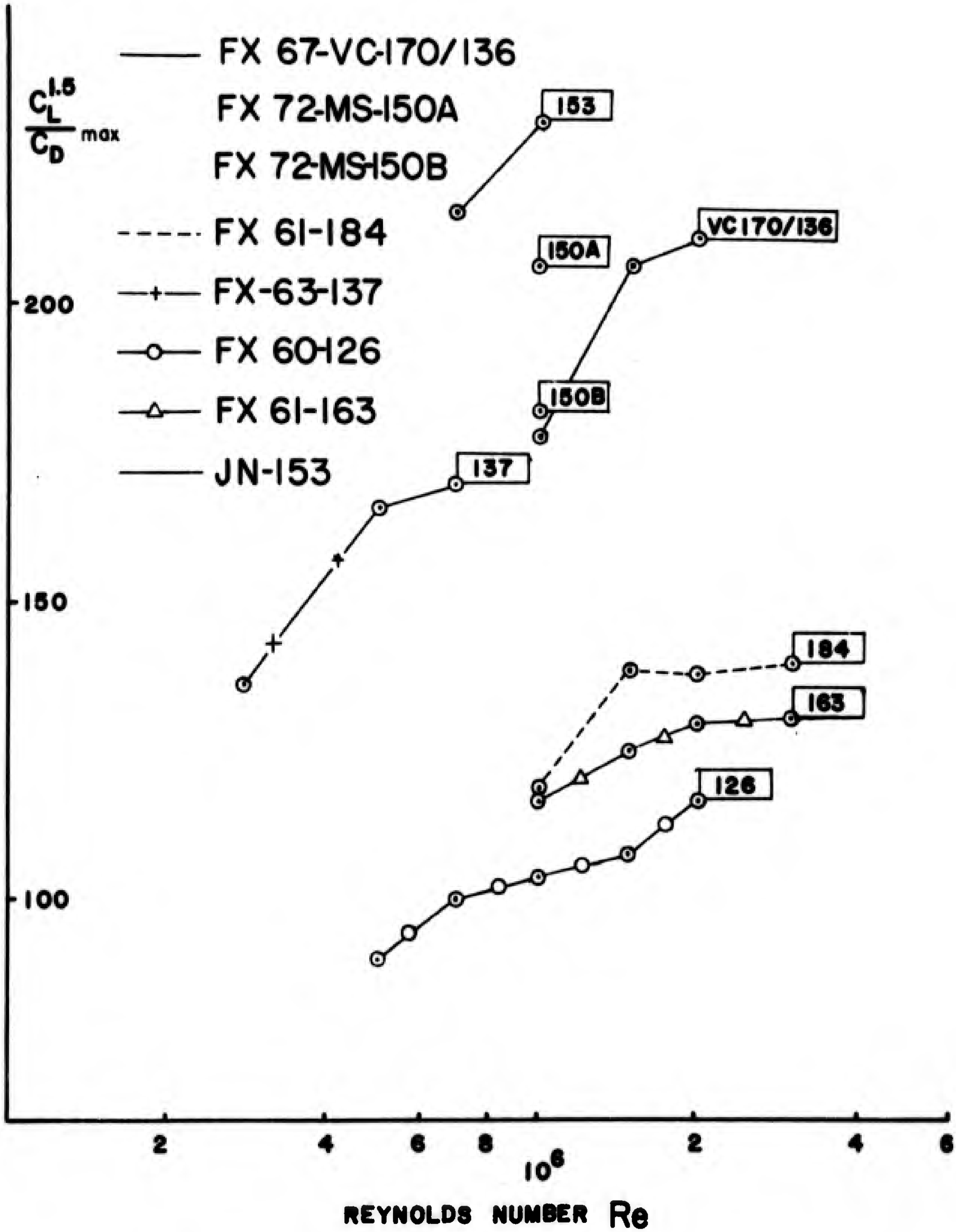

Figure 33. Maximum sink speed parameter for several airfoils as a function of Reynolds number

data was applied to a wing geometry like Volmer Jensen's Swingwing. The results (see Figure 29) for the finite span wing gave a maximum lift coefficient of 2.43 and a cruise lift coefficient of 1.505. In comparison to the Swingwing performance data in Table 2, this represents a 3.84% increase in the maximum lift coefficient and a 14.9% increase in the cruise lift coefficient for an aircraft like the Swingwing with a JN-153 airfoil.

VERIFICATION OF THE COMPUTER PROGRAM

In order to check the present program development, an independent verification of the performance of the JN-153 given by the Eppler inverse program was carried out. The Lockheed Airfoil computer code, as described in NASA CR-1843, solves the direct airfoil problem and requires that the coordinates, Mach number, Reynolds number, and angle of attack be used as input. Its solution gives the velocity distribution, boundary layer development, lift coefficient, and drag coefficient as an output. The airfoil coordinates given by the Eppler program for the JN-153 and the designed flight conditions were used as input to the Lockheed Airfoil Program. The Lockheed program gave a lift coefficeent of 2.09, which is the same result that the Eppler program gave, and a drag coefficient of 0.0129, which is 13.4% lower than that given by the Eppler program. A comparison of the velocity distributions of the two programs is given in Figure 24 showing that the same basic potential flow velocity distribution was calculated in both methods. This was considered to be a sufficient check on the present program development.

CONCLUSIONS

The present study demonstrates that a variational problem in optimal incompressible airfoil design can be defined and solved to produce the coordinates of an airfoil which could be considered optimal for its specified mission. This was accomplished by using calculus of variations techniques to determine the velocity distribution which would maximize the lift coefficient on a monoelement airfoil section and by using Eppler's inverse program to calculate the airfoil section coordinates from the optimal velocity distributions with some parametric adjust ments so that a practical and realistic airfoil would result. The specific mission for which the airfoil was designed is a high performance ultra-light glider that requires high lift coefficients as low Reynolds numbers. It should be noted that the performance data given for the JN-153 is theoretical and should be substantiated by experimental wind tunnel tests.

In order to check the present program development, an independent verification of the performance of the JN-153 given by the Eppler inverse program was carried out. The Lockheed airfoil computer code, as desiribed in NASA CR-1853, was employed for this purpose. Basically it took the coordinates from the output of the Eppler program and by solving the direct airfoil problem attempted to recover the lift coefficient, drag coefficient, and input design velocity distribution. The results checked quite well and were considered to be a sufficient verification of the correctness of the airfoil design computer code used within this study.

As was stressed in the body of this part, the optimization can only be as accurate as the model used in the boundary layer calculations. An example of the inaccuracy of the model used in the preceding analysis is that the second order effect of wall curvature upon the boundary layer has been neglected. In order to find a true optimum solution, the problem should be defined by using an incompressible fluid model which would adequately describe the phenomena of separation, laminar and turbulent flow, and account for all other significant viscous effects. The magnitude of this problem shows that the area of aerodynamic optimization is still in its infancy and that many advances are yet to come.

PART II

WIND TUNNEL STUDIES ON AN AIRFOIL DESIGNED FOR MAXIMUM LIFT AT LOW REYNOLDS NUMBER

INTRODUCTION

The JN-153 airfoil design that evolved from the Part I study and illustrated in Figure 34 was the basis for the present program undertaken in The University of Texas low speed wind tunnel. This program had two major goals. Firstly, comparisons were made between theoretical pressure coefficient data and measured pressure coefficient data, and between the overall lift and drag performance and the predicted performance. Secondly, a series of experiments was performed using externally radiated sound on the JN-153 section to determine the effects of flow disturbances in the form of radiated sound on maximum lift coefficient and drag. The works of Collins[50], Brown[51], Chang[52], and others have indicated a beneficial effect, for some airfoils, from sound on lift and drag in the post stall regime. That is, sound energy had the capacity to reattach the flow at incidences beyond the normal stalling point. This idea was applied to the JN-153 optimal airfoil to determine if the sound could provide further benefits to its high lift characteristics.

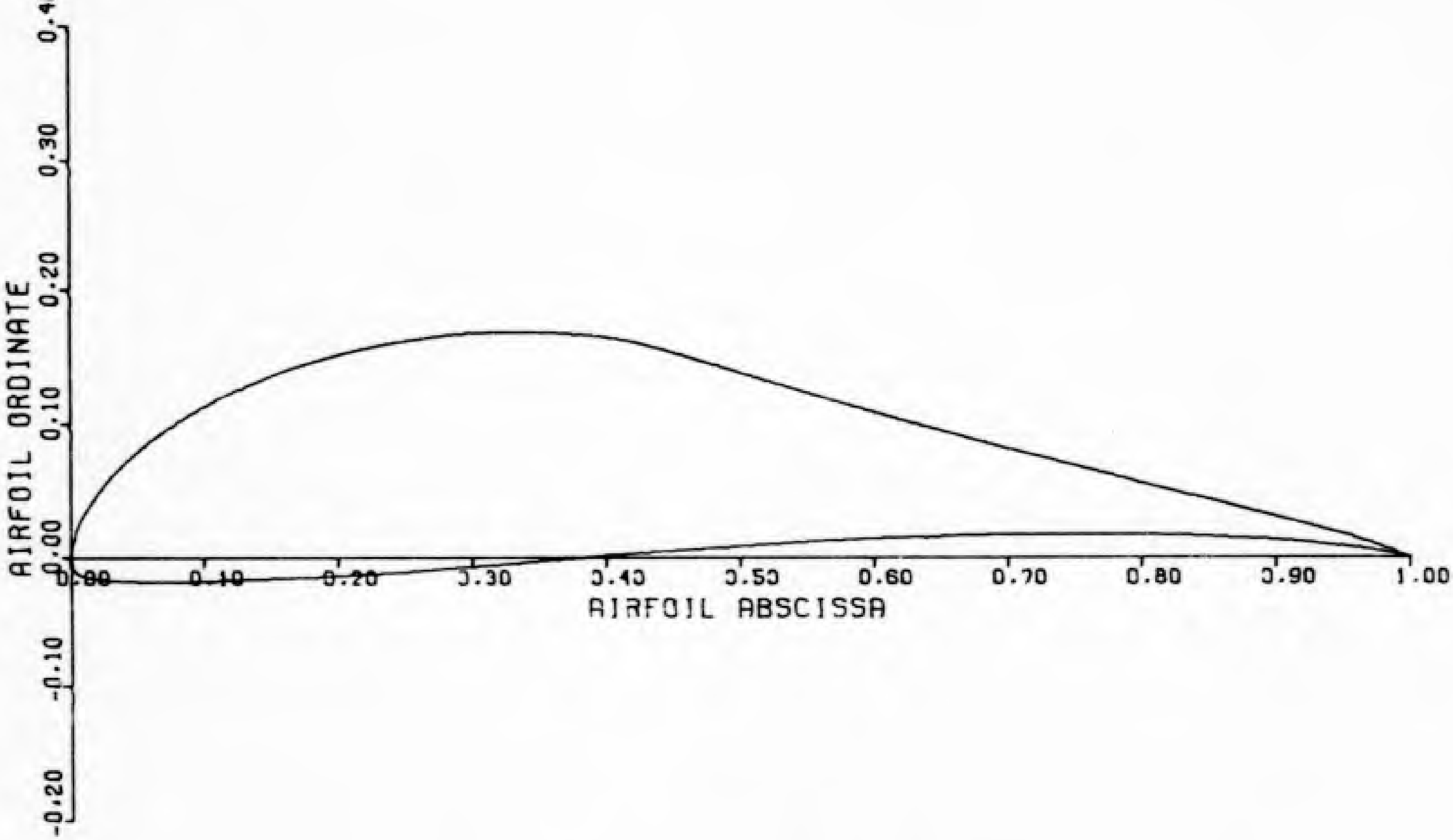

Figure 34. The JN-153 Optimal Airfoil.

MODEL DESIGN AND CONSTRUCTION

A significant problem with the construction of an airfoil section for aerodynamic testing is that of providing a sufficiently accurate airfoil profile to yield good results. In addition, there must be enough room in the wing to install all of the necessary tubing for surface pressure measurement. Thus, a large chord length would be an advantage. However, another primary problem of aerodynamic testing is the wind tunnel wall interference with the flow field. This implies the requirement for a small chord length airfoil section, and some best compromise must be made.

A chord length of twelve inches was chosen for the JN-153 wing. Although somewhat large as far as tunnel interference is concerned, it was large enough to facilitate construction. Wind tunnel wall interference effects would have to be compensated for. A twelve inch chord wing had been used in The University of Texas wind tunnel before and had produced data closely approximating published data by the use of tunnel interference correction factors. Similar corrections were applied in the present study.

To insure best accuracy in the area where surface pressure measurements were made, a four inch wide section of the wing was milled from a solid aluminum block. (See Figure 35) The static pressure taps to measure local pressure were placed in the center of this section. The pressure taps (.020" diameter holes) were drilled perpendicular to the surface. Each of the small holes intersected a larger hole drilled from the end of the center section. Pressure taps were concentrated in regions of expected rapid pressure change, i.e., around the nose and near the start of the pressure recovery

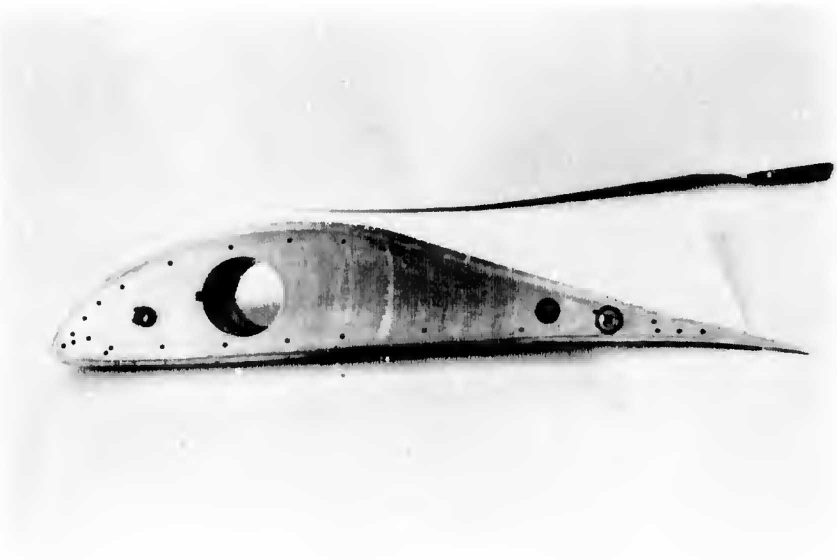

Figure 35. End View of the Machined JN-153 Center Section.

Figure 36. Tubing Mounted in the JN-153 Center Section.

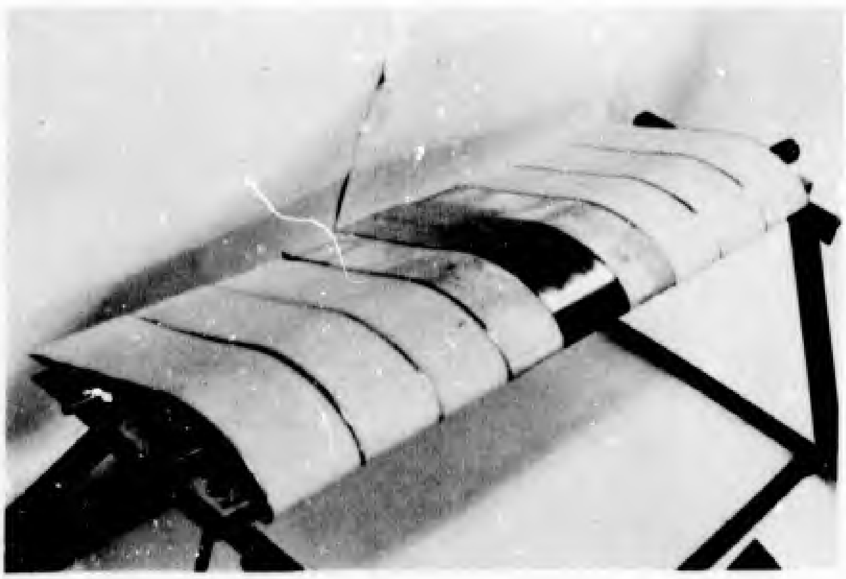

Figure 37. The JN-153 Wing.

region, while the remainder of the pressure taps were more uniformly distributed. (Figure 35). The milled center section was made in The University of Texas engineering machine shop. The profile was specified by 120 coordinate points.

The aluminum center section was assembled on a 1 3/16 inch steel tube main spar and a 3/8 inch threaded rod rear spar. The main spar was chosen to be stiff enough to provide small deflections (< .1") under the maximum load that might be expected on this wing. The threaded rear spar was employed to maintain proper rib spacing. The pressure taps were connected out beyond the end of the spar with .060" O.D. stainless tubing. One end of each piece of tubing was epoxied into its connecting hole in the end of the center section, run through a slot cut in the spar, and out the end of the spar. There were a total of thirty-one pressure taps. (Figure 36).

The remainder of the wing on either side of the center section was built up around aluminum ribs from urethane foam and fiberglass. The aluminum ribs were milled to the profile shape, then foam blocks were glued between them and sanded down to the rib contour. A hobby sanding filler was painted over the foam to give it a smooth surface and to control the tendency of the foam to increase in volume after sanding.

The completed foam blocks were mounted on the spar on both sides of the center section, and were covered with fiberglass cloth and polyester resin. After curing, the plastic surface was sanded to a smooth finish. (Figure 37)

To increase the effective aspect ratio of the wing, clear acrylic end plates were installed at the tips. Each end plate was 17 inches by 21 inches, with the leading edge cut in an 8 1/2 inch radius.

WIND TUNNEL TEST FACILITY

The University of Texas wind tunnel is a conventional closed circuit single return type. The test section is a rectangular open jet with dimensions 22 inches by 36 inches, and length of 38 inches. The tunnel speed is continuously variable between 0 and 120 ft/sec. Turbulence factor is .005.[53]

Tunnel speed is determined by measuring the dynamic pressure in the test section with a pitot tube connected to an inclined manometer.

The entrance to the diffuser section of the wind tunnel can be left as a rectangular squared off lip or can be faired in by a detachable "bell mouth" that will smoothly guide the flow back into the tunnel. (Figures 38 and 39).

Experience has shown that, with the bell mouth removed, there exists a region of separated flow on the bottom wall of the diffuser section when a wing in the test section is generating significant lift. Consequently, the bell mouth is used whenever possible.

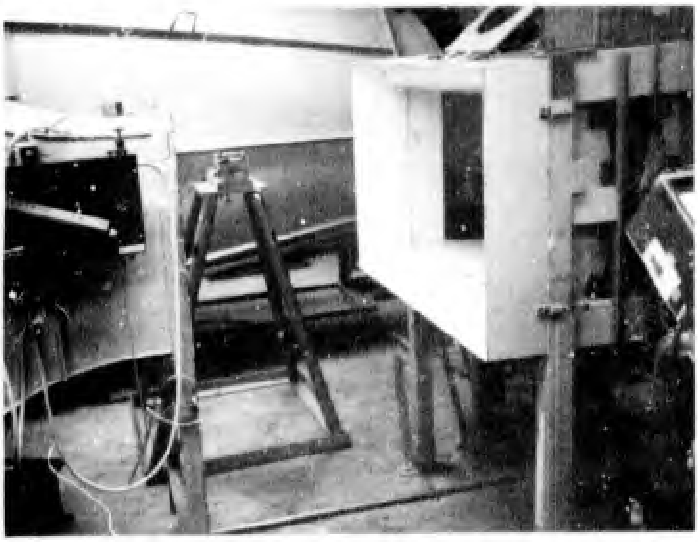

Figure 38. Wind Tunnel Test Section with Bell Mouth in Place.

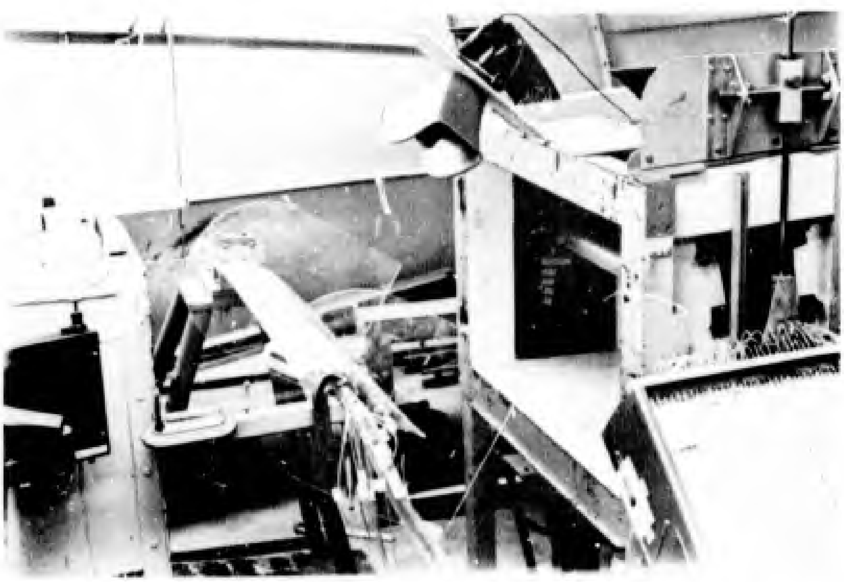

Figure 39. Wind Tunnel Test Section without Bell Mouth Ready for Test of Wing. (Note End Plates on Wing).

EXPERIMENTAL PROCEDURE

The data to be acquired from this series of tests was exclusively static pressure measured at various points along the airfoil profile. Therefore, the pressure measurement had to be accurate and reliable. A primary requirement to assure this accuracy was that there be negligible leaks in the pressure carrying system. Considerable effort was expended to make certain that none of the thirty-one ports and connecting tubing leaked at any point. This was done before the foam outer sections of the wing were assembled on the spar. Each pressure tap was temporarily sealed and the free end of its connecting tube attached to an inclined manometer. A pressure difference was put on the system. If the leak rate was less than the allowable limit, then the sealing was considered acceptable. The allowable limit was .1 psf/min.

Knowing the exact location of each static port on the airfoil was also important. Therefore, the coordinate location of each pressure tap was measured. A height gauge and surface table were used. For chordwise measurement the chordline was oriented vertically, and for thickness measurement, the chordline was horizontal. Figure 40 presents measured points plotted over the true profile.

After the above checks for accuracy were done, testing could begin. The tube from each surface pressure tap was connected by a flexible line to one manometer tube of a 40 tube oil-filled inclined manometer board. The angle of the manometer board could be varied between zero degrees and 90 degrees. The board was photographed to record the pressure distribution of

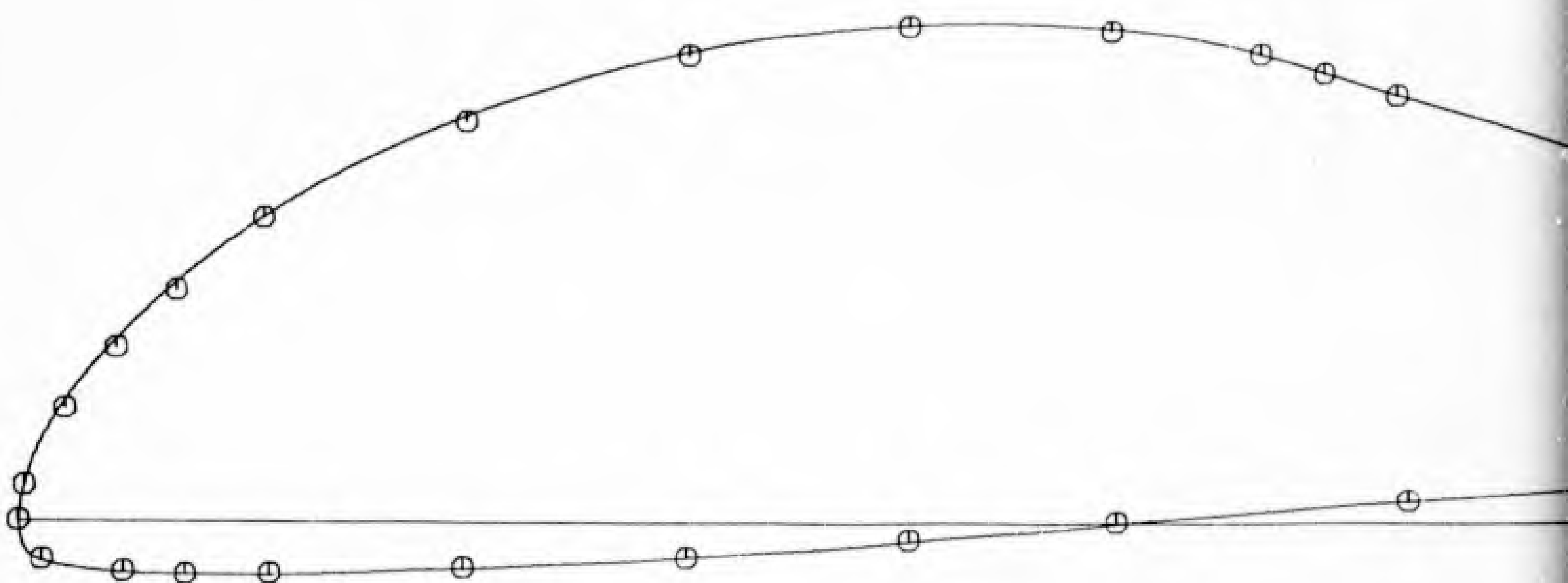

Figure 40. The Measured Locations of Pressure Taps in Relation to
(Line contour represents theoretical profile while act
at the end of the line in center of symbol.)

2

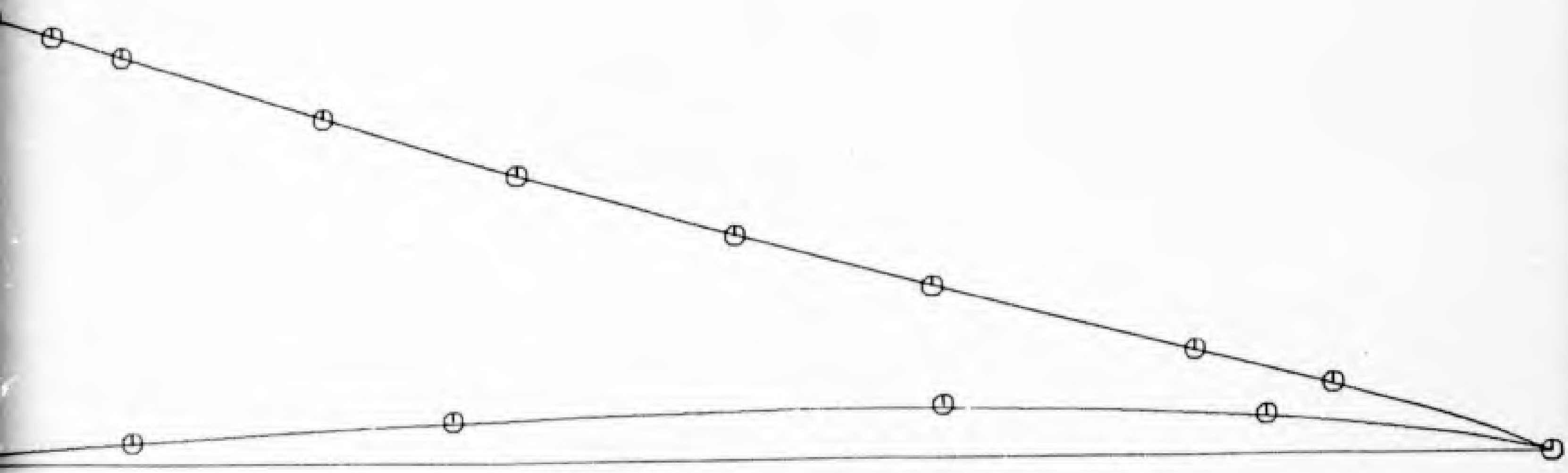

Taps in Relation to the True Profile of the JN-153.
l profile while actual measured profile is located
symbol.)

each run. From this photograph the pressure data was extracted. On the back of each photo other pertinent data was recorded (dynamic pressure, temperature, barometric pressure, incidence of the wing, and angle of the manometer board). The specific gravity of the manometer oil was .866.

There was no mechanism for changing the airfoil incidence while the tunnel was operating. Therefore, each change in incidence required shutting off the tunnel, loosening the clamps on the wing spar and adjusting the angle by hand. A pendulum clinometer was used to measure the angle of the wing reference line to the gravity direction. This reference line was at an angle of 15.3 degrees to the chordline of the wing. The gravity direction is fairly close to and was assumed perpendicular to the undisturbed flow direction of the wind tunnel.

The tests performed with externally radiated sound utilized loudspeakers to supply the sound energy. The sound tests were conducted following the procedure of the basic static aerodynamic tests, with the exception that the bell mouth was removed because of interference with the speaker mounting. (Figure 39). The speaker was mounted out of the air stream, pointed directly at the surface of the wing about 24 inches away from it. Most sound effects were expected in the stalled regions of the airfoil, so the speaker was placed to radiate sound directly on the surface where the flow was separated or nearly separated. When the upper surface flow was separated, the speaker was above and behind the wing, and when the bottom surface flow was separated, the speaker was directly below the wing.

Each experimental run consisted of setting the desired incidence and tunnel dynamic pressure, then turning up the sound to the desired frequency and power level (input power level). The appropriate parameters were recovded and the manometer board photographed.

The sound pressure level (SPL) at the surface of the wing was measured independently of the aerodynamic test, with the wind tunnel off. A condenser microphone, connected to an rms voltmeter was placed near the surface of the wing and aimed at the speaker. The oscillator and power supply were turned to the same frequency and power level recorded for one of the aerodynamic experiments. Output of the voltmeter was recorded. This process was repeated for each frequency and power level used in the aerodynamic tests.

TUNNEL INTERFERENCE CORRECTIONS AND DATA REDUCTION

The measured data consists of thirty-one measurements of static pressure at various points around the airfoil. This information can be used directly for comparison of local pressure (or pressure coefficient) with predicted local pressures. But generally, the desired information is the total force or force coefficients acting on the airfoil. Total force is computed by integrating the measured pressures, by some method, over the surface of the wing. An algorithm, coded for the digital computer, was written to accomplish this purpose.

The basic structure of the algorithm is to compute chordwise and normal forces independently by: dividing each dimensional direction into a number of incremental units (usually 100), finding the local pressure at each increment by interpolating with a fourth order polynomial fit, and then summing the products of the local pressure and these small elements. The dimensionless coefficients are then found by dividing by qS.

Considering the relatively large size of the wing compared to the test section of the wind tunnel, it is apparent that some form of interference correction was necessary to approximate the performance of a true isolated two-dimensional section. Three sources supplying correction factors to incidence and lift coefficient are available. All three had basic similarities. Two of these sets of correction parameters, Pankhurst and Holder's and that from AGARD, were coded as Fortran subroutines and combined with the pressure integration program to produce the overall integrated and corrected force coefficients.[54,55] This corrected data was the best information available from the test program.

Blockage corrections were not assumed to be necessary due to the direct measurement of the dynamic pressure at the entrance to the test section. No other correction was attempted.

RESULTS

The static aerodynamic performance of the JN-153 low-Reynolds number, high-lift airfoil design was given a preliminary experimental evaluation in The University of Texas 3' x 4' Low Speed Wind Tunnel. The influence of external disturbances in the form of radiated sound on this performance was also investigated.

Some of the measured velocity profiles (V_{local}/V_∞ vs. chordwise station) are presented for several angles of attack in Figures 41, 42, and 43. The predicted velocity profile for each angle of attack was also plotted over the measured data. The predicted and measured values are not in complete agreement, that is, the measured local velocity along the top surface of the airfoil is somewhat lower than the predicted values. The measured local velocity along the airfoil's bottom surface, however, matches the predictions quite well. The measured location for the onset of pressure recovery region was close to the predicted values only at the higher incidences.

Since the lift force on the airfoil is proportional to the area enclosed by the velocity profile, it is evident that the experimentally determined lift coefficient at any angle of attack must be smaller than the theoretical lift coefficient. The experimentally determined and theoretically estimated lift coefficient versus angle of attack data are plotted in Figure 44. The maximum lift coefficient measured in the wind tunnel was always below the predicted value of $C_L = 2.0$ for the cruise angle of incidence.

The drag coefficients computed from the measured data are given in Figure 45 for reference only. Because the drag force was much smaller than the lift force, and because there was a significant correction to incidence due to lift, the drag coefficients presented here cannot be considered reliable measurements. The use of a wake rake in a larger tunnel would be the best way to obtain accurate drag coefficients.[56] These qualitative data, however, do suggest the presence of a drag bucket.

A comparison of the JN-153 airfoil to a conventioaal NACA five digit airfoil commonly used in general aviation showed that the JN-153 maximum lift surpasses that of the typical older airfoil. An NACA 23018 (which is comparable in thickness to the JN-153) had a maximum lift coefficient of nearly 1.4 at $Re = 3.1 \times 10^6$. This performance is representative of conventional airfoils.[57] The JN-153 had a much better maximum lift coefficient (1.87) at a significantly lower Reynolds number (Re = 700,000). Comparing the JN-153 to a recently designed maximum lift airfoil showed, however, that it did not achieve the maximum design potential. The FX 72-MS-150-B, designed by Wortmann, had a maximum lift coefficient in excess of 2.0 at a Reynolds number near to that of the JN-153 ($Re = 10^6$).[58] The JN-153 is somewhat thicker than the Wortmann airfoil.

Unfortunately, this study cannot conclude that the lack of performance in the experimental airfoil was due exclusively to an inadequate boundary layer model or to other modeling inaccuracies in the design analysis. The small wind tunnel facility and possible manufacturing inaccuracies in duplicating the airfoil profile contributed to the uncertainty in correlating the experimental results with the predicted analytical performance. Error producing factors include: 1) an airfoil too large for the wind tunnel requiring excessive wall interference corrections, 2) undeterminable three-dimensional end effects of the flow, and 3) deviation from the true coordinates of the airfoil due to manufacturing tolerances.

The oversize wing required extreme corrections to lift and incidence to account for the effects of the boundaries of the flow field. The corrections were larger than anticipated. Incidence corrections, due to lift interference effects, of ten degrees were typical. Lift coefficient corrections ranged up to .24. In some instances corrections were fifty percent of the measured value. Also, flow visualization studies indicated that the large airfoil caused much of the flow to spill out of the wind tunnel. This factor was not taken into account in the derivation of the lift interference corrections.[60] This placed some doubt on the validity of the correction factors applied.

A graphic example of the interference between the tunnel walls and the lifting airfoil was discovered during the tests with radiated sound. With the wind tunnel bell mouth removed for sound testing, the corrected maximum lift coefficient as calculated from the data, taken without any sound energy input, jumped up to 2.0. This result was confirmed for several repeated runs. However, the separated flow inside the diffuser for this condition and the continued loss of flow outside the tunnel gave these lift coefficients no better credence. Tha data can be improved only by testing this size airfoil in a larger wind tunnel. Such tests are being planned for the new University of Texas 5' x 7' Subsonic Wind Tunnel now nearing completion.

The measurement of the pressure tap locations on the completed airfoil (see Figure 40) showed that the profile at the center of the wing did not follow the true coordinates for the airfoil. A deviation of $\pm$ 0.010 inc. was observed. How much effect this deviation has on the performance can be determined only by tests in a larger facility and on a more accurate model.

Adding to the previously mentioned difficulties was the fact that the airfoil was built without spanwise pressure taps. A spanwise distribution of pressure could possibly have shown how closely the flow approached a two-dimensional condition. In an alternate attempt to confirm the two-dimensionality of the flow, end plates of various sizes were fitted on the airfoil. The two points included in Figure 44 show the results of those tests. Increasing the size of the end plates did not change the measurements significantly. This would indicate that the flow was sufficiently two-dimensional. Yet when yarn tufts were placed on the airfoil near the end plates, there was always an indication of a spanwise component in the flow. Thus, no conclusion can be drawn, and the question should be further studied in a larger wind tunnel with two-dimensional wall inserts.

The results of the second part of this test program were designed to investigate the influence of flow disturbances on the JN-153 airfoil performance. The disturbances were introduced in the form of sound of a specific frequency radiating on the wing. The results from the sound tests are presented in the form of sound pressure level (SPL) versus lift (or drag) coefficient. Each discrete sound frequency is marked with a unique symbol. The Reynolds numbers for all sound tests were much lower than the airfoil design Reynolds number. It was found that sound had less influence at higher tunnel speeds (Reynolds number). Previous investigations with sound have been at very low Reynolds numbers.[61,62]

Externally radiated sound, in all cases, had a detrimental effect of the lift and drag of the JN-153. This was contrary to previously reported observations. Figures 46 and 47 show how sound affected the lift and drag of the JN-153 at two different incidences, $\alpha_u = 31.9°$ and $\alpha_u = 20.0°$ (α_u is the uncorrected incidence). In both cases the flow was separated over about 50 percent of the top surface before the application of sound energy. The decrease in lift coefficient when the wing was radiated with sound is apparent. There is possibly some frequency dependent behavior for $\alpha_u = 31.9°$. It appears as though higher frequencies caused a larger decrease in the lift coefficient for a constant power level (Figure 46). Not enough data points were obtained at other incidences, however, to make comparisons for frequency dependence. The variation of sound influence with frequency is fairly well documented.[61,62]

Alongside each lift curve is the corresponding drag coefficient curve. The drag coefficient data must be taken as a purely qualitative indication because of the uncertainty of the drag calculations. For both $\alpha_u = 31.9°$ and $\alpha_u = 20.0°$, the tendency is toward higher drag with increasing SPL.

Figure 48 presents lift and drag coefficients under sound influence for $\alpha_u = 28.8°$. The no-sound flow state was unstalled, but the application of a low power sound field caused immediate separation of the flow over a large part of the upper surface. The effect of this separation on both lift and drag was pronounced.

The result of radiating sound energy onto a boundary layer is to initiate a premature transition, causing the transition point to move upstream. This action in the JN-153 boundary layer apparently forced the separation point to move upstream also. In other words, it decreased lift and increased drag.

Collins[61] noticed an apparent opposite effect from sound energy radiating on an older (NACA 2412) airfoil. A closer look at the JN-153 airfoil in the U.T. wind tunnel, however, indicated that the features can actually be similar. In both cases, the application of sound energy caused reattachment of a certain class of separated flows around the airfoil which was at an incidence beyond the normal stalling incidence. The different behavior between the JN-153 and these airfoils under sound influence may be explained by the boundary layer condition at the normal separation point. The JN-153 boundary layer was always fully transitioned and turbulent before reaching the pressure recovery region, but the NACA four digit airfoils had pressure recovery (and separation) within the laminar boundary layer and allow the flow to travel further into pressure recovery before separating.

During the course of testing the JN-153, a rudimentary confirmation of this hypothesis was performed. At low angles of attack, the JN-153 exhibited a local velocity peak on the bottom surface near the leading edge. Behind this peak was a steep adverse pressure gradient. If the JN-153 were stalled in the negative lift direction, then the separation occurred in the region of a velocity peak. The boundary layer on this part of the airfoil was experimentally determined to be laminar at the design Reynolds number. Sound energy was radiated onto the airfoil in this condition and the effects on the local pressure were determined. Figures 49 and 50 show the C_L vs. SPL curves for low angles of attack. After application of sound energy, the lift coefficient exhibited a slight increase at one incidence (Figure 49) and no detectible change at another (Figure 50). The integrated force did not change significantly, but the local pressure coefficient in the region near the separation point was affected appreciably. Figure 51 shows the surface pressure coefficients at several chordwise stations for $\alpha_u = 1.25°$. Coefficients both with and without sound effects are presented. The same information for $\alpha_u = 1.87°$ is given in Figure 52. At both these incidences the sound energy caused reattachment of the separated flow, consequently restoring the low local pressure coefficient.

These results support the argument that sound is effective primarily in flow reattachment with a laminar boundary layer separation in the presence of a large pressure peak.

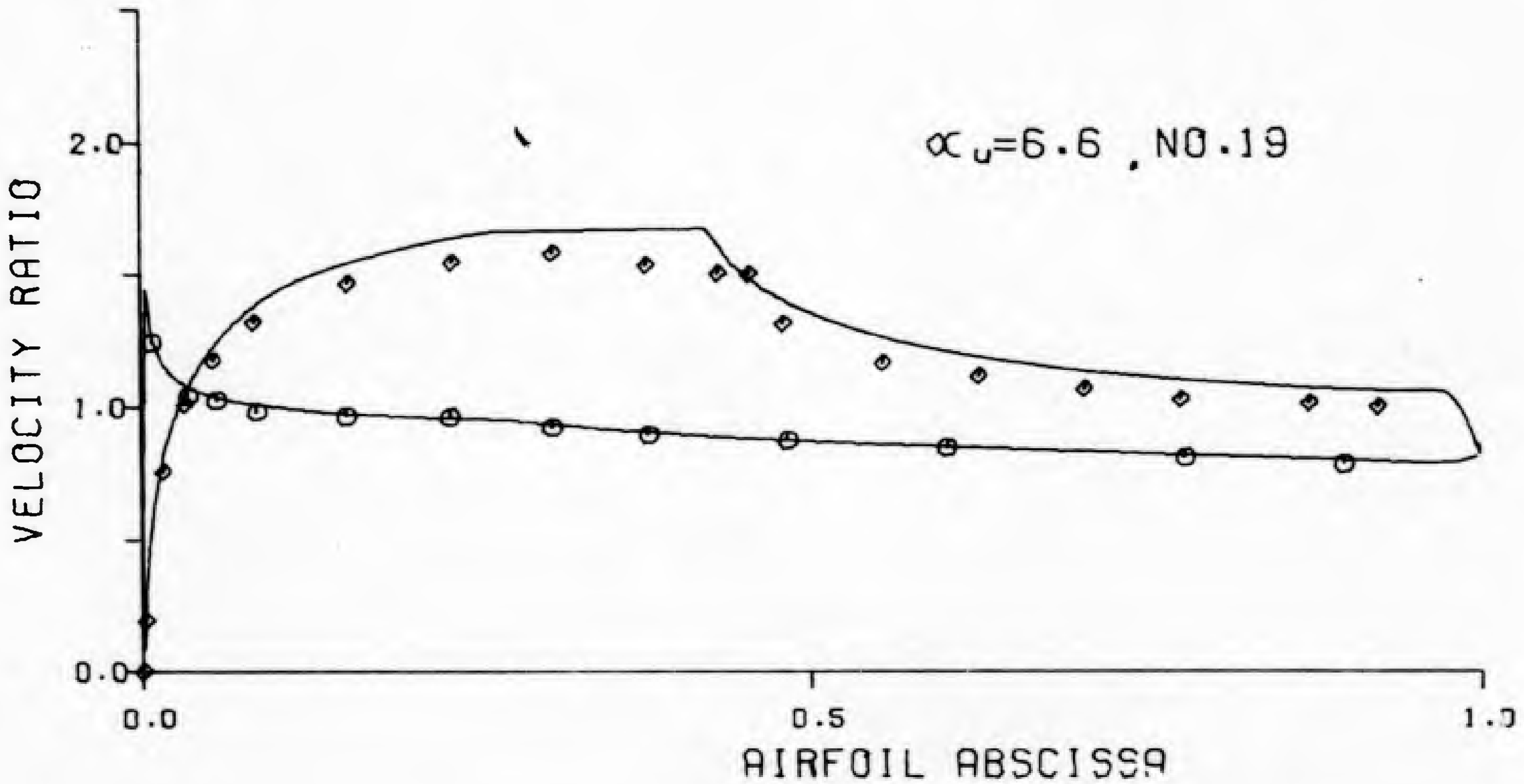

Figure 41. Velocity Distribution of JN-153, Measured Distribution Compared to Theoretical Distribution for α_c=0.8°, R_e=700,000. (α_c is the corrected incidence)

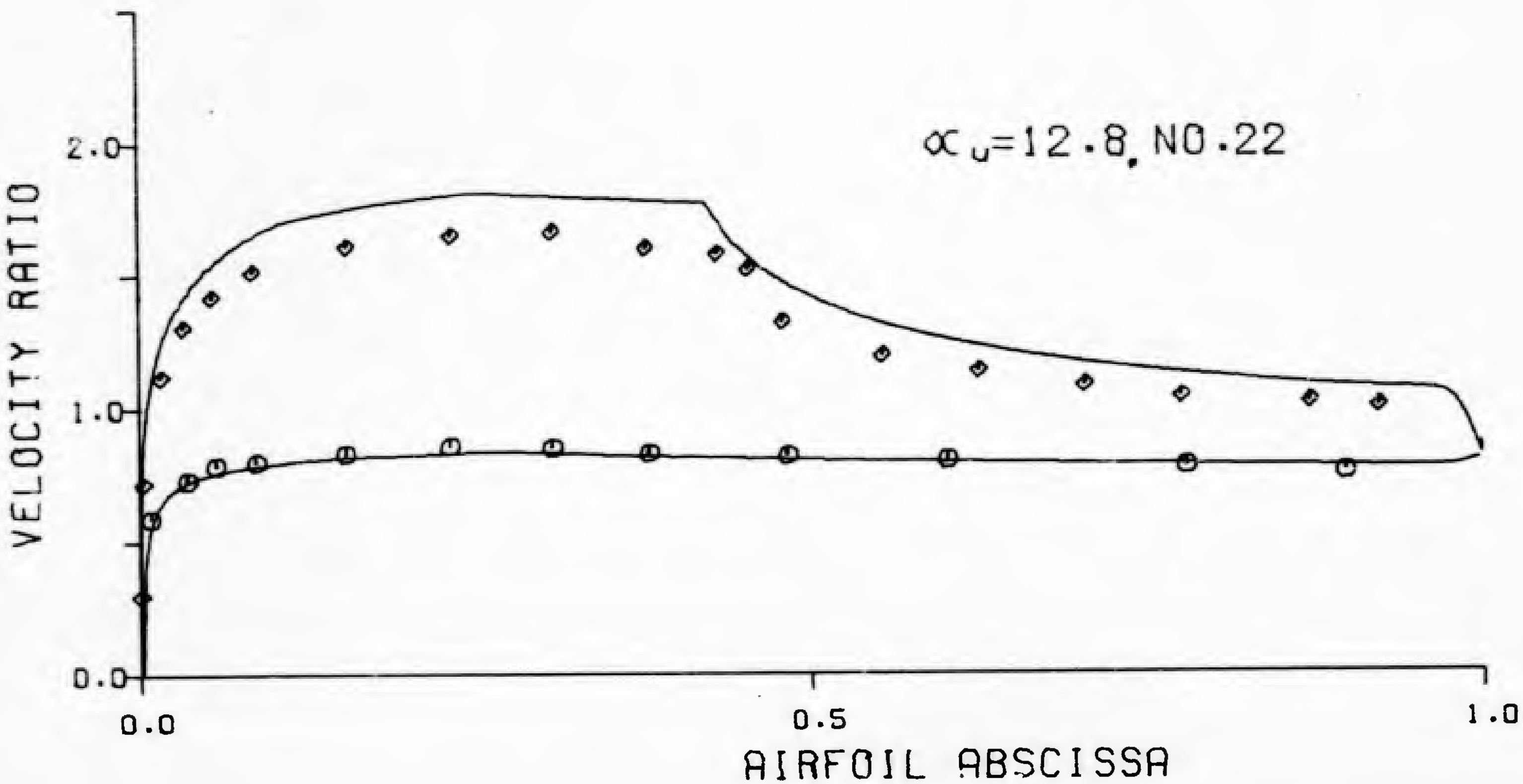

Figure 42. Velocity Distribution of JN-153, Measured Distribution Compared to Theoretical Distribution for α_c=4.2°, R_e=700,000.

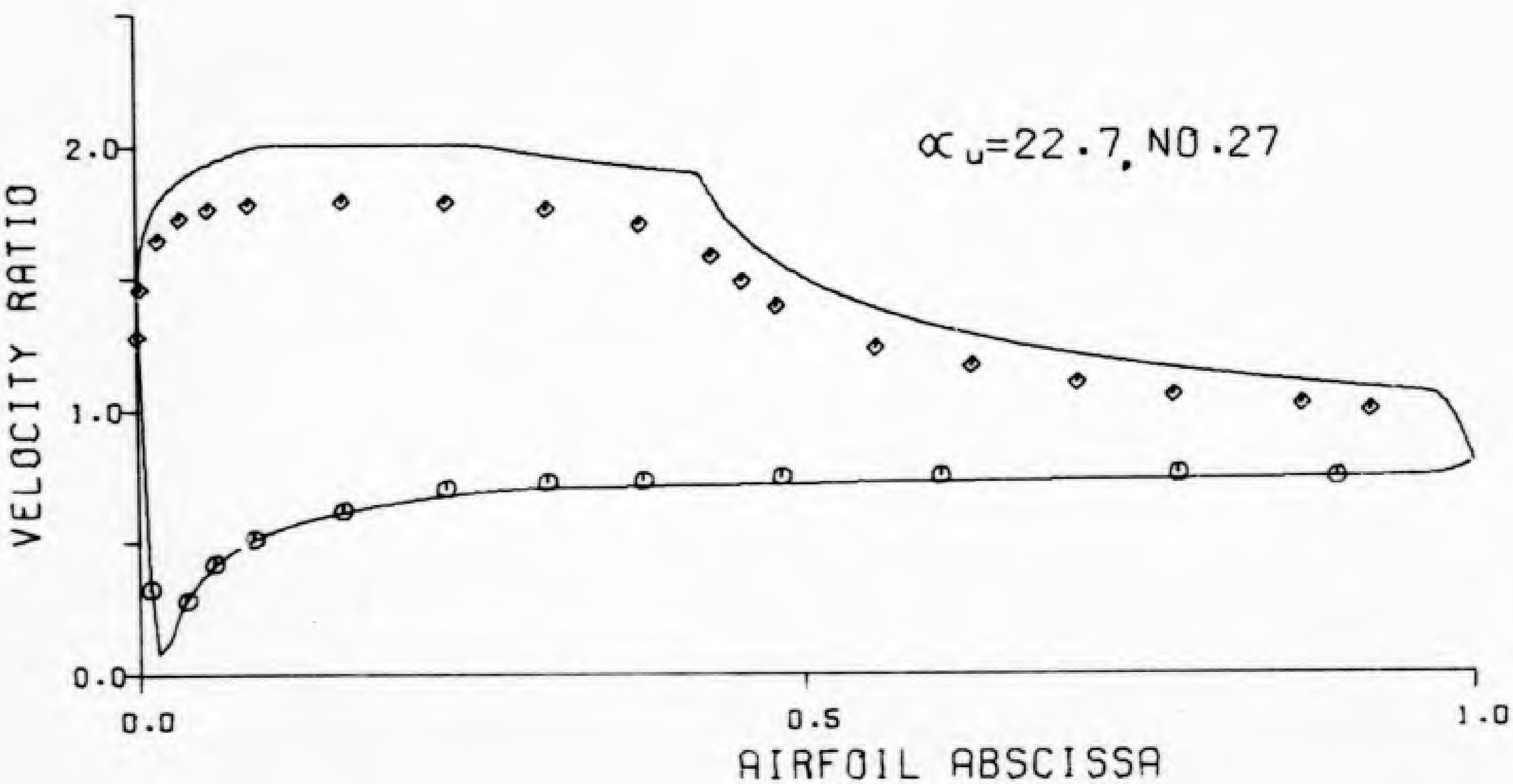

Figure 43. Velocity Distribution of JN-153, Measured Distribution Compared to Theoretical Distribution for α_c=10.6°, R_e=700,000.

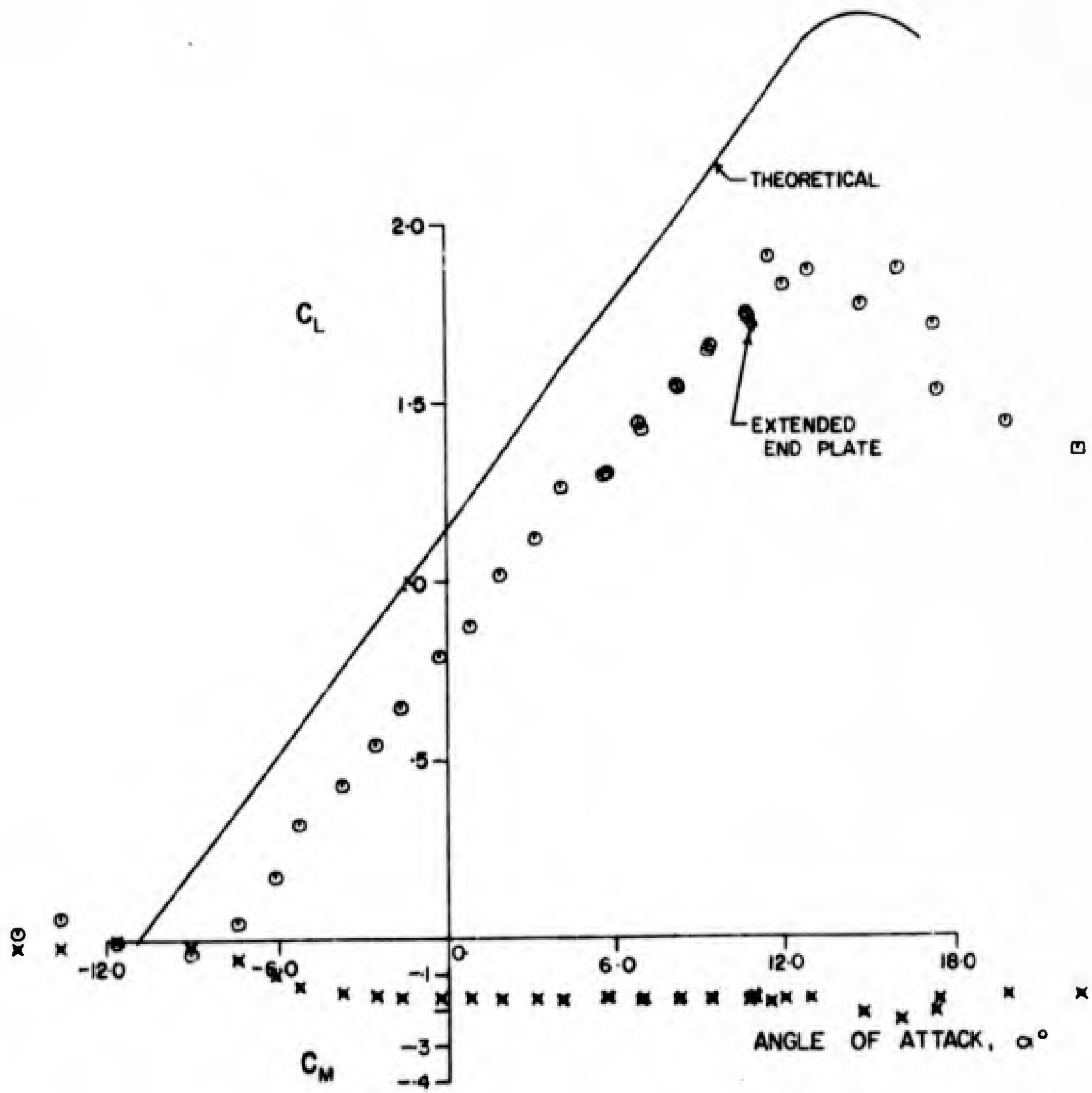

Figure 44. Corrected Lift Coefficient and Moment Coefficient versus Angle of Attack for the JN-153.

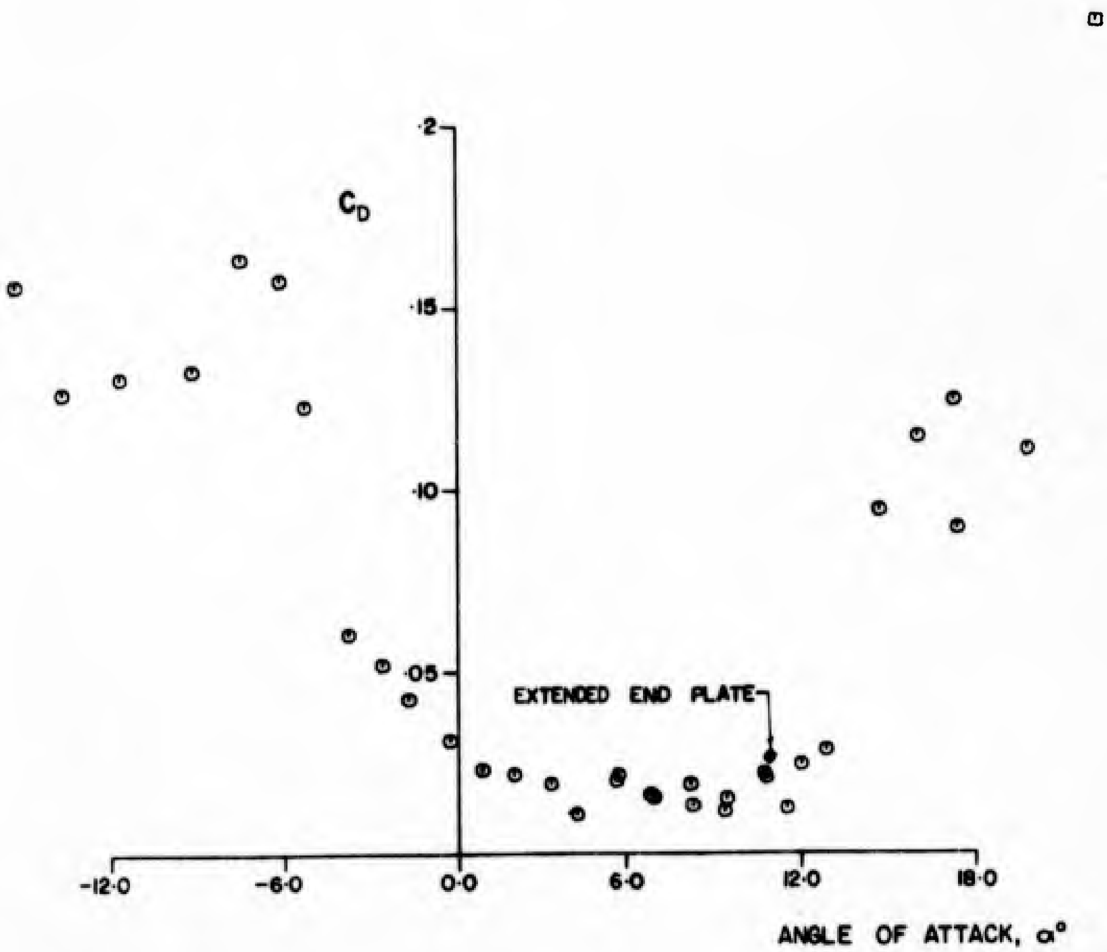

Figure 45. Drag Coefficient versus Angle of Attack for the JN-153.

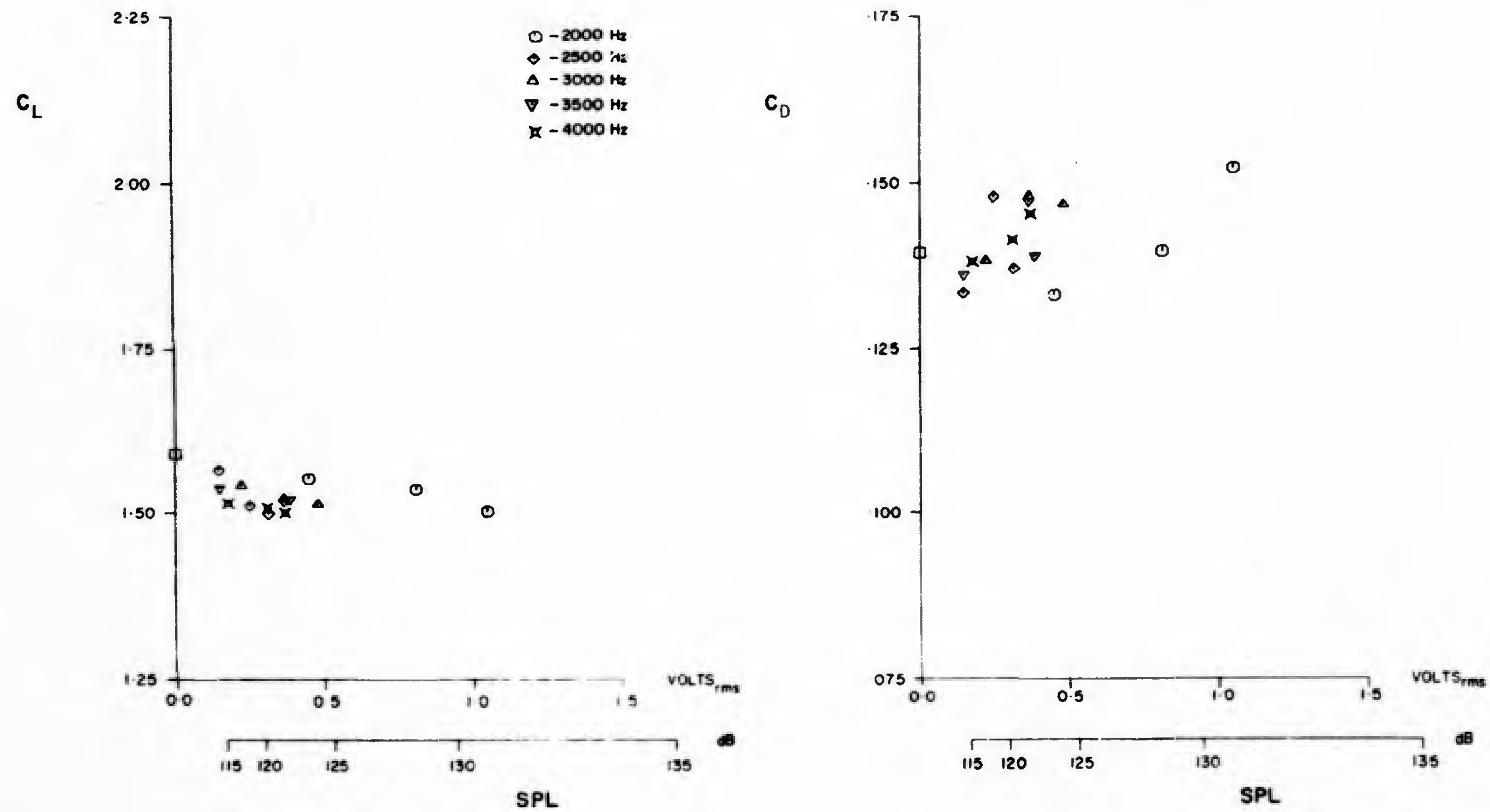

Figure 46. C_L versus SPL and C_D versus SPL for α_u=31.9°, R_e=498,000.

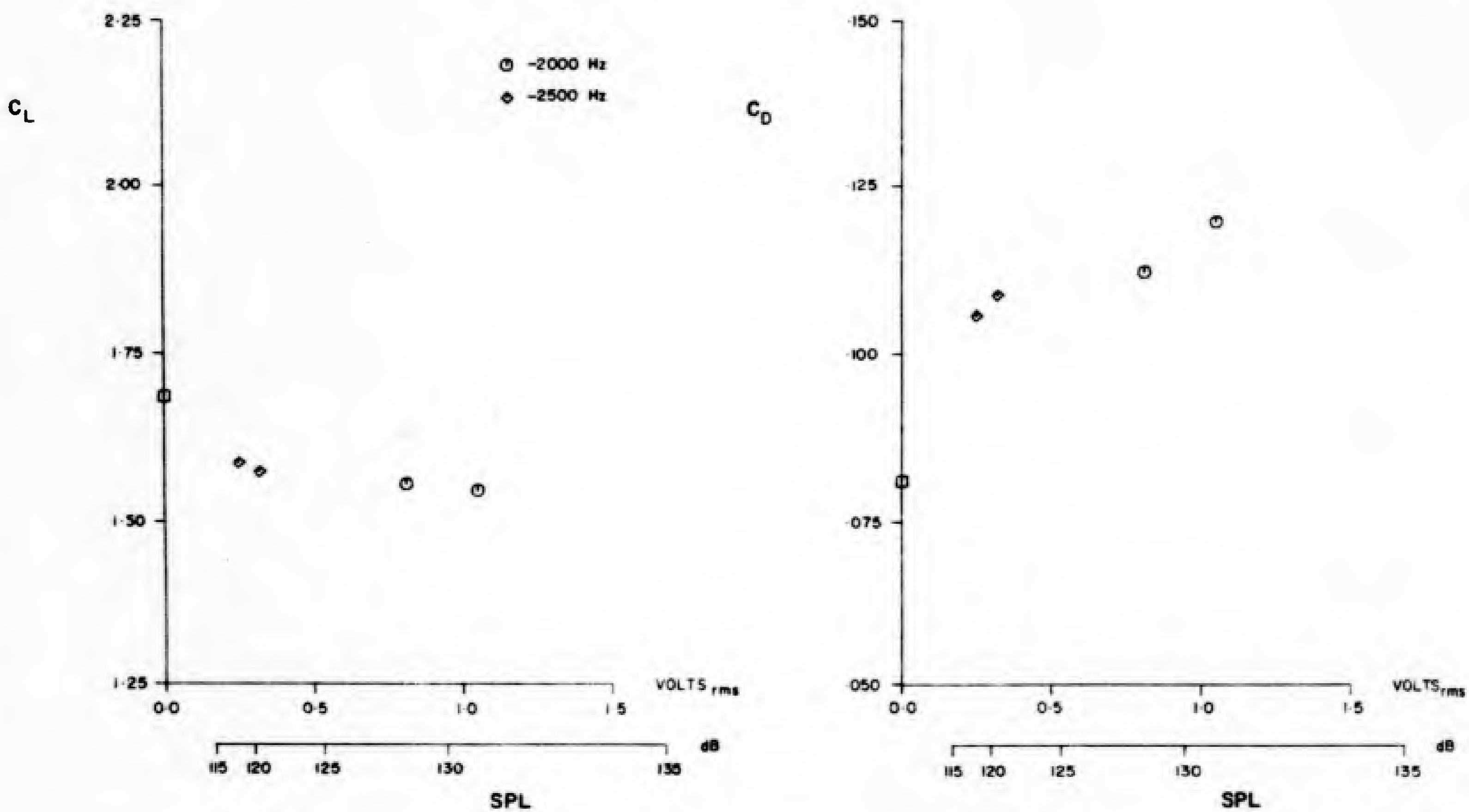

Figure 47. C_L versus SPL and C_D versus SPL for α_u=30.0°, R_e=498,000.

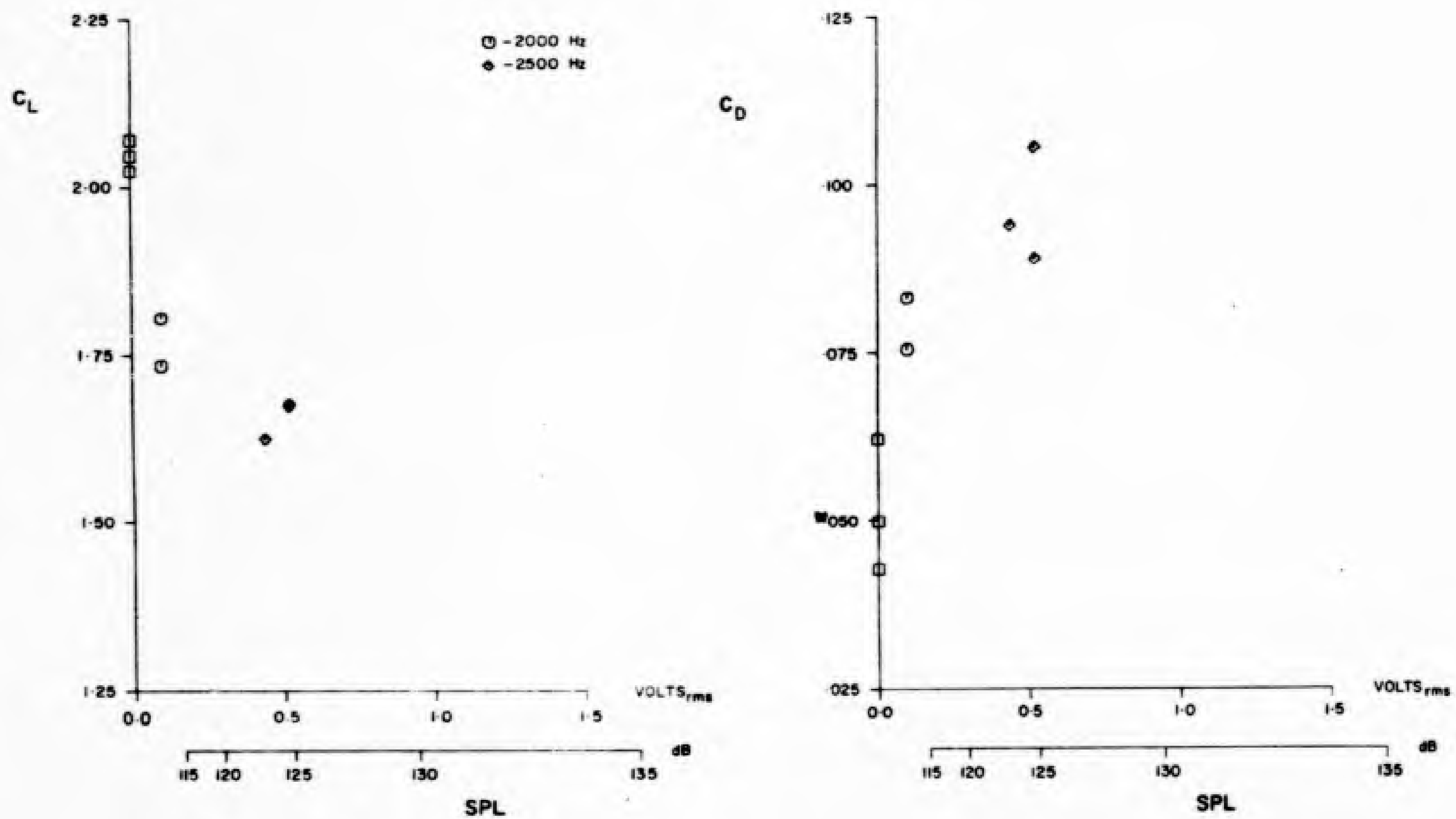

Figure 48. C_L versus SPL and C_D versus SPL for α_u=28.8°, R_e=500,000.
(Note higher C_L max without wind tunnel bell mouth.)(See Figures 38 and 39)

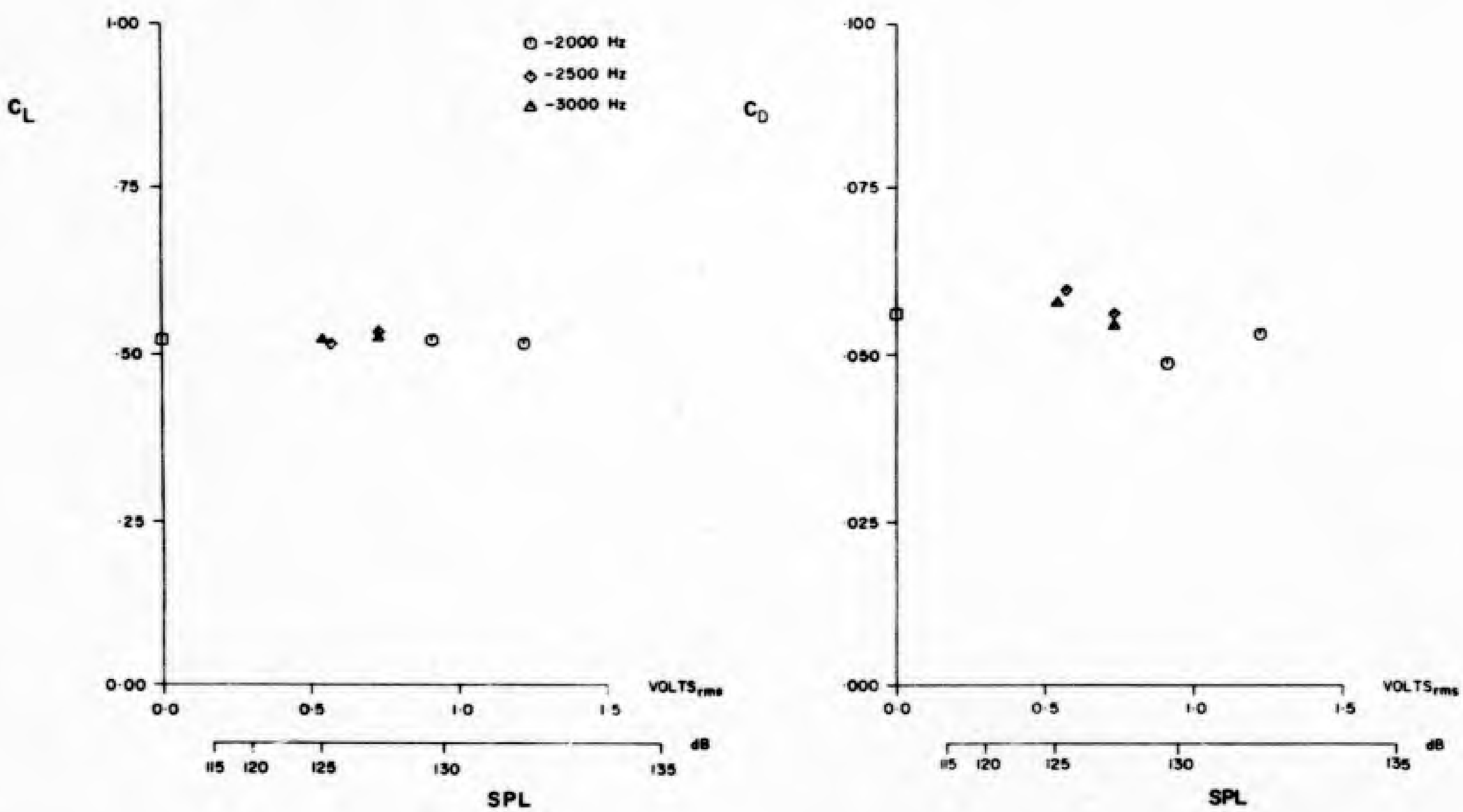

Figure 49. C_L versus SPL and C_D versus SPL for α_u=1.25°, R_e=499,000.

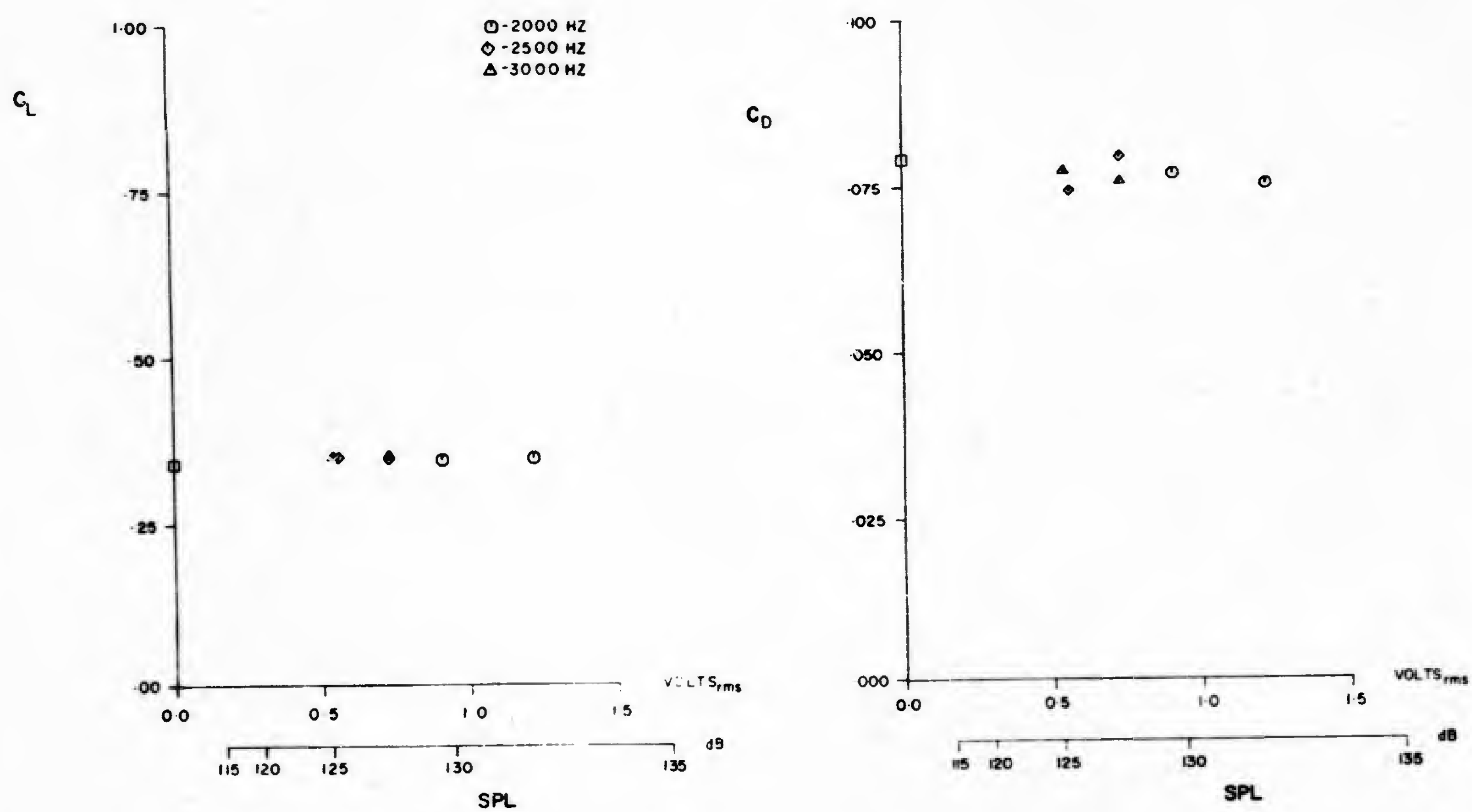

Figure 50. C_L versus SPL and C_D versus SPL for $\alpha_u = -1.87°$, R_e=498,000.

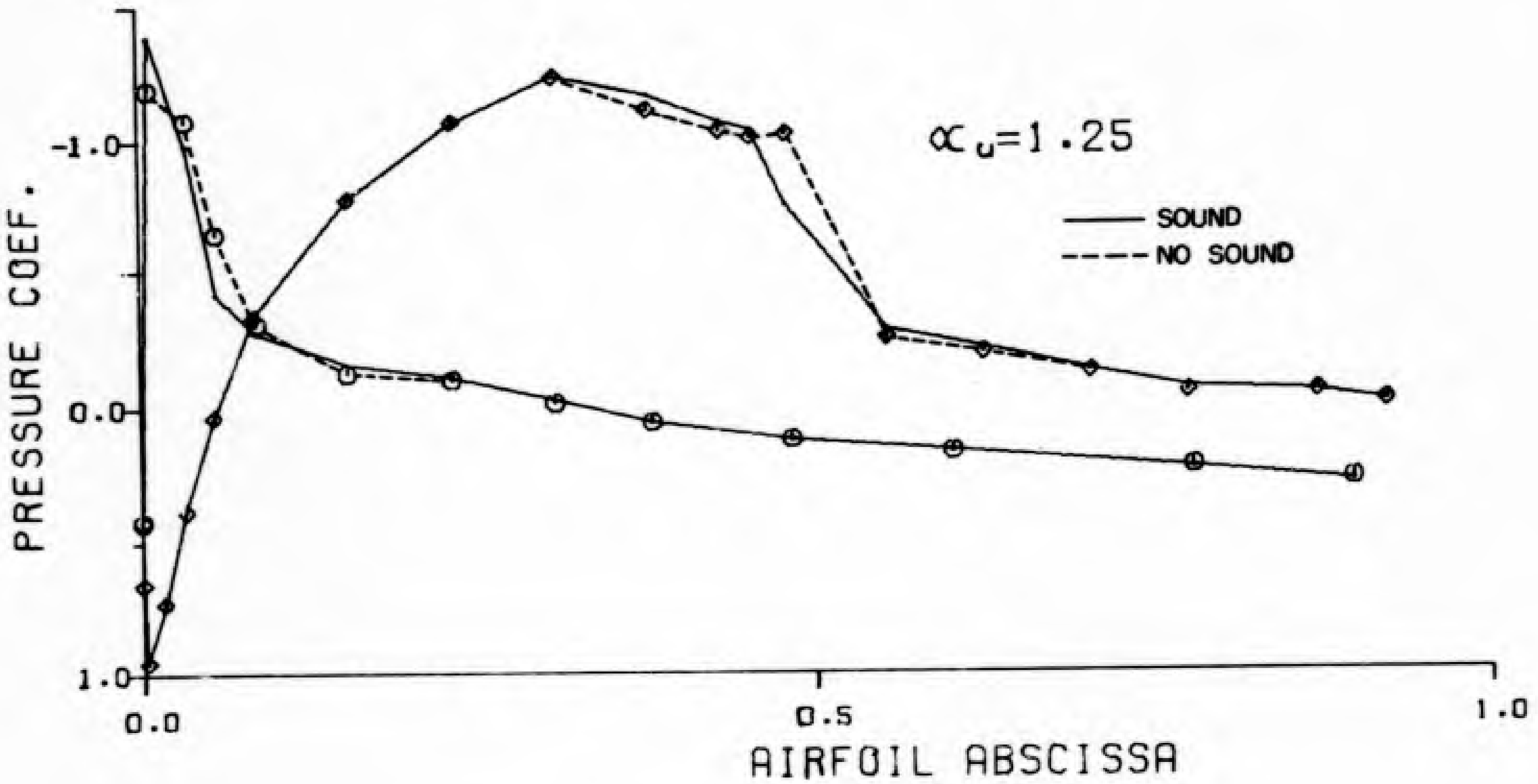

Figure 51. Pressure Coefficient at Low Incidence, with and without Sound.

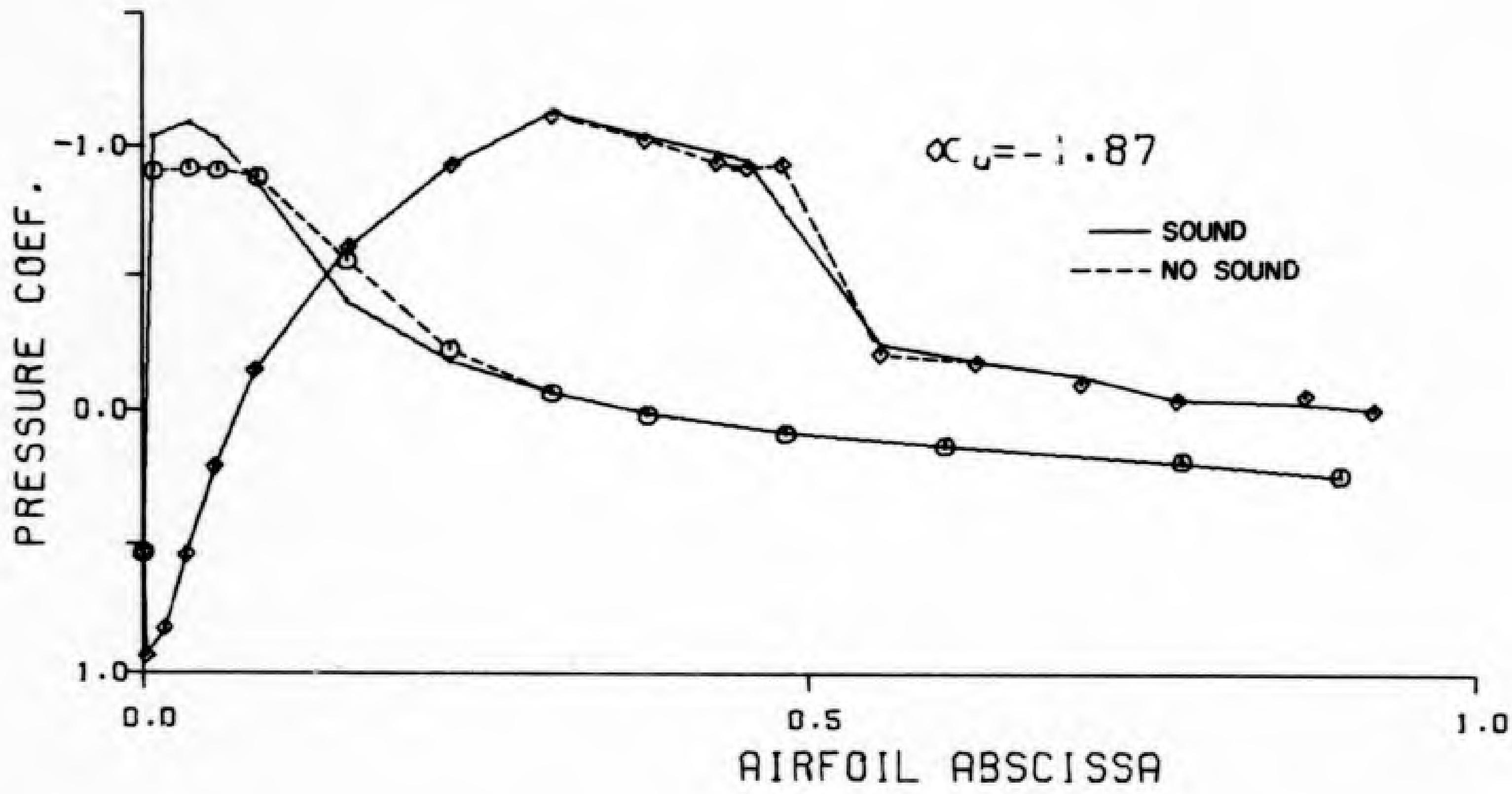

Figure 52. Pressure Coefficient at Low Incidence, with and without Sound.

CONCLUDING REMARKS

It has been shown that an airfoil, such as the JN-153, designed to maximize lift by employing optimization techniques, can have significantly better lifting ability than a conventional airfoil for Reynolds numbers less than one million. It has not achieved the ultimate performance predicted and this could be due to various factors in the experiment. Consequently, it has not been conclusively shown that the theoretical analysis is unrealistic. Further testing in a better facility is required.

As for the effect of sound on aerodynamic performance, it seems apparent that a well designed airfoil will achieve no advantage from radiated sound. Only those airfoils having a steep adverse pressure gradient in a laminar boundary layer with leading edge stall characteristics have been shown to benefit significantly from radiated sound.

REFERENCES

[1] von Karman, T., Aerodynamics, Ithaca, 1957, p. 21.

[2] Abbot, I., and A. von Doenhoff, Theory of Wing Sections, New York, 1949, p. 112

[3] Wortmann, F.X., "Progress in the Design of Low Drag Airfoils," Boundary Layer and Flow Control, edited by G. Lachmann, London, 1961, p. 748.

[4] Ibid, p. 750.

[5] Thwaites, B., "A New Family of Low Drag Wings with Improved C_L Ranges," ARC R and M No. 2292.

[6] Lighthill, M., "A New Method of Two Dimensional Aerodynamic Design," ARC R and M No. 2112.

[7] Wortmann, F.X., "A Critical Review of the Physical Aspects of Airfoil Design at Low Mach Numbers," MIT Symposium 1972, Technology and Science of Motorless Flight, Cambridge, Mass.

[8] Stratford, B.S., "The Prediction of Separation of the Turbulent Boundary Layer," Journal of Fluid Mechanics, Vol. 5, 1959.

[9] Matsumiya, K., and S. Uchida, "An Analytical Study of a Favorable Velocity Distribution for a Low Drag Aerofoil," Nagoya University Faculty of Engineering Memoirs, Vol. 18, May 1966.

[10] Squire, H., and A. Young, "The Calculation of the Profile Drag of Aerofoils," ARC R and M No. 1838.

[11] Abbot, I., and A. von Doenhoff, p. 84.

[12] Wortmann, R.X., Experimentelle Untersuchungen an neuen Laminar profilen fur Segelflugzeuge and Hubschrauder, Z. Flug W.,5, 228(1957). MOS translation TIL/T A906.
"Experimental Investigation of New Laminar Profiles for Sailplanes and Helicopters," British MOS translation TIL/T A906.

REFERENCES (continued)

[13]Curle, N., and H. Davies, Modern Fluid Dynamics, Vol. 1 Incompressible Flow, Princeton, 1968, p. 198.

[14]Granville, P., "The Calculation of Viscous Drag of Bodies of Revolution," David Taylor Basin Report No. 849, 1953.

[15]Wortmann, F.X., "Progress...

[16]Miley, S.J., "An Analysis of the Design of Airfoil Sections for Low Reynolds Numbers," Dissertation: Mississippi State University, January 1972.

[17]Owen, P. and L. Klanfer, "On the Laminar Boundary Layer Separation from the Leading Edge of a Thin Airfoil," ARC, Current Paper No. 220.

[18]Wortmann, F.X., "Concerning an Improvement of the 63-618 Airfoil," Soaring, May 1962.

[19]Eppler, R., "Direkte Berechnung von Tragflugelprofilen aus der Druckverteilung," Ingenur - Archiv, Vol. 25. No. 1, 1957. "Direct Calculation of Wing Profiles from the Pressure Distribution," translation.

[20]James, R., "A New Look at Two-Dimensional Incompressible Airfoil Theory," McDonnell Douglas Report DC-J0918/01, May 1971.

[21]Pick, G. and D. Lien, "The Development of a Two-Dimensional High Endurance Airfoil with given Thickness Distribution and Reynolds Number," MIT Symposium 1972, Technology and Science of Motorless Flight, Cambridge, Mass.

[22]Schlichting, H., Boundary Layer Theory, New York, 1968.

[23]Stevens, W., S. Goradia, and J. Braden, "Mathematical Model for Two Dimensional Multi-Component Airfoils in Viscous Flow," NASA CR 1843, July 1971.

[24]Wortmann, F.X., "A Critical Review...

[25]Wortmann, F.X., "Progress...

REFERENCES (continued)

[26]Wortmann, F.X., "Design of Airfoils with High Lift at Low and Medium Subsonic Mach Numbers," AGARD CP 102(1972), Lisbon.

[27]Owen, P.,and L. Klansfer, "On the Laminar ...

[28]Wortmann, F.X., "Progress...

[29]Wortmann, F.X., "Design...

[30]Wortmann, F.X., "Experimentelle...

[31]Abbot, I. and A von Doenhoff, p. 84.

[32]Schlichting, H., p.714.

[33]Granville, P., "The Calculation...

[34]Wortmann, F.X., "Experimentelle...

[35]Wortmann, F.X., "Ein Beitrag zum Entwurf von Laminarprofilen für Segelflugzeuge und Hubschrauber," Z. Flug W. 3, 333(1955). "A Contribution to the Design of Laminar Profiles for Sailplanes and Helicopters," British MOS translation TIL/T A903.

[36]Truckenbrodt, E., "A Quadrature Method for the Calculation of the Turbulent and Laminar Friction Layer," Ingenur - Archiv, 20(1952), p. 211-228.

[37]Stratford, B.S., "The Prediction...

[38]Miele, A. (editor), Theory of Optimum Aerodynamic Shapes, Applied Mathematics and Mechanics Series, Vol. 9, New York, 1965, p. 2.

[39]Liebeck, R.H. and A.I. Ormsbee, "Optimization of Airfoils for Maximum Lift," Journal of Aircraft, Vol. 7, No. 5, Sept.-Oct. 1970.

REFERENCES (continued)

[40]Eppler, R., "E. gebnisse gemeinsamer Anwendung von Grenschicht und Profiltheorie," Z. Flug W , 8(1960)9., "The Results of a Joint Application of Boundary Layer and Airfoil Theory," translation.

[41]Miley, S., "An Analysis...

[42]Liebeck, R.H., "A Class of Airfoils Designed for High Lift in Incompressible Flow," Journal of Aircraft, Vol. 10, October 1973, pp. 610-617.

[43]Strand, T., "Exact Method of Designing Airfoils with Given Velocity Distribution in Incompressible Flow," Journal of Aircraft, Vol. 10, November 1973, pp. 651-659.

[44]Wortmann, F.X., "A Critical Review...

[45]Pick, George S. and Douglas A. Lien, "The Development of..., pp. 218-248.

[46]Narramore, Jimmy, "Development of a Computer Aided Airfoil Design Procedure," Master's Thesis, The University of Texas at Austin, 1973.

[47]Eppler, R., "Direkte Berechnung von...

[48]Stratford, B.S., The Prediction of Separation...

[49]Miley, S.J., "An Analysis of the Design...

[50]Collins, Frank G. and James Zelenevitz, "Influence of Sound upon Separated Flow over Wings," AIAA Journal, Vol. 13, March 1975, pp. 408-410.

[51]Brown, F.M.N., private communication and movie films, Austin, Texas, 1972.

[52]Chang, P.K., "Drag Reduction of an Airfoil by Injection of Sound Energy," Journal of the Aeronautical Sciences, Vol. 28, No. 9, September 1961, pp. 742-743.

[53]Collins, Frank G. and James Zelenevitz, "Influence of Sound...

[54]Pankhurst, R.C. and D.W. Holder, Wind Tunnel Technique, Sir Isaac Pitman and Sons, Ltd., London, 1952.

[55]Garner, H.C., et al., Subsonic Wind Tunnel Wall Corrections, NATO Advisory Group for Aerospace Research and Development, Paris, 1966, pp. 49-52.

[56]Pope, Alan and John J. Harper, Low Speed Wind Tunnel Testing, John Wiley and Sons, Inc., New York, 1966, pp. 305-317.

[57]Abbott, Ara H. and Albert E. Von Doenhoff, Theory of Wing...

[58]Wortmann, F.X., "Airfoils with High Lift/Drag Ratio at a Reynolds of About One Million," NASA CR-2315, Motorless Flight Research, 1972, pp. 197-204.

[59]Schubaur, G.B. and H.K. Skramstad, "Laminar Boundary Layer Oscillations and Transition on a Flat Plate," NACA Rept. 909, 1948.

[60]Garner, H.C., et al., Subsonic Wind Tunnel...

[61]Collins, Frank G. and James Zelenevitz, "Influence of Sound...

[62]Chang, P.K., "Drag Reduction of an Airfoil...

[63]Pierpont, P.K., "Bringing Wings of Change: NASA's Airfoil Research Program," Astronautics and Aeronautics, Vol. 13, No. 10, October 1975, pp. 20-27.

APPENDICES

APPENDIX I

MAXLFT PROGRAM TO DETERMINE OPTIMUM VELOCITY DISTRIBUTIONS

The MAXLFT program was developed to determine optimum velocity distributions which maximize the lift coefficient. The analysis and equations used in the optimization section were incorporated into a FØRTRAN program in order to speed the calculations.

The input cards and formats are depicted in Table A-1.

TABLE A-1

INPUT FOR MAXLFT PROGRAM

Card 1 FORMAT(8A10)

Title card - may contain any characters in columns 1-80.

Card 2 FORMAT(4F10.0,I5)

- RE - Reynolds number based on chord length
- CPT - trailing edge pressure coefficient
- SP - lower surface length to stagnation point (may be set to zero for only upper surface calculations)
- CHORD - airfoil chord length in feet
- LT - index to indicate laminar or turbulent flow in the acceleration region (LT $\leq$ 0 implies laminar flow; LT > 0 implies turbulent flow in the acceleration region)

Card 3 FORMAT(I5)

- ITT - iteration index. If ITT = 0, no iteration on VO takes place. If ITT = 1, an iteration of VO is carried out so that the transition length constraint may be plotted (laminar acceleration region flow at Reynolds numbers less than 4×10^6)

This program is on permanent file in binary form for convenient usage. The following deck structure is required

JOB CARD

EXEPF 4110 MAXL

END OF RECORD CARD

DATA CARDS (3)

END OF FILE CARD

APPENDIX II

USE OF EPPLER INVERSE PROGRAM TO CALCULATE AIRFOIL COORDINATES

The velocity distribution upon an airfoil's surface is dependent upon the angle of attack of the airfoil. When designing an airfoil the designer is concerned not just with one angle of attack, but with a range of angles of attack, or correspondingly, with a range of lift coefficients. This range may be defined by stall (separation) or by extent of laminar flow (drag bucket) on the upper surface at one end of the angle of attack range and by any of these conditions on the lower surface at the other end of the angle of attack range.

Figure 34 shows the potential flow velocity distribution about a member of the NACA laminar flow airfoils for three different angles of attack. The section data of this airfoil is given in Figure 35. A constant velocity distribution extending to 40% chord is produced on its upper surface at an angle of attack of 4.2° and similarly on its lower surface at -1.6° angle of attack. (These two angles of attack correspond to the boundaries of the drag bucket.) Examination of Figure 34 gives additional information which applies to the general airfoil design problem:

$$\frac{\partial}{\partial \alpha}\left(\frac{V}{V_\infty}\right)\Bigg|_{\text{upper surface}} > 0$$

$$\frac{\partial}{\partial \alpha}\left(\frac{V}{V_\infty}\right)\Bigg|_{\text{lower surface}} < 0$$

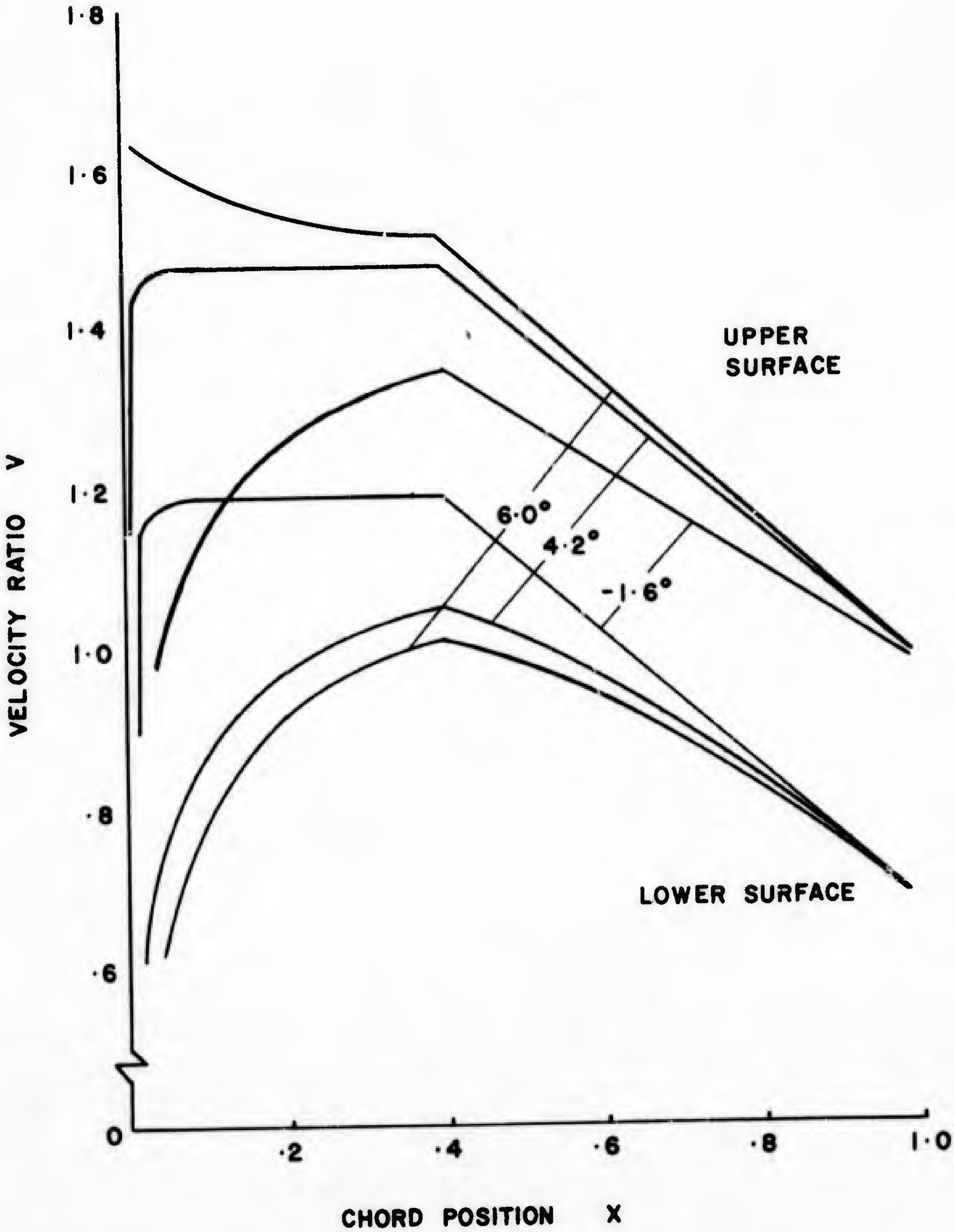

Figure A-II.1 Velocity distribution about a NACA laminar flow airfoil ($NACA\ 64_3$-618)

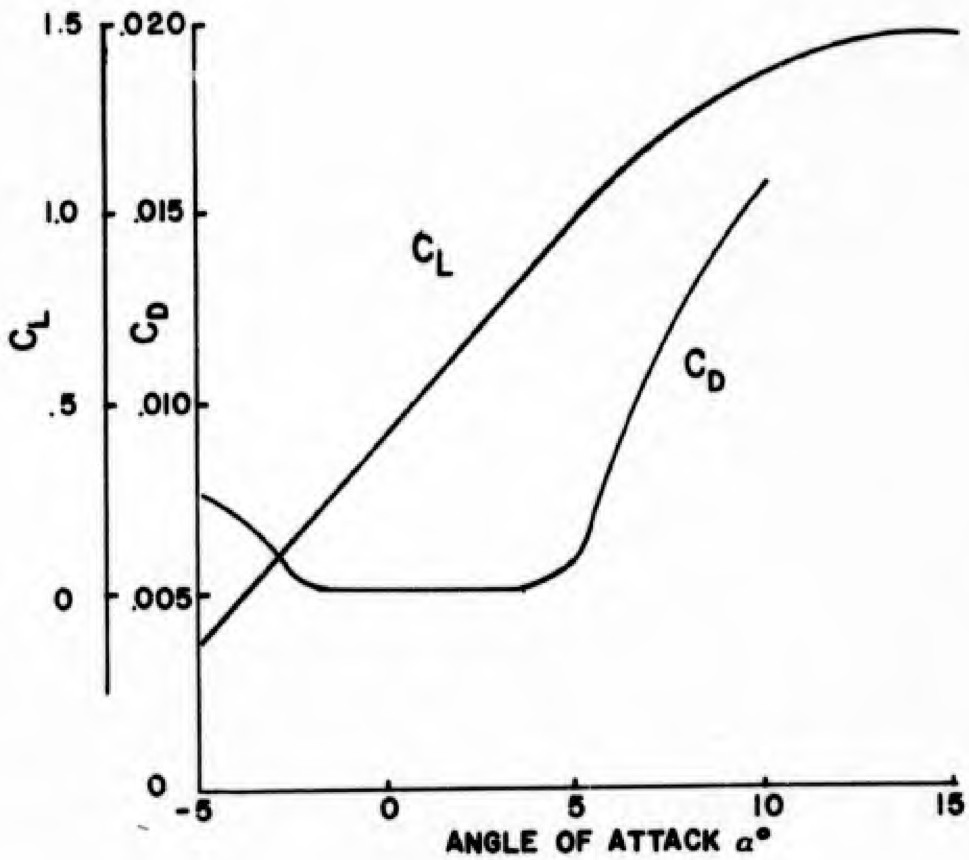

Figure A-II.2 Lift and drag coefficient as a function of angle of attack for the NACA 64_3-618

$$\frac{\partial}{\partial \alpha}\left[\frac{\partial}{\partial x}\left(\frac{V}{V_\infty}\right)\right]\Bigg|_{\text{upper surface}} < 0$$

$$\frac{\partial}{\partial \alpha}\left[\frac{\partial}{\partial x}\left(\frac{V}{V_\infty}\right)\right]\Bigg|_{\text{lower surface}} > 0$$

These relationships can also be derived from a theoretical basis and those interested in this analysis are referred to Miley's dissertation.

It should be noted that when designing an airfoil, one must specify not only the velocity distribution, but also the angle of attack at which this velocity distribution occurs. Eppler has simplified this requirement in his inverse solution.

The Eppler inverse program is based upon a conformal transformation from the flow about a circle to another plane containing the airfoil. Figure 36 shows the two planes and defines the symbols and nomenclature used. In all the airfoil surface segments, except the pressure recovery segment near the trailing edge of the airfoil, the angle of attack at which $\frac{\partial}{\partial x}\left(\frac{V}{V_\infty}\right) = 0$ in the segment is the required input. This in effect reduces the required input so that the numerical value of the velocity is not a specified input parameter. As an example, the design of the NACA laminar flow airfoil of Figure 34 would consist of specifying the position of the segment through $\cos \phi_i \simeq 2(\frac{x_i}{C}) - 1$ and the angle of attack for constant velocity in that segment. Since the position of the stagnation point is calculated in the program, it is left unspecified and the input would appear as follows

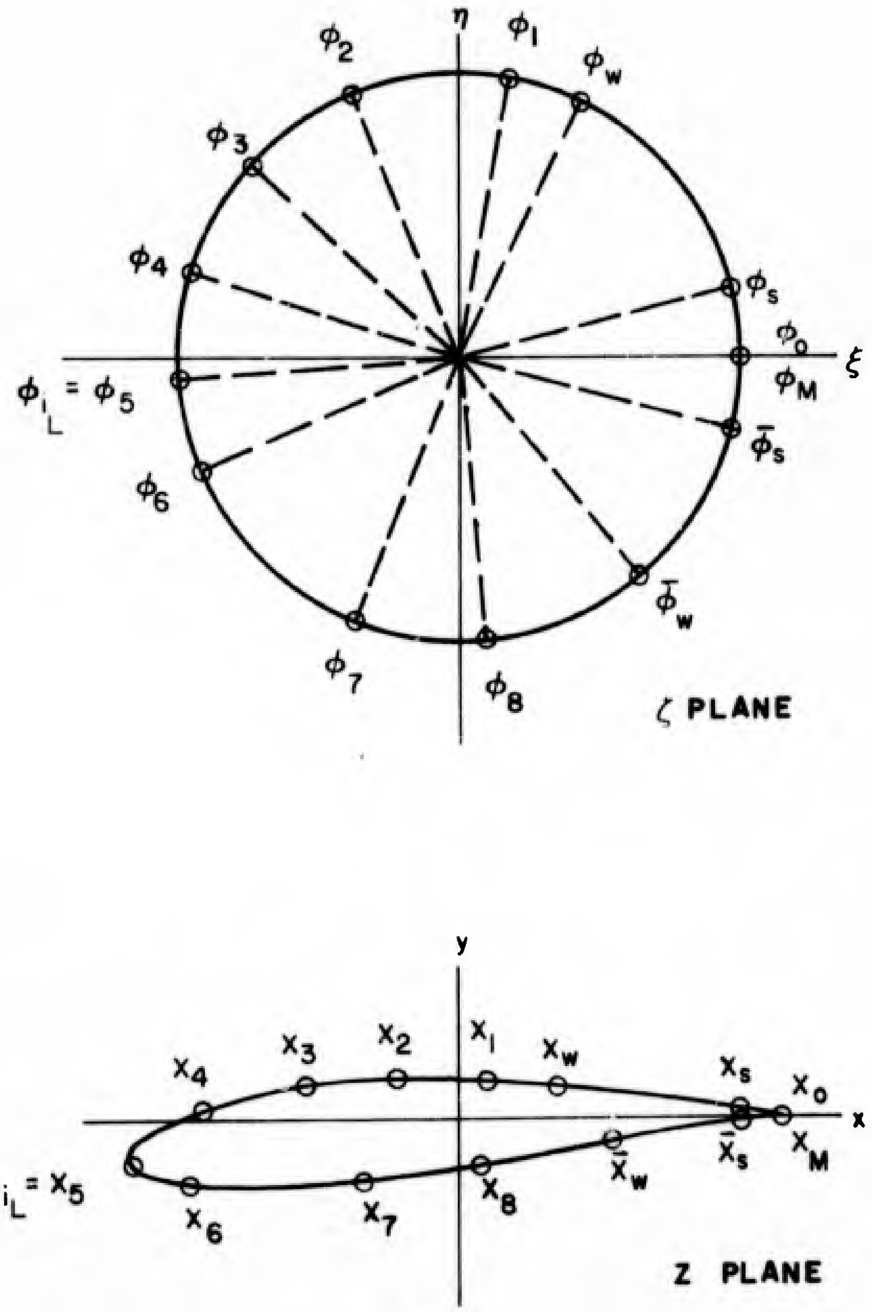

Figure A-II.3 Symbols and nomenclature for Eppler inverse solution program

Upper surface

$$\cos \phi_\omega \simeq 2(0.4) - 1 \rightarrow \phi_\omega \simeq 101°$$

$$\alpha_2 = 4.2°$$

$$\phi_1 = 96°$$

Lower surface

$$\bar{\phi}_\omega = 101°$$

$$\alpha_3 = -1.6°$$

$$\phi_3 = 264°$$

$$\phi_4 = 360°$$

This input adjusts the segment size and position of the start of the pressure recovery regions. The form of the velocity distribution in the adverse pressure gradient must also be specified.

There are three options available in the program for specifying the form of the large velocity decrease. The most convenient input parameters to use are the initial slope (ω') at the start of the pressure rise and a number related to the total amount of velocity decrease (ω). The parameters are illustrated in Figure 37.

Table A-2 gives the input cards and formats for the Eppler inverse program. The following deck structure is required

JOB CARD (TM = 10, PR = 33, PL = 800)
EXECPF 4110 ADP
END OF RECORD CARD
DATA CARDS
END OF FILE CARDS

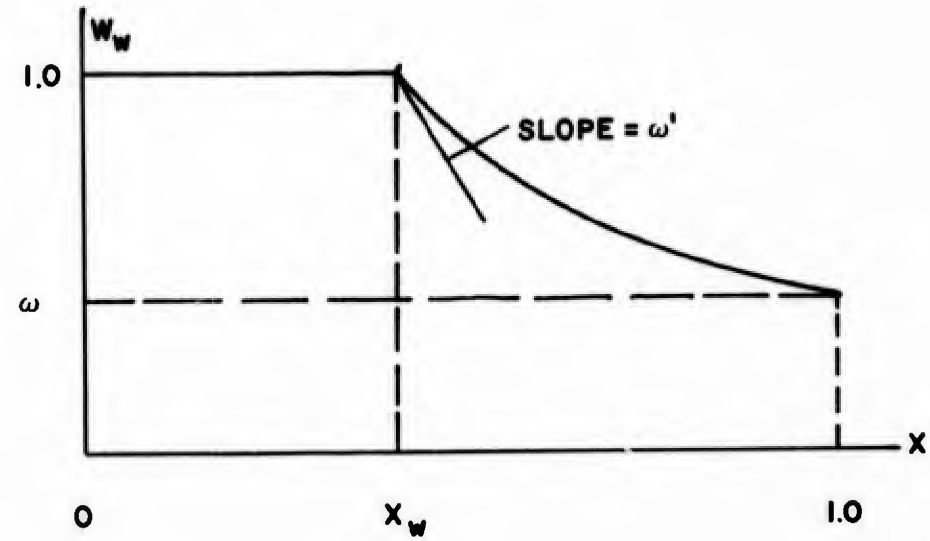

Figure A-II.4 Pressure recovery distribution parameters

The output includes a printout of the coordinates and boundary layer development and an ink plot of these at the specified angle of attack. (If more than one angle of attack is calculated, only the last is plotted.)

Since this program requires a few iterative runs to get the desired characteristics, it is advisable not to plot until the input is exactly correct. The following deck and control cards will give the print out with no plot

```
     JOB CARD (TM = 10, PR = 33)
     READPF 4110 ADP
     COPYBR ADP AAA 3
     RUN S
     REWIND LGO
     COPYBR LGO AAA
     SKIPR ADP 3
     COPYBR ADP AAA 13
     AAA
     END OF RECORD CARD
     SUBROUTINE DRME (X,Y,VF,S)
     DIMENSION X(121), Y(121), VF(121), S(121)
     CL = 0.0
     DO 3 I = 2, 121
     DS = S(I - 1) - S(I)
     VAVG = VF(I) + VF(I - 1)
     CL = CL + DS * VAVG
   3 CONTINUE
     WRITE (6, 8) CL
   8 FORMAT (/, 5X, *CL = *, F15. 6)
     RETURN
     END
```

END OF RECORD CARD

DATA CARDS

END OF FILE CARD

TABLE A-2

INPUT FOR EPPLER INVERSE PROGRAM

Card 1 FORMAT(16A4)

Title Code Card - this card lists the titles of all the cards to follow

Example:

TRAITRA2ALFAAGAMABSZRE ENDE

Card 2 FORMAT(A4, 6X, 2F5.2)

ABSZ - title code

NKR - this number determines the number of points to be calculated around the airfoil (use 120.) Note: $ABGR = \frac{360.}{NKR}$

ABFA - the segment factor (normally equal to one)

Example:

ABSZ 12000 100

Card 3 FORMAT(A4, 6X, 14F5.2)

AGAM - title code

AGAM(i) - these values control the output mode. The following example is the advised form

Example:

AGAM 100 100 100 000 100

Card 4 FORMAT(A4, I6, 14F5.2)

TRAI - title code

I - profile identification number

$\left.\begin{matrix} a_i \\ \alpha_i \end{matrix}\right\}$ - a maximum of 7 pairs of these values in degrees $\left(a_i = \frac{\phi_i}{ABGR}\right)$ where ϕ_i is the end of the <u>ith</u> segment in degrees on the circle to be transformed. The profile nose is specified by setting $a_i = 0$. (Note: If more than 7 segments are required, as many as 3 more TRAI cards may be added thus giving up to 28 segments)

Example:

TRAI 153 3200 1740 4150 900 5140 1700 000 2200 8620 -50012000 000

Card 5 FORMAT(A4, 6X, 3F5.2, 2F5.3, 3F5.2, 2F5.3, F5.2, F5.3)

TRAI - title code

λ^* - $\lambda^* = \frac{\phi_S}{ABGR}$ where ϕ_S is related to the trailing edge closing length. This should be applied to the last 3 to 5% of airfoil chord with ϕ_S chosen accordingly

λ - $\lambda = \frac{\phi_\omega}{ABGR}$ where ϕ_ω is related to the start of the pressure recovery region

mode 1 - choose mode 1= 1.0 so that ω' and ω may be specified in the next two words

ω' - slope at the start of the pressure recovery region on the upper surface

ω - specifies the amount of pressure to be recovered on the upper surface

$\bar{\lambda}^*$ - same as λ^* except applies to lower surface

$\bar{\lambda}$ - same as λ except applies to lower surface

mode 2 - control for next two words. Choose mode 2 = 1.0 so that ω' and ω may be specified

$\bar{\omega}'$ - slope at the start of the pressure recovery region on the lower surface

$\bar{\omega}$ - specifies the amount of pressure to be recovered on the lower surface

itmod - determines the mode of iteration for closure of the airfoil section itmod = 0.0 no iteration

1.0 iteration with α_i on upper surface

2.0 iteration with α_i on lower surface

3.0 iteration with α_i on upper and lower surface

Ksoll - determines the cross section at the trailing edge. Sensible values are between 0.0 and 1.5

Example:

TRA2 666 3300 100 4000 550 660 0 0 0 0 200 500

Card 6 FORMAT(A4, I6, 14F5.2)

ALFA - title code

NA - number of angles of attack to be computed. (Note: Only the last angle of attack velocity distribution is plotted)

Ai - the angles of attack for which velocity distributions and boundary layer calculations are to be made

Example:

ALFA 1 1700

Card 7 FORMAT(A4, 6X, 5(2I1, 3X, F5.3))

RE title code

MA - controls boundary layer suction in program (Set MA = 0 for no suction)

MU - controls transition criterion mode

MU = 0 transition by laminar separation

= 1 transition when UK1 - UK < 0

= 2 transition when UK1 - UK ≤ 0

= 3 transition when

$\ln(Re \cdot U \cdot \theta) \geq 18.4 \cdot H_{32} - 21.74$

(agrees best with Eppler's experiments)

= 4 transition when

$\ln(Re \cdot U \cdot \theta) \geq 18.4 \cdot H_{32} - 22.10$

REN - the Reynolds number multiplied by 10^{-6}.
(Note: Up to 5 sets of MA, MU, REN may be run)

Example:

RE 03 700

Card 8 FORMAT(A4)

ENDE - title card. Signifies end of input and initiates normal termination of the program.

Example:

ENDE